# Mapping of Genes Involved in Hereditary Skeletal Dysplasia in Pakistani Families

A dissertation submitted in the partial fulfillment of the requirements for the degree of Doctor of Philosophy

in

**Biotechnology**

**by**

**Ayesha Zaka**

**Reg # 56-FBAS/PHDBT/F15**



**Department of Biological Sciences**

**Faculty of Sciences**

**International Islamic University Islamabad, Pakistan**

**2023**

Skeletal dysplasias - Genetic aspects - Pakistan
Genetic disorders - Economic " - "
Human genetics - Research - Pakistan
Medical " - Economic aspects
Health care - Economic aspects - Pakistan
Public health - Pakistan - Economics
Genetic mapping - Pakistan

# Mapping of Genes Involved in Hereditary Skeletal Dysplasia in Pakistani Families



**Supervisor**

**Dr. Shaheen Shahzad**

**Assistant Professor**

**Department of Biological Sciences**

**Faculty of Basic and Applied Sciences**

**International Islamic University Islamabad, Pakistan**

**2022**

## FINAL APPROVAL

It is certified that we have read the thesis submitted by **Ms. Ayesha Zaka** and it is our judgment that this project is of sufficient standard to warrant its acceptance by the International Islamic University, Islamabad in partial fulfillment of the requirements for the degree of Doctor of Philosophy in Biotechnology.

**Chairperson** ________________________

Department of Biological Sciences

International Islamic University Islamabad, Pakistan

**Dean, Faculty of Basic and Applied Sciences** ________________________

International Islamic University Islamabad, Pakistan

**Date:** ______________

# CERTIFICATE

It is certified that we have read the thesis submitted by **Ms. Ayesha Zaka** and it is our judgment that this project is of sufficient standard to warrant its acceptance by the International Islamic University, Islamabad, in partial fulfillment of the requirements for the degree of Doctor of Philosophy in Biotechnology.

## COMMITTEE

**Supervisor:** **Dr. Shaheen Shahzad**

**External Examiner 1:**
**Dr. Peter John, Professor,**
**ASAB, NUST**

**External Examiner 2:**
**Dr. Aneesa Sultan, Associate Professor,**
**Department of Biochemistry, QAU**

**Internal Examiner:**
**Dr. Asma Gul, Associate Professor,**
**Department of Biotechnology, IIUI**

**Date:** 22nd March, 2023

## DECLARATION

It is certified that work done on this PhD Biotechnology research thesis **"Mapping of Genes Involved in Hereditary Skeletal Dysplasia in Pakistani Families"** is purely conducted by me. All the material is prepared by myself and has not been copied from anywhere; however, some text and figures have been used which are properly referenced.

**Ayesha Zaka**

## RESEARCH PUBLICATIONS

1. Zaka, A., Shahzad, S., Rao, H. Z., Hashim, Y., & Basit, S. (2021). A novel homozygous frameshift mutation in the DCC gene in a Pakistani family with autosomal recessive horizontal gaze palsy with progressive scoliosis-2 with impaired intellectual development. American journal of medical genetics. Part A, 185(2), 355–361. https://doi.org/10.1002/ajmg.a.61952
2. Zaka, A., Shahzad, S., Rao, H. Z., Kanwal, S., Gul, A., & Basit, S. (2021). An intrafamilial phenotypic variability in Ellis-Van Creveld syndrome due to a novel 27 bps deletion mutation. American journal of medical genetics. Part A, 185(10), 2888–2894. https://doi.org/10.1002/ajmg.a.62360
3. A Novel Homozygous Nonsense Mutation in FLNB gene causes Spondylocarpotarsal Synostosis Syndrome in a Consanguineous Pakistani Family (Submitted)
4. A Novel Homozygous Missense Mutation in CUL7 causes 3M Syndrome in a Consanguineous Pakistani Family (Submitted)

***Dedicated***

***To***

***My Family***

# TABLE OF CONTENTS

# LIST OF FIGURES

# LIST OF TABLES

# LIST OF ABBREVIATIONS

| | |
|---|---|
| ISDS | International Skeletal Dysplasia Society |
| INCDB | International Nomenclature of Constitutive Diseases of Bones |
| FGFR3 | Fibroblast Growth Factor Receptor 3 |
| SADDAN | Severe Achondroplasia with Developmental Delay and Acanthosis nigricans |
| COL2A1 | Collagen Type 2 Alpha 1 |
| OI | Osteogenesis Imperfecta |
| GAG | Glycosaminoglycans |
| NGS | Next Generation Sequencing |
| DNA | Deoxyribonucleic Acid |
| WGS | Whole Genome Sequencing |
| WES | Whole Exome Sequencing |
| MSC | Mesenchymal Stem Cells |
| VEGF | Vascular Endothelial Growth Factor |
| Wnt | Wingless |
| TGF-β | Transforming Growth Factor Beta |
| SHH | Sonic Hedgehog |
| IHH | Indian Hedgehog |
| FGF | Fibroblast Growth Factor |
| DSBS | Developmental Split Brain Syndrome |
| HGPPS | Horizontal Gaze Palsy with Progressive Scoliosis |

| | |
|---|---|
| DCC | Deleted in Colorectal Cancer |
| ACC | Agenesis of corpus callosum |
| ROBO2 | Roundabout Guidance Receptor 2 |
| EVC | Ellis van Creveld |
| EVC2 | Ellis van Creveld 2 |
| CCDC8 | Coiled-Coil Domain Containing 8 |
| OBSL1 | Obscurin-Like Cytoskeletal Adaptor 1 |
| SCT | Spondylocarpotarsal synostosis |
| FLNB | Filamin B |
| FMD1 | Frontometaphyseal dysplasia 1 |
| OPD1 | Otopalatodigital syndrome 1 |
| MNS | Melnick-Needles syndrome |
| OMIM | Online Mendelian Inheritance in Man |
| MESP2 | Mesoderm Posterior BHLH Transcription Factor 2 |
| PAP | Postaxial Polydactyly |
| PAPA | Postaxial Polydactyly Type A |
| PAPB | Postaxial Polydactyly Type B |
| ZNF141 | Zinc Finger Protein 141 |
| MIPOL | Mirror Image Polydactyly |
| PIT1 | Pituitary Transcription Factor 1 |

| | |
|---|---|
| RUNX2 | Runt-related Transcription Factor 2 |
| ATF4 | Activating Transcription Factor 4 |
| PTHrP | Parathyroid hormone-related protein |
| MAPK | Mitogen-activated protein kinase |
| CNP | C-type Natiuretic Peptide |
| PI3K | Phosphoinositide 3-kinase |
| ERK | Extracellular Signal-Regulated Kinase |
| PKCα | Protein Kinase C – alpha |
| ACH | Achondroplasia |
| MIM | Mendelian Inheritance in Man |
| CNS | Central Nervous System |
| mRNA | Messenger ribonucleic acid |
| KDa | Kilodalton |
| CHD | Calponin Homology Domain |
| ABD | Actin Binding Domain |
| PVNH | Periventricular Nodular Heterotopia |
| DLL3 | Delta-like Canonical Notch Ligand 3 |
| DSL | Delta-serrate-lag2 |
| EGF | Epidermal Growth Factor |
| TM | Transmembrane |
| SD | Spondylocostal Dyostosis |
| LMBR1 | Limb Development Membrane Protein 1 |
| SHH | Sonic Hedgehog |

| | |
|---|---|
| ZPA | Zone of Polarizing Activity |
| PPD | Preaxial Polydactyly |
| HCH | Hypochondroplasia |
| GHRHR | Growth hormone releasing hormone receptor |
| AMDM | Acromesomelic Dysplasia, Maroteaux type |
| AMDG | Acromesomelic Dysplasia, Grebe type |
| AMDH | Acromesomelic Dysplasia, Hunter-Thomson type |
| SHFM | Split hand-foot malformation |
| KPK | Khyber Pakhtunkhwa |
| EDTA | Ethylene diamine tetraacetic acid |
| ul | Microliter |
| mg | Milligram |
| $MgCl_2$ | Magnesium chloride |
| TE | Tris-EDTA |
| NaCl | Sodium chloride |
| rpm | Revolutions per minute |
| nm | Nanometer |
| BWA | Burrows-Wheeler Aligner |
| GATK | Genome Analysis Toolkit |
| gnomAD | Genome Aggregation Database |
| dbSNP | Single Nucleotide Polymorphism Database |
| SNP | Single Nucleotide Polymorphism |
| Rs | Reference SNP |

| | |
|---|---|
| ExAC | Exome Aggregation Consortium |
| SIFT | Sorting Intolerant From Tolerant |
| PolyPhen | Polymorphism Phenotyping |
| PCR | Polymerase Chain Reaction |
| Tm | Melting Temperature |
| bp | Base pair |
| min | Minute |
| DTCS | Dye Terminator Cycle Sequencing |
| NaAc | Sodium Acetate |
| SLS | Sodium Lauryl Sulfate |
| MRI | Magnetic Resonance Imaging |
| PDB | Protein Data Bank |
| PROVEAN | Protein Variation Effect Analyzer |
| UCSC | University of California Santa Cruz |
| SNAP | Screening for Non-acceptable Polymorphisms |
| PhD-SNP | Predictor of human Deleterious Single Nucleotide Polymorphisms |
| mvPPT | Pathogenicity Prediction Tool for missense variants |
| ACMG | American College of Medical Genetics |
| SD4 | Syndactyly Type 4 |
| TPTPS | Triphalangeal thumb–polysyndactyly syndrome |
| ROC1 | Regulator of Cullins-1 |
| DOC1 | Downregulated in Ovarian Cancer-1 |
| FBXW8 | F-box and WD repeat domain containing 7 |

# ACKNOWLEDGEMENTS

*All praise and thanks is for Allah who fashioned man in the most perfect of proportions, and opened the doors of knowledge and learning for him. Without His Mercy and Help, we would not be capable of accomplishing anything.*

*I owe my gratitude to a lot of people who played a critical role in the completion of this research work and dissertation. I would like to acknowledge my mentor and supervisor Dr. Shaheen Shahzad, Assistant Professor, IIUI for her kind mentorship, encouragement, cooperation and able supervision at every step throughout the course of my doctorate degree. I would also like to acknowledge the Chairperson, Department of Biological Sciences, Dean FBAS, all the faculty members and staff of the department for their support and cooperation.*

*I am obliged to the Higher Education Commission, Pakistan for granting me Indigenous PhD Scholarship which enabled me to complete my research work. I am also thankful to HEC-NRPU Project for providing research facilities. I owe my thanks to Dr. Sulman Basit, Assistant Professor, Centre for Inherited Diseases, Taibah University Madinah, Saudi Arabia, Dr. Saima Siddiqi, Chief Scientific Officer, Institute of Biotechnology and Genetic Engineering, Islamabad, and Dr. Jia Nee Foo, Assistant Professor, Lee Kong Chian School of Medicine, Nanyang Technological University, Singapore for helping with whole exome sequencing of samples at their research facilities as well as providing valuable input and suggestions in the data analysis.*

*Words fail me as I try to acknowledge my loving parents. The real credit for whatever I have achieved goes to them for their unconditional love, prayers, moral and* *material support throughout my life. Without them by my side, I would never have been able to complete this degree. I would also like to acknowledge my loving parents-in-law for their prayers, support and encouragement, which always lifted my spirits. My siblings and other family members kept encouraging and supporting me too.*

*My friends and fellow scholars Ms. Ambreen Sher, Ms.Ifrah Shafqat and all fellows of Genomic Research Lab, Department of Biological Sciences, IIUI, who made the journey worthwhile with their good company and support. I would also like to thank Dr. Nida Rafiq, Dr. Noor ul Ain, Ms. Memona Rashid, and Ms. Maha Yusuf for their invaluable assistance in radiological interpretation, WES result interpretation and in silico analysis. Ms. Yasmin Hashim, Ms. Sadia Kanwal, Mr. Tasadduq and Mr. Shafqat deserve acknowledgment for their assistance in collecting the samples.*

*The participating patients and their families deserve special acknowledgment for extending their cooperation throughout the course of the project.*

*Last but not the least, I would like to mention the love of my life, my dear husband Dr. Hadi Zahid Rao. His professional input in diagnosis, his assistance at every step, the confidence he has in my abilities, the pride he takes in my work, and the patience with which he stands by my side in the face of everything makes him the real hero of this project. And of course, my young son, Muhammad Umar Rao, the coolness of my eyes, deserves special mention for his patience and cooperation as his mother spent long hours in the laboratory and huddled over the laptop.*

***Ayesha Zaka***

# ABSTRACT

Skeletal dysplasias are a broad and varied group of diseases, many of which cause serious disabilities or significantly impact the quality of life. Fewer than 500 distinct abnormalities have been identified; however, they collectively afflict about three out of every 10,000 people. While other organ systems may also be affected, bone and cartilage are the primary targets of skeletal dysplasias. Clinical diagnosis of skeletal dysplasias has relied on rigorous phenotypic characterization, skeletal radiography, and genetic testing. Next-generation sequencing (NGS) technologies, such as whole exome and whole genome sequencing, have dramatically improved molecular diagnosis. Proper genetic and molecular diagnosis provides opportunities for targeted treatment, involvement in clinical trials, and customized medical follow-up.

Here, in this dissertation, eight consanguineous families with skeletal deformities were characterized clinically and genetically. After the families expressed their consent, pedigrees were constructed, blood samples were taken and detailed clinical examination was performed. Whole-exome sequencing (WES) was performed on multiple members of each family. WES data was filtered and likely pathogenic variants were shortlisted. Primers were designed for the variants of interest, and Sanger sequencing was performed for all affected and unaffected individuals to validate the segregation of the variant in accordance with the disease phenotype and mode of inheritance. In silico tools were used to assess the pathogenicity of shortlisted variants. Protein modeling and docking studies were also carried out in selected families to study putative impact of variant on the structure and function of protein.

Novel pathogenic variants identified in this study include *DCC* variant in HGPPS-2, *EVC* variant in EvC Syndrome, *CUL7* variant in 3M Syndrome, *FLNB* variant in spondylocarpotarsal synostosis syndrome, *DLL3* variant in spondylocostal dyostosis and *LMBR1* variant in non-syndromic polydactyly; whereas, known variants in two different genes *FLNA* and *FGFR3* were identified in two families segregating otopalatodigital syndrome-2 and achondroplasia respectively.

Together, the research findings broaden the genetic and phenotypic range of skeletal dysplasias, and show that using whole-exome sequencing technology in conjunction with thorough phenotyping is an effective way to identify disease-causing variations in people with congenital skeletal diseases.

# INTRODUCTION

Skeletal dysplasia is the collective name given to more than 450 genetically heterogeneous abnormalities of the skeletal system. These are primarily bone and cartilage growth and remodeling disorders. Prevalence of this disease is estimated to be 3-4 out of every 10,000 births (Cassart, 2010). The patients display abnormalities in differentiation, linear growth and maintenance of their appendicular and axial skeleton. The phenotypic spectrum can vary from death of newborn to only mild growth retardation in adults (Parnell and Phillips, 2012). Skeletal dysplasias are difficult to diagnose in utero, especially when there is no family history or molecular diagnostic marker (Dighe *et al.,* 2008).

Skeletal dysplasias generally manifest as abnormalities in growth, integrity and shape of bones. Other organ systems may also be affected concomitantly. Mode of inheritance of skeletal dysplasias may be X-linked or autosomal, recessive or dominant. Many of the genetic variations, pathways and molecular mechanisms causing skeletal dysplasias have been identified. However, there are still many gaps in the literature regarding the genetic basis of several kinds of skeletal dysplasias (Kim *et al.,* 2021).

The International Skeletal Dysplasia Society (ISDS) was founded in 1999 to ensure that the numerous diverse entities grouped together as skeletal dysplasias were properly characterised using clinical, genetic, and radiological data. This society formulated the International Nomenclature of Bone Constitutional Diseases (INCDB). (Mortier *et al.,* 2001).

In 2019, the International Skeletal Dysplasia Society's Nosology Committee reviewed and updated the tenth and most recent version of the Nosology and Classification of Genetic Skeletal Disorders. The latest Nosology includes 461 disorders divided into 42 groups on the basis of clinical, radiographic, and/or genetic characteristics (Table 1.1). Interestingly, pathogenic mutations impacting 437 distinct genes were discovered in 425/461 (92%) of these illnesses (Mortier *et al.*, 2019).

The Nosology groups 1–8 are based on a shared underlying mechanism or gene. The radiographic alterations to specific bone structures or the affected segment are localised in groups 9–17. Macroscopic criteria in combination with clinical aspects define groups 18–20. Mineralization aspects are considered in groups 21–25 and 28. Group 27 refers to a vast group of lysosomal illnesses that affect the skeleton. Exostoses, ecnhondromas, and ectopic calcification are examples of illnesses with so-called aberrant skeletal component development. Several unique molecular pathways causing hypophosphatemic rickets have been discovered by Group 26. Group 30 illnesses are overgrowth syndromes with a skeletal component that forms the diagnostic criteria for a specific disease. Inflammation and bone involvement are characteristics of Group 31 diseases. Finally, dysostoses are studied in groups 32–42, which include anatomical criteria as well as embryonic development principles (Warman *et al.*, 2011; Mortier *et al.*, 2019).

Individually, skeletal dysplasias are rare but almost always severe disorders. Affected individuals usually manifest with major complications affecting their quality of life. Loss of normal structural cartilage also affects motility. Understanding the underlying genetic interplay and expected complications is vital to provide the best care to patients (Zelzer & Olsen, 2003).

In the last few decades, positional cloning and linkage analysis have helped to identify the genes for skeletal dysplasia in more than 150 diseases. This information has led to improved prenatal and postnatal diagnosis. However, in several cases, the causative genes remain unidentified. Filling the missing gaps will improve the quality of life of patients, by improving treatment and diagnosis (Bonafe *et al.,* 2015).

In the last few decades, NGS has become the tool of choice to identify causative variants. NGS is a high-throughput method of DNA sequencing that can be used to identify pathogenic variants (Hodges *et al.*, 2007; Schuster, 2008; Parla *et al.*, 2011). Generally, NGS includes three steps: library preparation, amplification, and sequencing (Turner *et al.*, 2009). Through NGS, we can sequence whole genomic DNA called whole genome sequencing (WGS) as well as only the coding regions (exome) called whole exome sequencing (WES). Coding regions comprise almost 1 percent of genomic DNA. Among hereditary disorders, almost 85 percent are caused by variations in coding regions. Therefore, sequence analysis only of coding regions of the genome can reveal causative genes in most of the cases (Ku *et al.*, 2012).

Relative cost-effectiveness, and ease of data analysis has made WES the foremost platform for analyzing human genetics. Millions of variants can be detected in an individual's genome, and then filtered to identify the variants of interest (Boycott *et al.,* 2013, Vassy *et al.,* 2017).

This study will help clinicians in the diagnosis of genetic skeletal disorders. At clinical level, some of the skeletal disorders can be treated by surgical intervention and physical therapy with the help of pediatricians, orthopedists, and physical therapists. For example, extra digit in polydactyly patients is surgically removed. Similarly, some abnormalities of spinal curvature may be treated by surgical intervention followed by exercise and physical therapy (Umair *et al.,* 2019). Findings of present study would be helpful for geneticists in establishing genotype-phenotype correlation. Families having history of genetic skeletal disorders can take benefit from the present study through genetic counseling and prenatal testing. This study will bring awareness among people where consanguineous marriages are common to prevent recessive genetic disorders.

**Aims and objectives**

The main aim of the study is to search for the genes causing different types of skeletal dysplasias and their associated pathogenic mutations with the following objectives:

a- Identification and recruitment of families segregating hereditary skeletal dysplasia from different regions of Pakistan.

b- Clinical Examination of the affected members in each sampled family

c- To determine the genotypic and phenotypic variation in skeletal dysplasia in Pakistani families.

d- To identify the novel genetic mutations involved in the pathogenesis of clinically diverse Pakistani families affected with skeletal deformities.

# LITERATURE REVIEW

## 2.1 Human Skeleton

All vertebrates have an internal skeleton. The human skeleton is a very complex and advanced structural framework. It performs a range of important functions in the human body (Rimoin *et al.,* 2007). The skeletal system consists of three types of cells (osteoblast, osteoclast and chondrocyte), and two types of tissues (cartilage and bone). Skeletal dysplasias are caused by any kind of abnormality in any one or more of these components (Rimoin *et al.*, 2007).

The skeletal system of human is composed of 270 bones at birth, which gradually fuse such that there remain a total of 206 bones at adulthood (Figure 2.1). These 206 bones in an adult skeleton include 126 appendicular bones, 74 axial, and 6 ossicles (Savarirayan and Rimoin, 2002; Ross *et al.*, 2006). The skeleton is divided into appendicular and axial skeleton. Upper and lower limbs, pectoral girdle and the pelvic girdle comprise the appendicular skeleton. Appendicular skeleton supports the body weight and allows and aids locomotion. Skull, spinal column, ribs and all associated bones form the upright axial skeleton which supports the body (Helms & Schneider, 2003).

Some of the functions of the skeletal system include: movement, support, protection of vital internal organs (brain, spinal cord, lungs, heart and blood vessels), production of blood cells, storage of calcium and iron, and regulation of blood sugar, via a hormone called osteocalcin (Blottner *et al.*, 2006; Clarke, 2008).

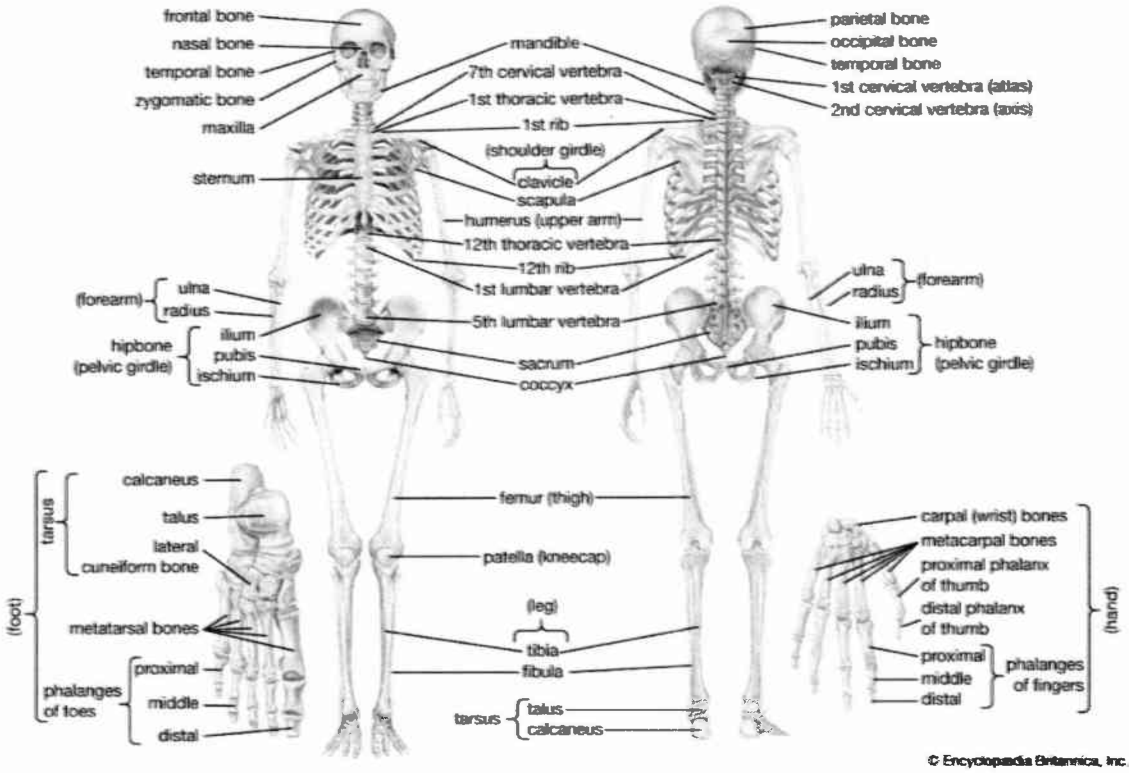


**Figure 2.1 Bones of the human skeleton** (britannica.com/science/human- skeleton)

### 2.1.1 Bone

Bone is made up of osteoblasts, osteoclasts, blood vessels, hematopoietic cells, and stroma, which is a living and growing connective tissue (Kini & Nandeesh, 2012). It is a rigid and hard structure which can regenerate. Up to 99 percent of total body calcium is found in the bone matrix. Collagens, proteoglycans, hyaluronic acid, and minerals and ions such as sodium, potassium, bicarbonates and phosphates are present in the bone. Bone cells (osteocytes) are involved in bone formation and resorption, as well as blood production (hematopoietic cells) and immunology (Artner, 2003).

Bone can be divided into five classes based on their morphology: long bones, short bones, irregular bones, flat bones, and sesamoid bones. All these bones perform specific functions in the body, and are shaped accordingly (Clarke, 2008).

Long bones have a diaphysis (a central cylindrical shaft) and an epiphysis (a hollow region housing the medullary cavity) (Figure 2.2). The epiphyseal plate is the region where diaphysis meets the epiphysis (Laurin *et al.*, 2011). Periosteum covers the outer surface of the bone and attaches it to ligaments and tendons, while endosteum lines and protects the inner surface (Kini & Nandeesh, 2012).

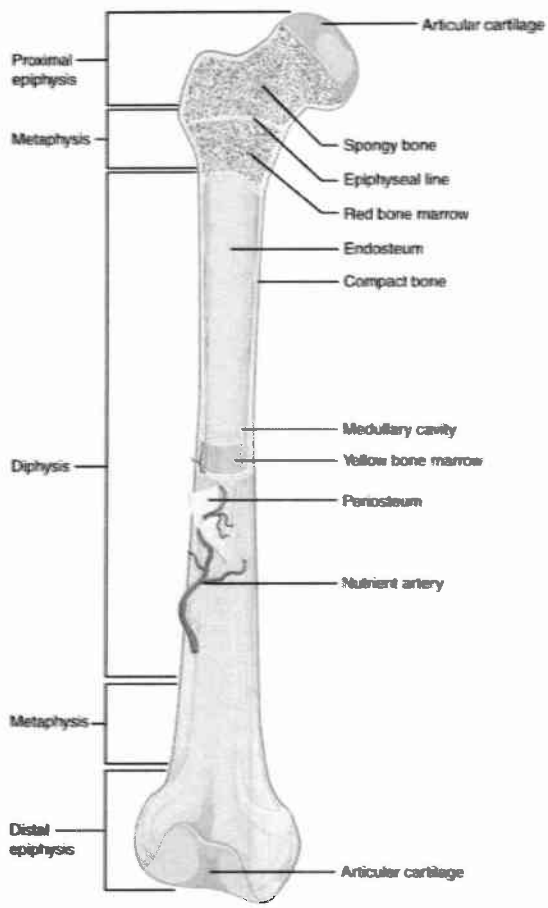


**Figure 2.2 Structure of a long bone** (Source: en.wikipedia.org/wiki/Long_bone)

### 2.1.2 Cartilage

Cartilage is an avascular resilient tissue with a high water content. It is composed of an extracellular matrix and chondrocytes. It is covered by the perichondrium which is a protective layer of connective tissue. Perichondrium maintains the shape of the cartilage, while providing it nutrition as per its requirement (Duynstee *et al.*, 2002). The embryonic skeleton initially appears as a cartilage template. This is replaced by bone during the embryonic period, except at specific areas where the elasticity of cartilage is required (Geister & Camper, 2015). Cartilage is divided into three categories based on histology:

- Hyaline cartilage: This type of cartilage can be found near the ends of long bones and ribs. It is made up mostly of tiny collagen fibres. It is gradually replaced by bone in childhood and growing age (Umlauf *et al.,* 2010).
- Fibrocartilage is a type of cartilage that can be found in the vertebral discs and joint capsules. It has strong collagen fibres and provide mechanical support (Umlauf *et al.,* 2010).
- Elastic cartilage: It is made up of multiple elastic fibres and is found in the external ear, auditory tube, and epiglottis (Umlauf *et al.,* 2010)

## 2.2 Bone Formation

Bone is a hard, living connective tissue that makes up the skeleton of vertebrates. Skeletogenesis begin at the embryonic stage when the ectoderm and endoderm give rise to multipotent mesenchymal stem cells (MSCs), which move to specific areas, and become predestined to achieve their skeletal fate. After condensation, these mesenchymal cells divide into cartilage cells (chondrocytes) and bone cells (osteoblasts). Skeletogenic cells initiate osteogenesis by intramembranous ossification and endochondral ossification. After birth, the skeleton continues to undergo a dynamic process of growth and remodeling (Zelzer and Olsen, 2003). Skeletal abnormalities can result from defects at any stage of skeletal development or growth (Mariani & Martin *et al.,* 2003).

### 2.2.1 Skeletal Patterning

Skeletal patterning is the process in which the size, shape and number of individual parts of the skeleton are defined. Patterning factors are the factors involved in this definition. This process involves the migration of cells from three different embryonic lineages i.e. lateral plate mesoderm, somites and neural crest. These cells migrate to their final sites to build the craniofacial skeleton, axial skeleton, and appendicular skeletons, respectively, throughout this phase (Koosha & Eames *et al.,* 2022).

Cells travel to the region of future skeletogenesis, where they first condense, and then differentiate into chondrocytes (which form the cartilage) or osteoblasts (which form the bone) (Bi *et al.,* 1999).

### 2.2.2 Bone Development and Growth

The first step in bone development and growth is the condensation of mesenchymal stem cells from the neural crest or mesoderm. The condensed mesenchyme can then follow the routes of endochondral or intramembranous ossification.

1- Endochondral ossification (chondrogenesis of condensed mesenchyme and then its conversion into mineralized bones) (Lefebvre and Bhattaram, 2010)

2- Intramembranous ossification (development of condensed mesenchyme directly into osteoblasts) (Lefebvre and Bhattaram, 2010)

Intramembranous ossification forms the bones of the craniofacial skeleton and sections of the clavicle, while endochondral ossification leads to the formation of all other bones including long bones (Karsenty *et al.,* 2009).

### 2.2.2.1 Intramembranous Ossification

Skeletal cells develop to prehypertrophic chondrocytes and concentrate in growth plate perichondrium and potential cranial bone locations during intramembranous ossification (Karsenty *et al.,* 2009). These cells now develop into either endothelial cells or osteoblastic cells. These initiate the formation of the extracellular matrix (Figure 2.3). Ossification centres form in the centre of each future bone. They start producing bony spicules in a circular pattern to begin extracellular matrix calcification. Sutures are fibrous and elastic bone development regions that occur between growing bones of the cranium. They harbor active, undifferentiated osteogenic cells, allowing them to create new bone cells necessary for bone development. At the age of two, they vanish and the skull bones fuse together. (Lefebvre & Bhattaram, 2010).

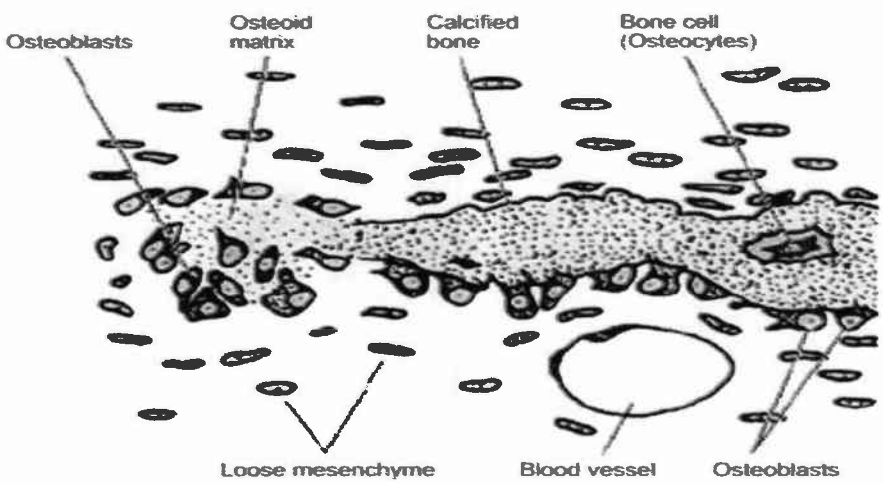


**Figure 2.3 Intramembranous Ossification**

Mesenchymal cells derived from the mesoderm migrate to the site where they will form future bone, and condense to form the osteoblasts. Osteoblasts produce un-calcified bone matrix (osteoid) and mineralize the bone matrix. Osteocytes are born from osteoblasts that remain trapped in osteoid matrix. Osteoblasts continue to line the surfaces of developing bones to produce bone matrix (source: https://www.ncbi.nlm.nih.gov/books/NBK10056/).

### 2.2.2.2 Endochondral Ossification

Endochondral ossification, in which cartilage analgen are created initially and then replaced by bone, forms the majority of the skeleton (Erlebacher *et al.,* 1995).

Endochondral ossification requires the formation of a growth plate. It is required for prenatal bone formation throughout early development, and also for postnatal development until the end of puberty.

Through a series of maturation processes, chondrocytes in the growth plate are organised into four layers: resting, proliferating, prehypertrophic, and hypertrophic chondrocytes (Figure 2.4). Hypertrophic chondrocytes produce a collagen X- rich extracellular matrix into which they deposit various factors such as the angiogenic factor and the vascular endothelial growth factor (VEGF) (Iyama *et al.,* 1991). The VEGF promotes blood vessel development from the perichondrium (Gerber *et al.,* 1999).

After migrating to the diaphysis, osteoblasts, osteoclasts, and hematopoietic cells create the major ossification centres as blood vessels invade the cartilage matrix. Hypertrophic chondrocytes die, osteoclasts breakdown cartilage matrix, while osteoblasts lay deposit bone matrix. Bone marrow is produced by hematopoietic cells, and the perichondrium develops into a bone collar within these centres. Postnatally, secondary ossification centres form in the epiphyses, forming a cartilage plate between the epiphyses (Florencio-Silve *et al.,* 2015; Chen *et al.,* 2018).

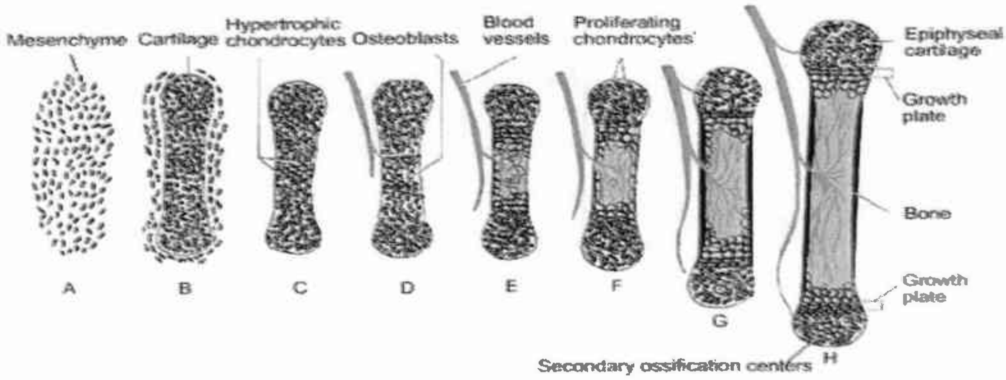


**Figure 2.4 Endochondral ossification**

Endochondral ossification begins with the formation of a cartilage template as mesenchymal cells condense and differentiate into chondrocytes (A, B). Primary ossification centres develop in the long bone shafts as a result of chondrocyte death and hypertrophy, which causes blood capillaries to invade (C). Osteoblasts replace cartilage with bone matrix and calcify it when the cartilage template is vascularized (D, E). The invasion of blood capillaries causes the formation of secondary ossification centres at the extremities of long bones, and the formation of growth plates occurs at the edges of long bones (F-H). The chondrocytes in growth plates, which are important for bone growth and creation, are organised into separate layers of resting, proliferating, and hypertrophic chondrocytes (Source: https://www.ncbi.nlm.nih.gov/books/NBK10056).

### 2.2.3 Bone Remodeling

When exposed to mechanical pressures or changing metabolic needs, a bone has the capacity to maintain its total bulk and undergo continual remodeling. The process of remodeling entails the removal of old bone and the formation of new bone through the coordinated action of osteoclasts and osteoblasts, respectively. Bone loss (osteoporosis) or excess bone buildup (osteopetrosis) are both caused by disruptions in remodeling. Components of the canonical Wnt signalling pathway are required for appropriate coupling of osteoblastic and osteoclastic activity (Issack *et al.,* 2008; Karner *et al.,* 2017).

Several cytokines, growth factors, and intercellular signals, such as Wingless/Integrated (Wnt), Sonic hedgehog (SHH), Indian hedgehog (IHH), Notch, and TGF-, tightly regulate skeletal patterning, condensation and differentiation of mesenchymal stem cells into chondrocytes, osteoblasts, and osteoclasts, and bone and cartilage growth and remodelling. Inherited skeletal conditions are caused by genetic differences in cytokines and growth factors (Lefebvre and Bhattaram, 2010; Long and Ornitz, 2013).

## 2.3 Genes Involved in Skeletal Dysplasias

Skeletal development processes and pathways are under specific and complex genetic control, and abnormalities of these pathways give rise to the various skeletal dysplasias. Various transcription factors, growth factors, and hormones are involved in the pathways of skeletal formation, growth and development. Skeletal anomalies may arise as a result of defects in any of the steps of skeletal development or growth (Karsenty and Wagner, 2002).

*HOX* genes, *IHH*, *COL2A1, FGFR3,* and *COL10A1* are some of the well-known transcription factors that are known to be a key player in bone development. Homeobox genes (*HOXA11*, *HOXA13* and *HOXD13*) guide the patterning of the appendicular skeleton (McGinnis & Krumlauf, 1992). Fetal cartilage formation is initiated by *SOX5*, *SOX6* and *SOX9*. *RUNX2* expressed by chondrocytes induces hypertrophy of chondrocytes and bone calcification (Long & Ornitz, 2013). *COL10A1*and osterix (*OSX*) also have a vital role to play in these processes. *ATF4* (activating transcription factor-4) regulates the maturation of osteoblasts (Wang *et al.,* 2009). Endochondral ossification depends on the proper activity of these growth factors, their receptors, cell matrix proteins and other associated genes. (Lefebvre & Bhattaram, 2010; de Crombrugghe *et al.*, 2001).

*SOX9* is a key regulator of chondrocyte differentiation from condensed cells. The Indian hedgehog (*IHH*), a hedgehog family member positively regulates chondrocyte proliferation (Bitgood and McMahon, 1995). It also controls the expression of parathyroid hormone–related peptide (PTHrP) in perichondrial cells. When the PTHrP/IHH pathway is disturbed, it produces a variety of skeletal abnormalities (Vortkamp *et al.*, 1996; Chen *et al.*, 2008).

The FGF pathway was one of the first to be linked to skeletal dysplasias. It is made up of 22 FGFs which signal via four FGF receptors. Components of the FGF pathway play key roles in suture closure in the skull and in limb development (Du *et al.,* 2012).

Fibroblast growth factors play vital functions in the entire process of skeletogenesis (De Crombrugghe *et al.*, 2001). Upon ligand binding, *FGFR3*activates the Stat1 transcription factor and the MAPK pathway, inhibiting chondrocyte proliferation and speeding up hypertrophy (Ornitz, 2005). Wnt, retinoic acid, TGF beta and C-type natriuretic peptide (CNP) all are key regulators of the growth plate before and after birth (Adams *et al.,* 2007; Mackie *et al.,* 2011). FGF signalling through FGFR1/2 has been shown to modulate the processes of development of osteoblast and formation of bone (Wilkie, 2005). Excess and reduced FGF signalling have been linked to a variety of skeletal diseases. Gain of function mutations in *FGFR3* cause constitutive activation of the protein (Naski *et al.,* 1996), which disrupts cartilage function during the linear formation of bone (Trujillo-Tiebas *et al.*, 2009). Achondroplasia (ACH; MIM 100800) is the most common form of dwarfism associated with excessive FGF signaling, as well as other related diseases (Hurst *et al.*, 2005).

## 2.4 Kinds of Skeletal Dysplasia in this Study

Rare skeletal dysplasias and underlying genetic causes diagnosed in the families recruited for this study are presented below.

### 2.4.1 Horizontal Gaze Palsy with Progressive Scoliosis 2 caused by *DCC* Mutations

Homozygous loss-of-function mutations in the axon guidance receptor *DCC* gene cause horizontal gaze palsy with progressive scoliosis (HGPPS-2), also known as developmental-split brain syndrome (DSBS) (OMIM 617542). Jamuar *et al.* (2017) were the first to describe it as a new syndrome. They reported two different homozygous intragenic deletions in the *DCC* gene in three HGPPS2 patients from two unrelated families. Premature termination and functional null alleles were the outcome of both mutations. (Jamuar *et al.*, 2017; Marsh *et al.*, 2017)

The absence of cerebral commissures, hypoplasia of the pons and midbrain, butterfly-shaped medulla, horizontal gaze palsy, and progressive kyphoscoliosis since childhood are the major hallmarks of HGPPS-2. Restrictive lung disease can develop in certain persons with severe scoliosis. This may necessitate spine surgery. Walking and talking are common developmental milestones that are delayed, and intellectual development might be abnormal. Mirror movements are also possible. The gait may be uneven, but it is not abnormal (Jamuar *et al.*, 2017; Zaka *et al.*, 2020). Only two *DCC* gene variants have been found worldwide in HGPPS-2 patients so far (Jamuar *et al.*, 2017).

The netrin-1 receptor protein is encoded by the *DCC* (deleted in colorectal cancer) gene. It belongs to the immunoglobulin superfamily of cell adhesion molecules and is a single-pass transmembrane glycoprotein (Keino-Masu, *et al.,* 1996). Originally, the *DCC* gene was assumed to serve as a tumour suppressor. The activity of *DCC* as a tumour suppressor is still debated because it has yet to be confirmed in vivo (Fearon *et al.,* 1990; Llambi *et al.,* 2001; Williams *et al.,* 2006; Bin *et al.,* 2015). *DCC,* on the other hand, has been proven to play a role in the development of the central nervous system (Keino-Masu *et al.,* 1996; Fazeli *et al.,* 1997; Srour *et al.,* 2009; Jamuar *et al.,* 2017; Marsh *et al.,* 2017).

Congenital mirror motions and/or corpus callosum agenesis have previously been linked to heterozygous truncating variations in the *DCC* gene (Marsh *et al.,* 2017; Bierhals *et al.,* 2018; Vosberg, *et al.,* 2019). Patients with HGPPS-2 (OMIM 617542), a "split-brain" condition characterised by the absence of cerebral commissures and clinical characteristics of scoliosis, horizontal gaze palsy, and intellectual development, have biallelic loss of function mutations in the *DCC*. It is similar to the HGPPS phenotype generated by a recessive *ROBO2* mutation (Jamuar *et al.,* 2017; Marsh *et al.,* 2018).

Two boys and an unrelated girl were characterised by Jamuar et al. (2017) as having the same phenotype of developmental delays, intellectual disability, horizontal gaze palsy, and early-onset progressive scoliosis. They were all born into consanguineous Mexican and Arabian families. Brain imaging revealed the following conditions: agenesis of the corpus callosum (ACC), absence of the anterior and hippocampal commissures, hypoplasia of the pons and midbrain, and a butterfly-shaped medulla caused by a midline cleft through the brain. Mirror movements were absent in the parents of the affected patients, implying variable or insufficient penetrance (Jamuar *et al.,* 2017).

### 2.4.2 Ellis van-Creveld Syndrome caused by *EVC* Mutations

Ellis-van Creveld syndrome (OMIM #225500) is an autosomal recessive chondroectodermal dysplasia with skeletal and extraskeletal characteristics, including ectodermal and congenital cardiac abnormalities. Short ribs and limbs (chondrodystrophy), dysplastic teeth and nails (ectodermal dysplasia), and postaxial polydactyly are all common symptoms. In 60 percent of people, congenital heart abnormalities or circulatory anomalies are discovered. (Nguyen *et al.,* 2016). Pérez-Andreu *et al.* 2015 estimated that 50 percent of those affected die in infancy due to cardiorespiratory issues.

The most common cause of this condition is mutations in the *EVC* and *EVC2* genes (Tompson *et al.,* 2007). The bulk of the mutations create a premature termination codon, which is likely to result in protein truncation and loss of function. (Aziz *et al.*, 2016; D'Asdia *et al.*, 2013).

EvC syndrome is a very rare condition, with only about 300 instances reported worldwide. Although the actual prevalence of the illness is unknown, it is expected to affect seven out of every million people (Al-Fardan & Al-Qattan, 2017). The Amish group has reported the majority of the instances (Baujat & Le Merrer, 2007). Even within the same family and with the same mutation, there has been significant heterogeneity in the severity and illness characteristics. It is well recognised that not every patient with EvC syndrome exhibits all of the symptoms. The existence or absence of a cardiac abnormality, as well as polydactyly of the feet, are common distinctions among patients. Syndactyly has been documented as well (Ibarra-Ramirez *et al.*, 2017; Rao *et al.*, 2017). Clinical and skeletal radiography examinations are frequently used to make the final diagnosis.

*EVC* is a 992 amino acid protein that is encoded by a 103 kb region on chr4p16.2. The *EVC* gene product is involved in skeletogenesis, as well as control and differentiation signalling between ectodermal and mesodermal derivatives (Caparrós-Martin *et al.*, 2013; Valencia *et al.*, 2009). It has also been linked to cardiogenesis (Liu *et al.*, 2018; Ruiz Perez & Goodship, 2009).

*EVC* and *EVC2* proteins are both essential for maintaining normal levels, according to knockout animal models. Both proteins form a complex that binds to primary cilia and influences the Hedgehog signalling pathway in a favourable way (Caparros-Martin *et al.*, 2013, Louie *et al.*, 2020). An abnormal response to Hedgehog signalling has been shown to cause chondrodysplasias in cell cultures and animal models (Louie *et al.*, 2020).

### 2.4.3 3M Syndrome caused by *CUL7* Mutations

3M syndrome (OMIM 273750) is a rare autosomal recessive syndrome that presents with characteristic features of intrauterine and postnatal growth retardation, facial dysmorphism, skeletal abnormalities and normal intelligence (Miller *et al*., 1975, van der Wal *et al*., 2001; Temtamy *et al*., 2006). 3M syndrome has multigenic, autosomal recessive inheritance pattern. Mutations in Cullin 7 (*CUL7*), coiled-coil domain-containing protein 8 (*CCDC8*) and obscurin-like 1 (*OBSL1*) are known to cause 3M syndrome (Huber *et al*., 2005; Hanson *et al*., 2009).

3M syndrome is characterized by low birth weight, severely retarded postnatal growth, and short stature. The affected individual has very distinctive facial features, including a triangular shaped face, fleshy tipped nose, anteverted nares, midface hypoplasia, dolichocephaly, full lips, prominent ears, pointed chin and frontal bossing. These features are more prominent in childhood, and become less pronounced in adults, which makes 3M Syndrome more difficult to diagnose in adults (van der Waal *et al.*, 2001; Temtamy *et al.*, 2006).

Radiological abnormalities are variable and also tend to become less pronounced with age. Reported anomalies include slender long bones, tall vertebral bodies, short thorax and hypoplastic ribs. Abnormalities of the bone are found to be less common in 3M syndrome in patients with *CUL7* mutations, as compared to patients with *OBSL1* and *CCDC8* mutations (Maksimova *et al.*, 2007).

As opposed to most other genetic growth disorders, intelligence of 3M syndrome patients remains normal. There is no reported delay in developmental milestones either. In some cases, in utero deaths of affected fetuses have also been reported (Huber *et al.*, 2009).

Mutations in the *CUL7* gene (MIM 609577) have been reported as the causative factor in more than three-quarters of 3M syndrome patients (Huber *et al.*, 2005). The *CUL7* gene encodes the cullin-7 protein. This protein plays an important role in the ubiquitin-proteasome system, as it regulates the assembly of the E3 ubiquitin ligase complex that tags proteins for ubiquitination (Sarikas *et al.*, 2008). *CUL7* has been found to be necessary for growth and development, including chondrogenesis, endochondral ossification, and lung development. (Tsutsumi *et al.*, 2008).

### 2.4.4 Spondylocarpotarsal Synostosis caused by *FLNB* Mutations

Spondylocarpotarsal synostosis syndrome (SCT) (OMIM #272460), commonly known as congenital synspondylism, is a skeletal abnormality marked by postnatal disproportionate short height, scoliosis and lordosis, carpal and tarsal synostosis, and vertebral fusions (Langer *et al.,* 1975; Krakow *et al.,* 2004).

In 1975, Langer *et al.* coined the term spondylocarpotarsal synostosis syndrome to describe the most common radiological and clinical characteristics of the disorder. The lunate–triquetrum and capitates-hamate bones are generally involved in carpal synostosis, and tarsal coalitions can cause club feet. Joint laxity, cervical spine instability, cleft palate, mixed hearing loss, pes planus, dental malformations, enamel hypoplasia, and facial dysmorphism are some of the other symptoms of this condition (Krakow *et al.,* 2004).

The filamins A, B, and C are involved in several important processes, including cell division and motility. They also provide cell structure, enable signal transduction and facilitate the transport of tiny solutes into and out of the cell (Yang *et al.,* 2017).

Krakow *et al.,* (2004) discovered that SCT patients in four unrelated spondylocarpotarsal synostosis (SCT) families had nonsense mutations in the FLNB gene, either in the homozygous or compound heterozygous state. The premature stop codons were all found within Filamin B repeat domain, hence, Krakow *et al.,* (2004) reported that SCT is caused by Filamin B truncation or absence. Flnb -/- mice were found to have phenotypic similarities to people with SCT, including short height and skeletal deformities (Farrington-Rock *et al.,* 2008).

Short height, scoliosis, block vertebrae, symphalangism, and tarsal synostosis were all signs of SCT in a 45-year-old Pakistani male, according to Assir & Wasim (2012), who presented the first case from Pakistan. In this investigation, however, no genetic data was available. Yasin *et al.* (2021) identified the first novel *FLNB* homozygous pathogenic variant in the Pakistani population.

### 2.4.5 Otopalatodigital syndrome 2 caused by *FLNA* Mutations

Otopalatodigital syndrome-2 (OPD) (OMIM #304120) is one of four congenital otopalatodigital syndromes. The phenotypic range of syndromes also includes frontometaphyseal dysplasia (FMD1; OMIM #305620), otopalatodigital syndrome-1 (OPD1; OMIM #311300), and Melnick-Needles syndrome (MNS; OMIM #309350).

Infants diagnosed with OPD2 have been reported to have characteristic facial dysmorphism, including hypertelorism, downslanting palpebral fissures, midfacial hypoplasia, microstomia, micrognathia, malformed and/or apparently low-set ears, and midfacial hypoplasia. Malformations of the central nervous system, heart (congenital heart abnormalities), gut, and genitourinary system are examples of extraskeletal malformations. From normal to modest intellectual disability, psychomotor development differs (Robertson *et al.,* 2003).

Brewster *et al.* (1985) reported two infants, a baby boy and his maternal uncle, with lethal skeletal dysplasia, manifesting as midface hypoplasia, downward-slanting palpebral fissures, cleft palate, a tiny thorax, and bowed limbs with nonexistent fibulae. Clinical, radiologic, and histologic data suggested that deficient intramembranous ossification is a major anomaly in OPD type II, according to Ogata *et al.,* (1990). Johnson *et al.,* (2008) described a brother and sister with OPD2 who had tracheomalacia and needed a tracheostomy to ease lower airway blockage.

It has been reported that OPD2 has an X-linked dominant inheritance pattern, and is caused by gain of function mutations in the gene *FLNA* (Xq28), which encodes filamin A (Robertson *et al.,*2003).

Robertson *et al.,* (2003) described *FLNA* mutations that lead to a spectrum of X-linked syndromes: otopalatodigital syndrome types I and II (OPD1 and OPD2), frontometaphyseal dysplasia (FMD1), and Melnick-Needles syndrome (MNS). All mutations were present in the actin-binding domain and repeat domains 3, 10, 14 and 15 of the gene.

Stefanova *et al.,* (2005) discovered heterozygosity for a deletion in the *FLNA* in 6 afflicted girls from a 4-generation pedigree with cranial hyperostosis and numerous skeletal deformities. Male offspring in this family died young as a result of the condition. Females' phenotypic were varied and modest, bridging the phenotypes of multiple OPD spectrum disorders. Zenker *et al.* (2006) proposed that X-inactivation is a major epigenetic regulator of the phenotype in females with FLNA-related skeletal dysplasias.

*FLNA* has 48 exons comprising 26 kb of genomic sequence and a 7.9-kb open reading frame (Fox *et al.,* 1998). Filamin A is encoded by this gene. Filamin A is a 280-kD actin-binding protein that regulates actin cytoskeleton rearrangement by interacting with integrins, second messengers and transmembrane proteins. By forming orthogonal networks of crosslinked actin filaments in the cytoplasm, filaments join membrane proteins to the actin cytoskeleton. Controlling cell shape and migration requires the remodelling of the cytoskeleton. (Maestrini *et al.,* 1993; Fox *et al.,* 1998).

### 2.4.6 Spondylocostal Dyostosis 1 caused by *DLL3* Mutations

Spondylocostal dysostosis 1 (OMIM # 277300) is a disorder in which the bones of the spine and ribs are malformed. Fusion of the vertebrae, hemivertebrae, and rib fusion with other rib abnormalities are the most common skeletal deformities. A natural consequence of these anomalies is a deformity of the chest and spine (severe scoliosis, kyphoscoliosis, and lordosis), which results in dwarfism (Mortier *et al.,* 1996).

In most cases, autosomal recessive spondylocostal dysostosis is detected in the neonatal era. This disorder causes infants' chests to be too tiny to expand properly, resulting in life-threatening breathing issues. Early-life breathing issues can be fatal; nevertheless, some people with breathing problems live into adulthood (Turnpenny *et al.,* 1999).

This syndrome was first documented in two siblings by Jarcho and Levin (1938). Castroviejo *et al.* (1973) described three Spanish sisters with spondylothoracic dysplasia. They had a small thorax, a short neck with limited mobility, winged scapulae, and scoliosis or kyphoscoliosis. There were rib anomalies in both form and quantity.

Turnpenny *et al.* (1999) used homozygosity mapping to do genome-wide scanning in families with autosomal recessive spondylocostal dysostosis. A significant connection to 19q13 was discovered. To assess human *DLL3* as a potential gene, Bulman *et al.* (2000) cloned and sequenced it. Mutations were discovered in three autosomal recessive spondylocostal dyostosis families. These were the first alterations in a human delta homolog, emphasising the importance of the Notch signalling system and its components in mammalian axial skeleton patterning.

Notch signalling is involved in somite segmentation, which is the process of separating future vertebrae and ribs from one another during early development. Somite segmentation is interrupted when the Notch signalling system is disrupted, leading in the deformity and fusion of the spine and ribs seen in spondylocostal dysostosis. *DLL3* (19q13.2), *MESP2* (15q26.1), *LFNG* (7p22.3), and *HES7* (17p13.1) are the four genes found so far that are all implicated in the Notch signalling pathway. Spondylocostal dysostosis is caused by mutations in these genes in about 25% of cases. Additional genes implicated in the Notch signalling system may possibly be linked to the disease (Penton *et al.,* 2012)

The *DLL3* gene codes for the DLL3 (delta-like 3) protein, which aids in the modulation of the Notch pathway, which is critical for the proper formation of vertebrae during embryonic development. During early development, the DLL3 protein and the Notch pathway are implicated in somite segmentation. Although the exact mechanism of somite segmentation is unknown, it appears to be dependent on the activity of multiple Notch pathway proteins, including the NOTCH1 protein, being turned on and off in a certain rhythm (Saga *et al.,* 2001). The DLL3 protein binds to the inactive NOTCH1 protein and either sequesters it or marks it for degradation, preventing it from being activated (Bulman *et al.,* 2000).

### 2.4.7 Polydactyly caused by *LMBR1* Mutations

Polydactyly is one of the dysostoses recognized by extra digit in upper and/or lower limbs (Malik, 2014). The disorder may be unilateral or bilateral, symmetrical or asymmetrical. On the basis of digit being affected, polydactyly is divided into preaxial polydactyly (PPD; extra digit located on thumb side), mesoaxial polydactyly (duplication of middle digits 2-4) and postaxial polydactyly (PAP; when extra digit locates on the little finger side) (Malik, 2014; Umair *et al.*, 2017b). Postaxial polydactyly is subdivided into PAP type A (PAPA; if the extra digit is well-developed) and type B (PAPB; when the digit is rudimentary). A very rare type of polydactyly is mirror-image polydactyly characterized by mirror-image duplication of digits. Polydactyly segregates as autosomal dominant as well as autosomal recessive entity.

Pre-axial polydactyly segregates in autosomal dominant form and is caused by heterozygous variants in *GLI3* and *ZRS/SHH* (Radhakrishna *et al.,* 1999; Lettice *et al.,* 2003; Wieczorek *et al.,* 2010). Five genes (*ZNF141*, *IQCE*, *ZRS/SHH*, *GLI3*, *GLI1*), and three other loci (13q21-32, 13q13.3-21.2, 19p13.1-13.2) have been associated with nonsyndromic post-axial polydactyly (Radhakrishna *et al.,* 1999; Zhao *et al.,* 2002; Wieczorek *et al.,* 2010; Umm-e-Kalsoom *et al.,* 2012, 2013; Umair *et al.,* 2017b; Palencia-Campos *et al.,* 2017).

*LMBR1* gene, located on 7q36.3, encodes for LMBR1 protein (limb development membrane protein 1). Another member of the same protein family as LMBR1 is known to be to be a lipocalin transmembrane receptor. Within an intron of this gene is a highly conserved, cis-acting regulatory module for the sonic hedgehog gene. Therefore, interruption of this genic area can change the expression of Sonic Hedgehog and impact limb patterning, although it is unknown if this gene has a direct role in limb development (Xu *et al.,* 2020).

According to Clark *et al.* (2000), Lmbr1 expression had an impact on the growing limbs of Hemimelic extra toes (Hx) mice. The Hx mutation results in preaxial polydactyly, hemimelia of the radius and tibia, on both forelimbs and hindlimbs (Knudsen and Kochhar, 1981). Acheiropody, characterized by hand and feet aplasia and bilateral congenital amputations of the upper and lower extremities is also linked to chromosome 7q36. Based on the genomic location of the gene and the phenotypic of Hx mice, LMBR1 could be a candidate for acheiropody. (Escemilla *et al.,* 2000).

Lettice *et al.* (2003) discovered that point mutations in a Sonic hedgehog (SHH) regulatory region on chromosome 7q36 cause preaxial polydactyly II. In mice models of PPD, SHH is expressed in an extra ectopic position at the anterior border, where it is normally expressed in the zone of polarising activity (ZPA) posteriorly in the limb bud. Lettice *et al.* (2003) discovered an enhancer element in the ZPA that drives normal *SHH* expression. The ZPA regulatory sequence (ZRS) is found inside intron 5 of the *LMBR1* gene, 1 Mb from the target gene *SHH*. In three independent families with PPD2 and one family with tibial hypoplasia with polydactyly, as well as in the Hx mouse mutant, the ZRS included point mutations that segregated with polydactyly (Lettice *et al.,* 2003).

Gurnett *et al.* (2007) investigated four families with triphalangeal thumbs and preaxial polydactyly, finding a mutation near the 5-prime end of the *LMBR1* ZRS in two families and a mutation in the ZRS in one. In a three-generation consanguineous Turkish kindred, Semerci *et al.* (2009) discovered a heterozygous mutation in the ZRS region of the *LMBR1* gene linked to isolated triphalangeal thumb-preaxial polydactyly syndrome.

### 2.4.8 Achondroplasia caused by *FGFR3* Mutations

The most prevalent primary skeletal dysplasia in humans is achondroplasia, a rare genetic condition. More than 90% of cases of disproportionately small height, popularly known as dwarfism, are caused by this type of dysplasia. (Vajo *et al.,* 2000). Every year, around 1: 20,000-30,000 cases are reported worldwide in newborns (Waller *et al*., 2008).

Achondroplasia follows an autosomal dominant inheritance pattern. Advanced paternal age is a recognised risk factor, and more than 80% of instances result from a spontaneous mutation. The phenotype can be recognised on prenatal ultrasonography, and by newborn examination since it clearly differs from other skeletal dysplasias. (Orioli *et al.*, 1995; Barbosa-Buck *et al.*, 2012).

Macrocephaly, frontal bossing, midface hypoplasia, short limbs, brachydactyly and genu varum are among the physical phenotypic characteristics (Pauli, 2019).

Early mortality, issues with the otolaryngology later in childhood, and an increased risk of obesity into adulthood are all linked to achondroplasia. Spinal stenosis, joint laxity, and thoracolumbar kyphosis may also appear in those who are affected (Schkrohowsky *et al.*, 2007).

During embryogenesis, the *FGFR3* gene acts as a negative modulator of skeletal growth and regulates endochondral ossification (Xue *et al.*, 2014). Achondroplasia was first related to dominant mutations in this gene (Shiang *et al.*, 1994; Unger *et al.*, 2017). Hypochondroplasia (HCH; OMIM 146000) and thanatophoric dysplasia (TD; OMIM 187600) types I (TDI) and II (TDII) were later linked to mutations in *FGFR3* gene. De novo mutations account for the majority of these autosomal dominant mutations. Wilkin *et al.* (1998) also discovered that the achondroplasia mutation G380R is only found in the paternal allele.

Achondroplasia (ACH), thanatophoric dysplasia types I and II (TD1 and TD2), and hypochondroplasia (HCH) are all autosomal dominant human skeletal abnormalities linked to point mutations in different regions of the *FGFR3* gene. It is believed that point mutations linked to these diseases result in constitutively activated FGFR3, which autophosphorylates in the absence of ligand and is no longer regulated by FGF binding (Harada *et al.*, 2009; Foldynova-Trantirkova *et al.*, 2012).

Skeletal dysplasias caused by *FGFR3* gene mutations have a wide phenotypic range. The severity ranges from moderate forms like HCH to deadly forms like TDI or TDII (Harada *et al.,* 2009; Xue *et al.,* 2014). Clinical diagnosis can be challenging in some cases due to phenotypic overlap, hence testing for the mutations underlying the condition is important (Almeida *et al.*, 2009; Xue *et al.*, 2014).

## 2.5 Skeletal Disorders in Pakistani Population

Cousin marriages are prevalent in the Pakistani society. Rare recessive genetic variants continue to accumulate and the rare phenotypes manifest as a result of increased incidence of consanguinity (>60 percent) (Hussain & Bittles, 1998). As a result, recessive diseases are more prevalent in this population.

In Pakistan, several investigations on the genetics of skeletal dysplasia have been undertaken. The first study looked at a large cohort of people living in two villages of Sindh. In many consanguineous marriages, dwarfism affected multiple individuals. A biallelic variation in *GHRHR* was discovered after molecular characterisation using linkage analysis and sequencing (Baumann & Maheshwari, 1997).

Genetic skeletal disorders are a diverse, rare, and distinct group of rare bone growth abnormalities that result in aberrant skeleton size and shape. In Pakistan, the prevalence, mutation spectrum, and regional distribution of genetic skeletal illnesses remain unknown. There have been no reports of disorders from any of the 19 groups listed in the "Nosology and Classification of Genetic Skeletal Disorders (2015 Revision)" from the Pakistani population. Next-generation sequencing technologies were used to identify mutations in the majority of instances (Umair *et al.,* 2019).

Variants in different genes have been discovered as the cause of several kinds of skeletal dysplasia in Pakistani patients with various inheritance patterns. Acromesomelic dysplasia (AMDM, AMDG, AMDH), Polydactyly, Mucopolysaccharidosis, Split hand/Split foot malformation (SHFM), and synpolydacyly are the most commonly documented skeletal abnormalities in Pakistan, accounting for 55.04 percent of all cases. The most common skeletal dysplasias are acromesomelic dysplasias (Maroteaux type, Grebe type and Hunter-Thompson type) (Mumtaz *et al.*, 2015; Ullah *et al.*, 2018; Umair *et al.*, 2015; Umair *et al.*, 2019).

Global genetic studies on inherited skeletal dysplasias are needed to better comprehend the genetic factors underlying the diverse kinds of dwarfism and its phenotypic expression. Due to the high number of consanguineous marriages and hence the odds of identifying appropriate families, the Pakistani population holds a lot of potential for genetic studies of recessive hereditary illnesses. Because many skeletal dysplasia syndromes have no known genetic etiology, the search for new genetic variants continues (Costantini *et al.*, 2021; Tang *et al.*, 2021).

# MATERIALS AND METHODS

The research work was approved by the Ethical Review Committee at International Islamic University, Islamabad. The workflow is illustrated in Figure 3.1.

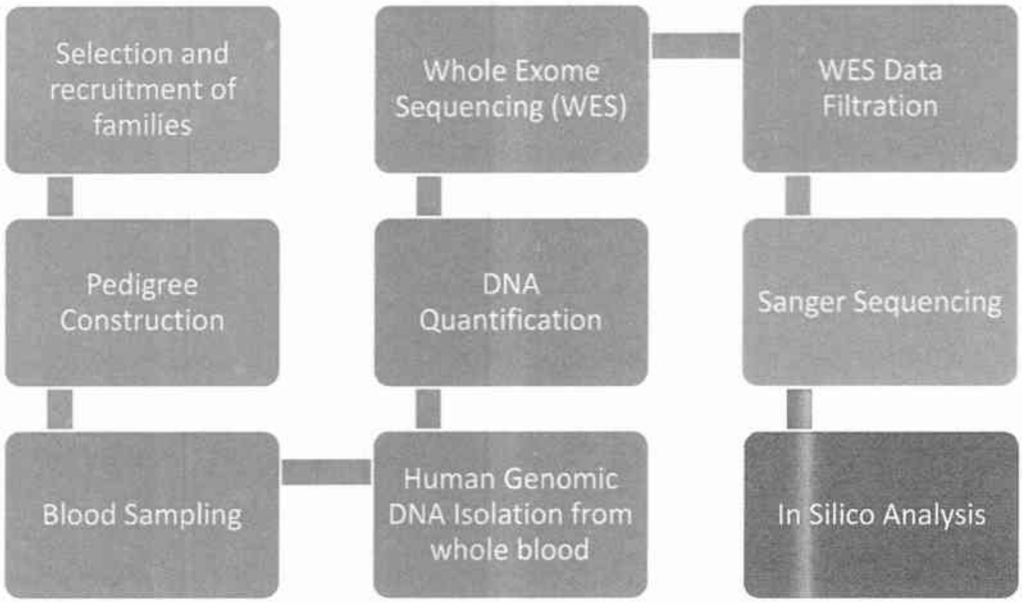


**Figure 3.1 Workflow showing the different steps carried out in the study**

## 3.1 Selection and Recruitment of Families

Eight consanguineous Pakistani families, with multiple members affected with skeletal dysplasia, were selected from different areas of Pakistan, including Punjab, Sindh, KPK and Azad Kashmir. All the family members taking part in the research project provided written informed consent for genetic/molecular analysis in accordance with the Helsinki Declaration (Carlson *et al.,* 2004).

## 3.2 Pedigree Construction

Pedigrees were created using the method outlined by Bennett *et al.,* (2008) based on the information provided by knowledgeable elder members of all the families included in the study.

In the pedigree, squares represent males and circles represent females. Unfilled shapes are used for normal individuals, and filled shapes for affected individuals. Crossed diagonal symbols are used to identify deceased people. Arabic numbers are used to identify people within a generation. Roman numerals represent different generations. Marriage is represented by the horizontal line, consanguinity by the double marriage line, and offspring by the vertical line. The line traced horizontally from the line of descent was known as the sibship line. Clinical information, images, radiographs, and thorough medical histories were gathered from all the affected members of the study's participating families at local government hospitals and private clinics.

## 3.3 Blood Sampling

Blood samples were collected from all the available family members, including both affected and unaffected members. The collected blood samples were stored in EDTA-coated vacutainer tubes at 4°C at the Genomics Research Lab (GRL), Department of Biological Sciences, International Islamic University, Islamabad. Later, DNA was extracted from them.

## 3.4 Genomic DNA (gDNA) Extraction from Blood

Phenol-chloroform method was used to extract DNA. This is considered the standard protocol for extraction of genomic DNA extraction (Sambrook *et al.*, 1989). Commercial kit method was also used to extract DNA from available blood samples.

### 3.4.1 DNA Extraction using Phenol-Chloroform Method

From the vacutainer tube, 0.75 ml of blood was taken in an Eppendorf tube. 0.75 ml of solution A (0.32 M Sucrose, 10 mM Tris pH 7.5, 5 mM $MgCl_2$, and 1%

(v/v) Triton X-100) was added to it and mixed. The tube was centrifuged at 13,000 rpm for 60 seconds. A dense pellet was obtained after discarding the supernatant. The pellet was resuspended in 400 ul of solution A, and was centrifuged at 13,000 rpm for 60 seconds again. Supernatant was again discarded to obtain the nuclear pellet. This pellet was resuspended in 400 ul of solution B (10 mM Tris pH 7.5, 400 mM NaCl, 2 mM EDTA pH 8.0). 12 ul of 20% sodium dodecyl sulphate (SDS), and 5 ul of proteinase K were also added to the Eppendorf tube.

The tube was then incubated at 37°C for 24 hours. 0.5 ml of a freshly prepared mixture of equal volumes of solution C (400 ul phenol and 10 mM Tris) and solution D (Chloroform and isoamyl alcohol; 24:1) were then added to it. The sample was centrifuged at 13,000 rpm for 10 minutes to obtain a distinct separation of layer. The upper aqueous layer was quantified and transferred to a new tube. Equal volume of solution D was added to it.

The tube was then centrifuged for a further 10 minutes at 13,000 rpm, and upper aqueous layer was again quantified and collected in a separate Eppendorf tube. Equal volume of chilled isopropanol (at -20°C) and 55 ul of 3 M sodium acetate (pH 6) were added to it. The DNA was then precipitated by repeatedly inverting the tube. 200 ul of chilled 70% ethanol was used to wash the DNA pellet. The tube was once more centrifuged for 7 minutes at 13,000 rpm. The tube was then dried for 10 minutes at 45°C in a drying oven. The DNA was dissolved in an appropriate volume (150–200 ul) of Tris-EDTA (TE) buffer. The sample was incubated in an incubator at 37°C for 24 hours.

### 3.4.2 DNA Extraction using Kit Method

Blood was kept in an EDTA tube at room temperature for 18 to 20 minutes. Lysis solution C (200 l; GenEluteTM Sigma Aldrich MO, USA), proteinase K solution (20 ul; 16.8UI), and blood (200ul) were thoroughly vortexed for 10–25 seconds and incubated for 15 minutes at 55–60 °C in a 1.5 ml micro-centrifuge tube (Axygen Inc., CA, USA). The addition of 220u l of 100% ethanol (BDH, England) was then followed by a 15–25 second vortex.

Each Gene Elute Miniprep Binding Column received 500 ul of Column Preparation Solution (CPS), which was then centrifuged for one minute at 10,000 rpm and the supernatant was discarded. After transferring the homogenised mixture from the incubation step to the prepared column, centrifugation at a speed of 12,000 rpm was performed for 2 minutes. The supernatant was discarded. The column was washed twice, once with pre-wash solution (500 ul) and once with wash solution (500 ul). Centrifugation was carried out in both steps for 12 minutes at a speed of 13,000 rpm, and the follow-through was discarded. Elution buffer (EB; 150 ul) was pre-heated to increase the concentration of DNA, and added to the column; centrifugation was then carried out for three minutes at 12,500 rpm, and the extracted DNA was stored at 4 °C.

## 3.5 DNA Quantification

By using a Nanodrop ND-1000 spectrophotometer (Life Technologies, USA) quantification of DNA was carried out at an optical density of 260nm.

## 3.6 Whole Exome Sequencing (WES)

WES was carried out at Lee Kong Chian School of Medicine, Nanyang Technological University, Singapore and at Centre for Inherited Diseases, Taibah University Madinah, Saudi Arabia.

Sonication was used to randomly shear three micrograms of genomic DNA into 100-160 bp fragments (Covaris E220, Woburn, MA, USA). DNA from 1-3 members of each family was analyzed using WES. Using the commercially available Sure Select XT Human All Exon Agilent 50Mb kit, exome enrichment was carried out. Prior to WES, the Bravo automated platform was employed for sample enrichment and preparation. On an Illumina HiSeq- 2500/4000 system, captured DNA fragments were sequenced.

The readings were analysed using Burrows-Wheeler Aligner (BWA) Enrichment application of Base Space. (Illumina Inc. 5200 Illumina Way, San Diego, CA, 92122, USA). In order to accomplish alignment, Burrows-Wheeler Aligner (BWA) was used, and Genome Analysis Toolkit (GATK) was utilised to call the variants (Li & Durbin, 2009). The entire set of called variants was annotated using Illumina Variant Studio v2.2. GRCh37 (Genome Reference Consortium Human Build 37) was used for data analysis.

### 3.6.1 Filtration of WES Data

Exome sequencing data was filtered for non-synonymous, homozygous variants if the disease's mode of heredity was predicted to be autosomal recessive, and non-synonymous, heterozygous variants if the disease's mode of inheritance was predicted to be autosomal dominant. Variants were further filtered by searching through online databases of genetic variations in humans (gnomAD, 1000 Genome, dbSNP, ExAc). Only variants with a frequency less than 0.01 were taken into consideration. To further shortlist pathogenic variants, Mutation Taster (Schwarz *et al.,* 2014), Polyphen2 (Adzhubei *et al.,* 2010) and SIFT (Sim *et al.,* 2012) were utilized.

Following validation of the pathogenicity of variants and their detrimental impact on the structure and function of proteins using PolyPhen-2, Mutation Taster, and SIFT, literature review was conducted to shortlist the variants that seemed to be related closely to the clinical phenotype observed in the affected individuals. The filters applied are shown in Figure 3.2.

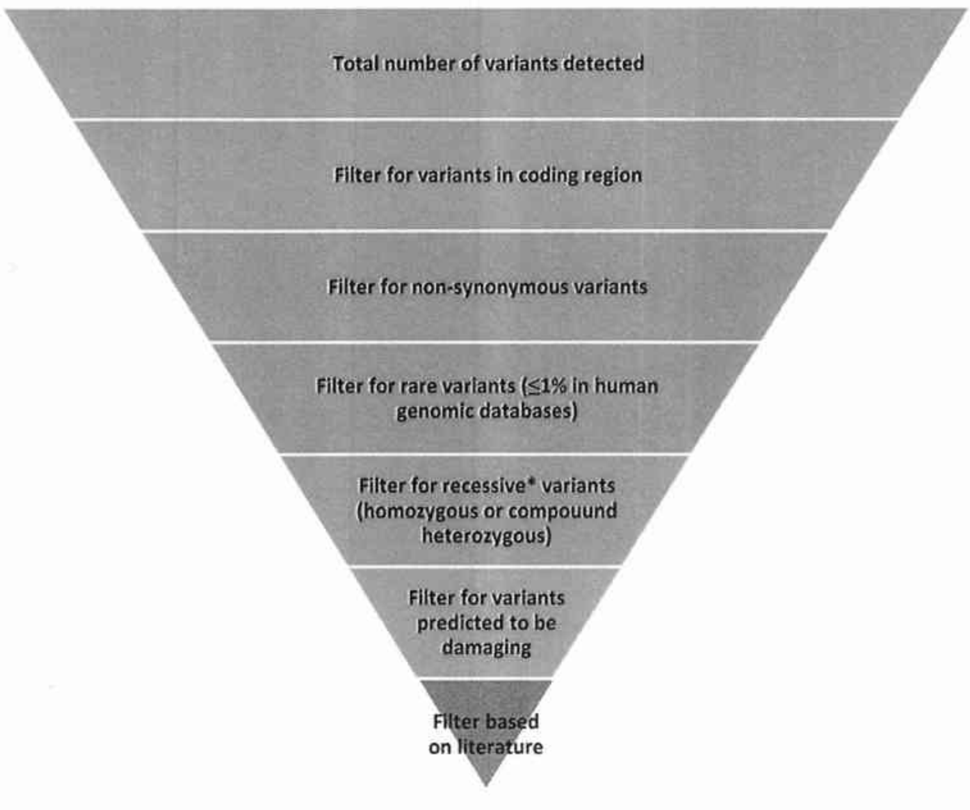


**Figure 3.2 Workflow showing the different filtration steps carried out during WES Data Filtration**

* For autosomal dominant variants, filtration for heterozygous variants is performed.

## 3.7 Sanger Sequencing

Primers were designed, exons of interest were amplified through PCR, and Sanger sequenced to validate segregation of the variant in all affected and unaffected members of the family.

### 3.7.1 Primer Design

Primers for the genes of interest were designed to validate correct segregation of the shortlisted deleterious variants in affected and unaffected family members. Primers were designed online using the Primer-3 software. Primer sequences are listed in Table 3.1.

**Table 3.1 List of primers used for candidate gene amplifications**

| Gene | Exon | Forward Primer | Reverse Primer |
|---|---|---|---|
| *CUL7* | 24 | 5'-GAGAGTCTGCTGGCGTTCTC-3' | 5'-ATCCTTTTGCTCGTGAAGGT-3' |
| *FLNA* | 3 | 5'-GGAACCTGAAGCTGATCCTG-3' | 5'-GGCACAGCTGTCCACCAG-3' |
| *DLL3* | 7 | 5'-ACTTCTCCGGCCTCGTCT-3' | 5'-TCCTGCGTCCTTAGGTTGTT-3' |
| *FLNB* | 21 | 5'-CCAAAGGAGCTGGTACTGGA-3' | 5'-TGAAGGGAGACCCAGGTATG-3' |
| *EVC* | 6 | 5'-AGCAAAAGACAAAAATACCATTGA-3' | 5'-TTTAAGTTACCTTGAAACATAGGTTGA-3' |
| *DCC* | 16 | 5'-CCACTGCCACTTTCCTTTCT-3' | 5'-GCATGCATATGTGTGCAAGTA-3' |
| *LMBR1* | 14 | 5'-TGATTTGCTTTTCTATGGGCCT-3' | 5'-AACAAGCTCTGCAGTTCTCC-3' |
| *FGFR3* | 9 | 5'-GAACGTTCAGCCTATCCACA-3' | 5'-AAGTTCTCGGCAGTCTCCAA-3' |

### 3.7.2 Polymerase Chain Reaction

#### 3.7.2.1 First Sequencing PCR

100 ng of extracted DNA, 20 pmoles of forward and reverse primer, 200 M dNTPs, 2.5 units of Taq DNA polymerase, and PCR buffer were included in the reaction mixture. Thermal cycling was performed under the following conditions: 95 °C for 5 min, then 40 cycles of 95 °C for 1 min, 53-58 °C for 1 min, 72 °C for 1 min, and finally a 10 min extension at 72 °C. The Palm-Cycler gradient thermal cycler was used to conduct PCR (Corbett Life Science, Australia).

In 0.2 ml PCR tubes, target exons were amplified. 2% agarose gel was prepared to analyze the PCR results. For purification after the first PCR, ThermoScientific GeneJET kit was employed, according to the standard instructions provided by the manufacturer. The purified product was again analyzed on 2% agarose gel.

#### 3.7.2.2 Second Sequencing PCR

Sanger sequencing was carried out in a total volume of 10µl by adding the following components (1µl sequencing buffer, 1-2µl purified PCR product, 3.5µl DTCS quick start kit, 1µl of primer (0.1µM), and 2.5-3.5 µl PCR water).

After thoroughly mixing all of the components, the 10 ul reaction mixture was run on the thermocycler T1 (Biometra, Germany) under the following conditions. A 50-second initial denaturation stage was followed by three steps with 25 amplification cycles: denaturation at 95°C for 12 seconds, annealing at 57 °C for 12 seconds, and extension of the amplified product at 62°C for 4 minutes.

Following a second successful PCR, the POP6 Protocol for ethanol precipitation step was used to achieve a second round of purification.

A fresh stop solution (SS) of 20 mg/ml Glycogen (0.5 ml) and 100 mM $Na_2EDTA$ was added to a fresh Eppendorf tube (2 ml).

Sequencing product was added to it, and it was subsequently centrifuged at 12,500 rpm for 20 minutes.

After discarding the supernatant, 150 μl of 70% ethanol was added to the tubes They were once more centrifuged for 10 minutes at 12,500 rpm. The samples were vacuum dried, while the supernatant was castoff.

The pellet was resuspended in sample loading solution (20 μl SLS) by vortexi ng for 5 to 10 seconds. All of the samples were loaded onto the sample loading t ray. DNA sequencer was used to perform sequencing (Beckman Coulter, CEQ880 0).

### 3.7.3 Analysis of Sanger sequencing data

BioEdit software was used to analyze variants and co-segregation in Sanger sequenced data. Ensembl Gene Sequence view (http://www.ensembl.org/index.html) was used to obtain the reference sequence of the gene of interest. The reference sequence was aligned with Sanger sequencing results in BioEdit software using Clustal W.

## 3.8 In Silico Analysis

The identified variants were analyzed using online pathogenicity prediction tools including SIFT, Mutation Taster, PolyPhen-2, MutPred2, PMut, PhD-SNP, mvPPT, SNAP, Panther, Meta-SNP, LRT, and GERP.

Three dimensional (3D) structure of the wild-type proteins was retrieved from Alpha fold protein structure database (Jumper *et al.,* 2021; Varadi *et al.,* 2022). Mutant structures were developed via Pymol (DeLano,2002) and I-Tasser (Yang &

Zhang, 2015). In order to remove bad contacts from the modelled structures, protein structures were energetically minimized via Chimera 1.14 (Pettersen *et al.,* 2004). Structural evaluation of these energetically minimized models was performed via PROCHECK Ramachandran plots (Laskowski *et al.,* 1993).

In order to have a clear understanding between the difference in structure of wild-type and mutant proteins, structural superimposition was performed via USCF Chimera (Pettersen *et al.,* 2004). PDBsum generate was employed to predict and compare the change in secondary structure elements of wild-type and mutant proteins (Laskowski, 2001).

In order to investigate the effect of mutant proteins on molecular interaction and binding affinity with other interacting proteins, molecular docking of wild-type and mutant proteins were performed via Cluspro web-server (http://cluspro.bu.edu/) (Comeau *et al.,* 2007).For visual depiction, Chimera 1.14 (Pettersen *et al.,* 2004) was employed. LigPlot+ (Laskowski *et al.,* 2011) was utilized to analyze protein-protein interactions and measure distances between interacting amino acids.

# RESULTS

In the present study, eight families were investigated for the underlying causes of prevalent skeletal dysplasias. These families were recruited from their native towns. Family descriptions are given along with the pedigrees, followed by detailed phenotypic, clinical and radiological findings of affected individuals. Results of genetic analysis are given along with the description of biallelic sequence variants resulting in deleterious mutations.

## 4.1 Family 1

Family 1 was collected from District Swabi, KPK Province. It comprised of four affected individuals. One affected individual was deceased at the time of sample collection. Three affected individuals along with their unaffected siblings, parents and relatives participated in the study (Figure 4.1).

### 4.1.1 Clinical Findings

We investigated at a large consanguineous Pakistani family that included three affected members (IV-1, IV-2, and IV-6) who were diagnosed with scoliosis, which was slight at birth and gradually increased over time (Figure 4.2).

The affected individuals had lateral curvature, disproportionate shoulders, unequal hips, and trunk asymmetry in addition to spinal malformation. They reported pain and discomfort in walking, and their gaits were altered. On radiographs, the dorso-lumbar spine was clearly kyphoscoliotic, with convexity to the right side (Figure 4.2). This was linked to early degenerative changes and a generalized reduction in bone density.

IV-1 was a 19-year-old male. He didn't exhibit any obvious developmental delays. He began to walk and speak at the normal age. He was diagnosed with moderate intellectual disability and chronic lung disease. He was diagnosed with horizontal gaze palsy and poor eyesight after an eye exam. There were no mirror movements observed. Individual IV-2 was 17 years old at the time of examination. He started walking at the age of 4 years, but was unable to speak properly. He was assessed to be intellectually normal. Eye examination revealed classic symptoms of horizontal gaze palsy.

Individual IV-6, at the time of the examination, was 9 years old. She met all the developmental milestones and had a normal intellectual capability. She exhibited mild horizontal gaze palsy.

Mirror movements were examined in parents, siblings, and both affected and unaffected children, but were found to be absent. The affected individuals had not undergone any scoliosis surgery or other corrective treatment. Brain MRI tests were performed for the three affected individuals. All three displayed abnormalities such absence of anterior commissure, hypoplasia, and corpus callosum agenesis (Figure 4.2). The four siblings' phenotypic traits are collected in Table 4.1. Table 4.2 compares the clinical characteristics of the affected individuals between this study and a prior study by Jamuar *et al.* (2017).

No apparent phenotypic abnormality was noted in the parents of the affected siblings. Mirror movements were also absent. MRI and any other radiological tests could not be performed on them, as they did not give their consent.

### 4.1.2 Genetic Findings

Pathogenic mutations were screened for in the variants found following the exome sequencing of two affected patients (IV-2 and IV-6) Variants were filtered according to standard process (Hashmi *et al.*, 2019). The non-synonymous variants in the coding region of the genome were selected. Variants with a frequency larger than 0.01, in human genetic databases, were excluded. Then, recessive variants that were predicted to be damaging were selected. (Table 4.3).

After applying the filtration steps, 38 variants were shortlisted. A homozygous frameshift variation (c.2399dupA, p.(Asn800Lysfs*11)) in exon 16 of the DCC gene (NM 005215.3) was chosen after thorough investigation since it was discovered to be strongly associated to the phenotype based on literature studies. Due to past reports linking DCC gene variants to progressive scoliosis, delayed intellectual growth, and distinctive radiological findings, the DCC gene variant (c.2399dupA) found in our family was regarded as the most likely candidate variant.

Primers were designed for the variant identified in the DCC gene. The region flanking the DCC gene variant was sequenced in both parents, the affected sibling, and the unaffected sibling. Analysis of the Sanger reads confirmed that the variant was fully segregating with disease phenotype in all family members (Figure 4.3). Sanger sequencing verified that all three patients carried the unique homozygous mutation; the parents were heterozygous carriers, which is consistent with the autosomal recessive inheritance pattern.

The variant was not found in 1000 Genomes Database, and Exome Aggregation Consortium (ExAc).

### 4.1.3 In silico Findings

The variant was identified as disease-causing by pathogenicity prediction tools (Table 4.4). The residues of interest were found to be conserved in orthologues (Figure 4.4). Comparison of modelled structure of normal and mutated protein showed that the mutated protein was truncated, as illustrated in Figure 4.5.

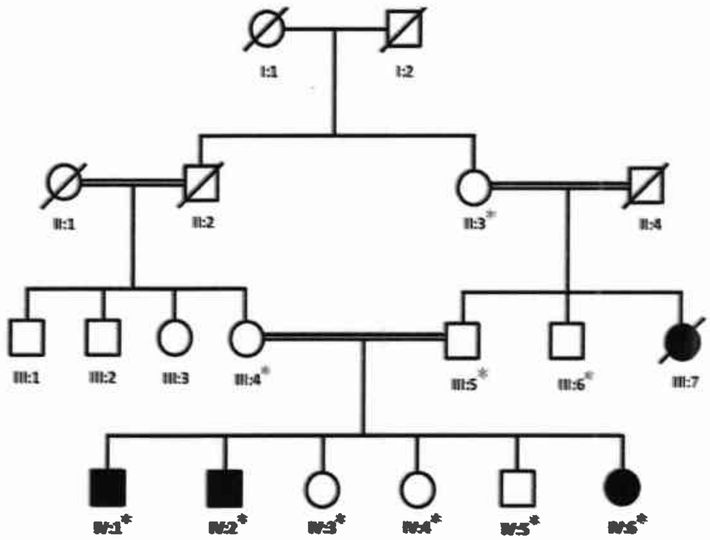


**Figure 4.1 Pedigree of Family-01**

Pedigree of a family segregating horizontal gaze palsy with progressive scoliosis-2 in an autosomal recessive manner. Asterisks show individuals available for this study.

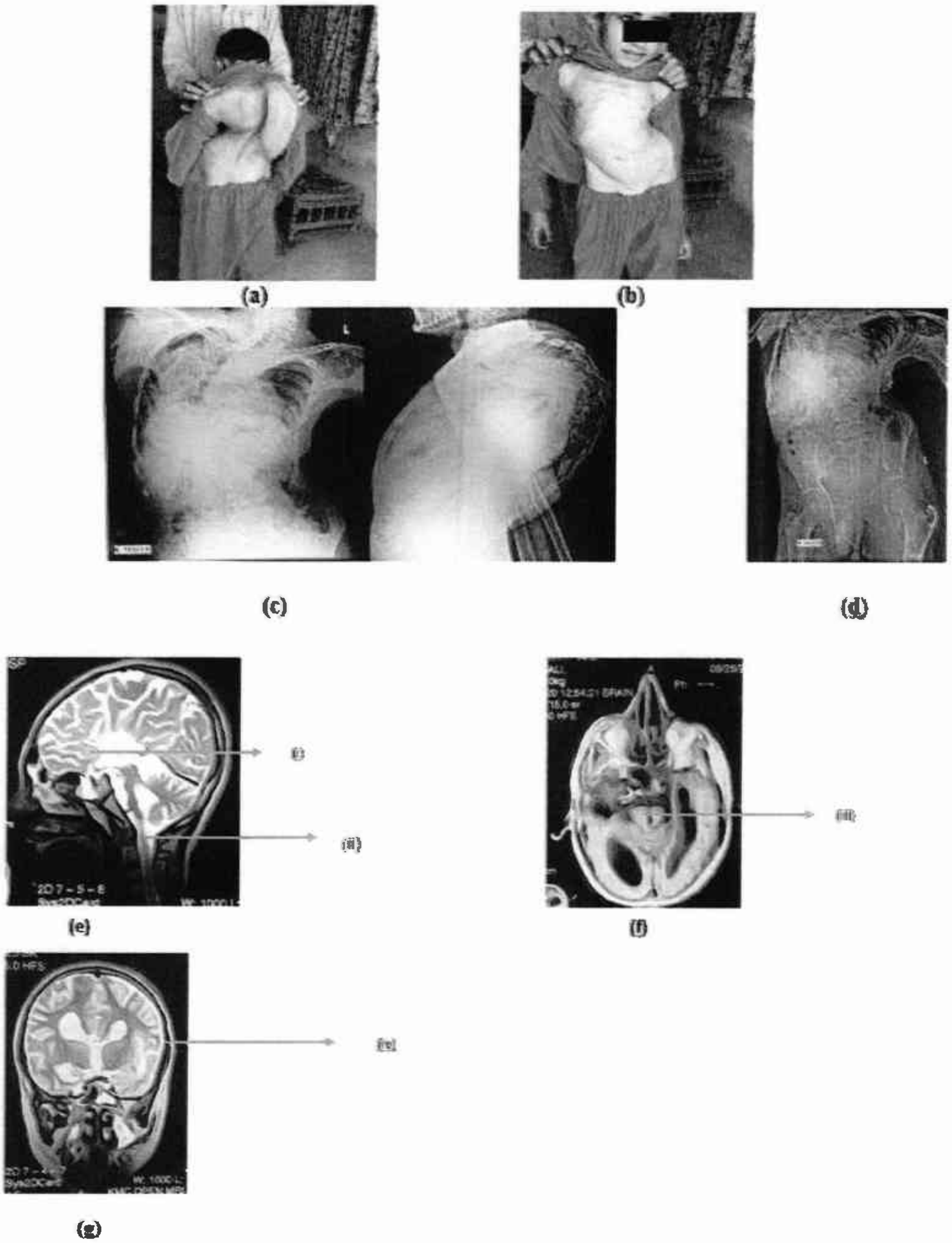

**Figure 4.2 Photographs and radiographs of Family-01**

Photographs of affected individuals IV-I (a) and IV-2 (b). Radiographs of an individual IV-I showing marked kyphoscoliosis in dorso-lumbar spine (c, d). MRI images of affected individual IV:1 (e-g). Sagittal image showing absent anterior commissure (i) and hypoplastic pons (ii). Axial images showing midline medullary cleft and butterfly-shaped medulla (iii) and agenesis of corpus callosum (iv).

**Table 4.1 Comparison of clinical features of affected individuals in Family-01**

| | Patient IV-1 | Patient IV-2 | Patient IV-6 |
|---|---|---|---|
| Gender | Male | Male | Female |
| Age | 19 yrs | 17 yrs | 6 yrs |
| Developmental delays | - | + | - |
| Intellectual disability | + | - | - |
| Mirror movements | - | - | - |
| Scoliosis | + | + | + |
| Agenesis of corpus callosum | + | + | + |
| Absence of cerebral commissures | + | + | + |

Key: (+) = presence of features; (-) = absence of features

**Table 4.2 Comparison of clinical features of affected individuals in Family-01 in this study and previous study by Jamuar *et al.* (2017)**

| | This report | | | Jamuar *et al.* (2017) | | |
|---|---|---|---|---|---|---|
| | Patient IV-1 | Patient IV-2 | Patient IV-6 | Family 1 Patient 1 | Family 1 Patient 2 | Family 2 Patient |
| Ethnicity | Pakistani | Pakistani | Pakistani | Mexican | Mexican | Arab |
| Consanguinity | + | + | + | + | + | + |
| Developmental Delays | – | + | - | + | + | + |
| Intellectual Disability | + | – | - | + | + | – |
| Mirror Movements | - | - | - | + | + | - |
| Scoliosis | + | + | + | + | + | + |
| Horizontal Gaze Palsy | + | + | + | + | + | + |
| Agenesis of corpus callosum | + | + | + | + | + | + |
| Absence of cerebral commissures | + | + | + | + | + | + |

Key: (+) = presence of features; (-) = absence of features

**Table 4.3 Filtration steps used to search for the disease-causing variant after Whole Exome Sequencing (WES) in Family-01**

| Filtration Steps | No. of variants detected |
|---|---|
| Total number of variants | 109,998 |
| Variants in coding region | 28,964 |
| Filter for non-synonymous variants | 17,229 |
| Rare variants (less than or equal to 1%) | 2,792 |
| Recessive variants (homozygous or compound heterozygous) | 261 |
| Predicted damaging | 38 |
| Related to the phenotype based on literature study | 1 |

**Table 4.4 Pathogenicity prediction of the shortlisted variant in *DCC* gene using online tools**

| Software | Score | Prediction | Comments |
|---|---|---|---|
| Mutation Taster | 1 | Deleterious | Frameshift<br>NMD<br>Protein features affected |
| SIFT | NA | NA | - |
| PolyPhen-2 | NA | NA | - |
| MutPred2 | 0.48 | Pathogenic | - |
| PMut | 92% | Disease-causing | - |

(a)

(b)

(c)

(e)

(d)

(f)

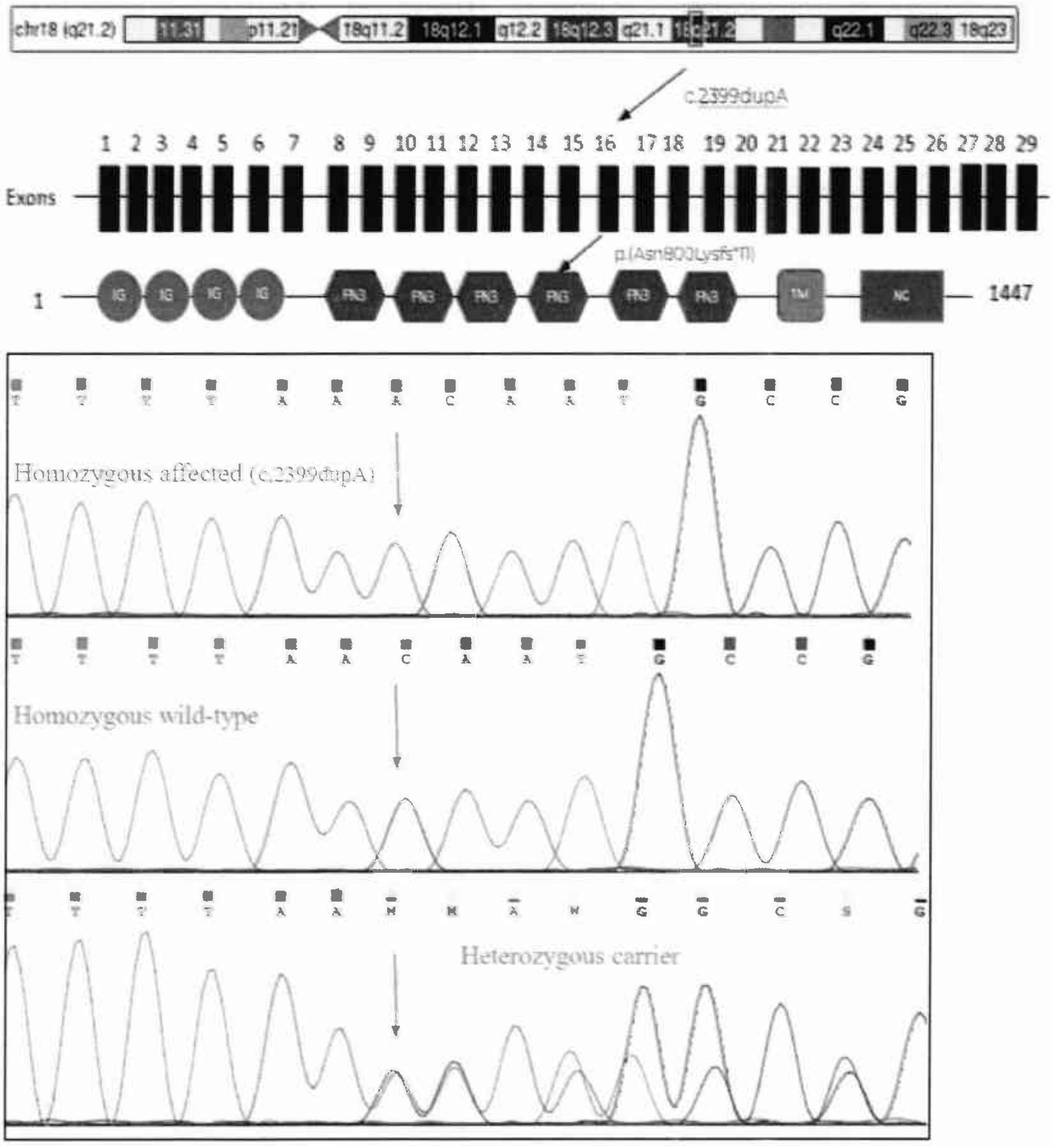


**Figure 4.3 Graphical representation of *DCC* gene, DCC protein and partial chromatograms of *DCC* gene**

(a) Representation of *DCC* gene at position 18q21.2 on chromosome 18 (Figure taken from UCSC Genome Browser)
(b) Representation of exons in *DCC* gene (NM_005215.3). The mutation c.2399dupA lies in the 16th exon.
(c) Representation of the domains in DCC protein (IG= Immunoglobulin domain; FN3= Fibronectin domain; TM= Transmembrane domain; NC= Neogenin-C domain). The mutation lies in the fourth fibronectin domain.

(d-f) Chromatogram showing partial sequence of an exon 16 of the *DCC* gene. Homozygous mutant sequence (of individual IV:1) (d), wild-type sequence (of individual IV:3) (e), heterozygous carrier (of individual III:4) (f). Arrows mark the point of mutation.

```
Human Mutated:   SSSHYVISLKAFKQCRRRSSSL*

Human Normal:    SSSHYVISLKAFNNAGEGVPLYESATTRSITDPTDPVDYYPLLDDFPTSVPD

P troglodytes:   SSSHYVISLKAFNNAGEGVPLYESATTRSITDPTDPVDYYPLLDDFPTSVPD

M musculus:      SSSHYVISLKAFNNAGEGVPLYESATTRSITDPTDPVDYYPLLDDFPTSVPD

M mulatta:       SSSHYVISLKAFNNAGEGVPLYESATTRSITDPTDPVDYYPLLDDFPTSVPD
```

**Figure 4.4 Multiple Sequence Alignment of DCC Protein**

Amino acid sequence comparison of DCC orthologues shows the conservation of the mutated residues across different species. Conserved residues are shown in green. Residues which have been mutated in the patients have been shown in red.

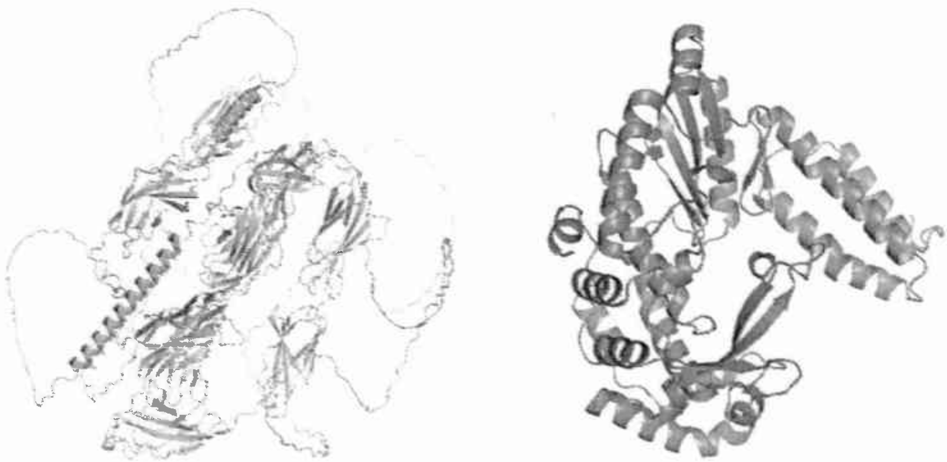

**(a)** **(b)**

**Figure 4.5 Structural models of wild-type and mutated DCC protein**

Comparison of wild-type DCC protein model (a) and mutated DCC protein model (b) demonstrates that the predicted mutated protein is truncated.

## 4.2 Family 2

Family 2 was a consanguineous family sampled from Azad Kashmir, Pakistan. It comprised four affected siblings. One affected individual was deceased at the time of sample collection. Three affected siblings and their parents participated in the study (Figure 4.6).

### 4.2.1 Clinical Findings

Clinical testing revealed that three affected siblings (II-1, II-2, and II-3) had isolated ulnar polydactyly/syndactyly, which was the initial diagnosis.

The proband II-1 was a 12-year-old female with severe postnatal growth retardation and developmental abnormalities despite having a normal birth weight (4 kg, >50th percentile). She weighed 19 kg and measured 105 cm at the time of the checkup. She was below the first percentile for both height and weight for her age. She had delayed speech, and also started walking at around 5 years. She had multiple oral frena, hypoplastic nails, bilateral postaxial polydactyly of the hands and feet, and malocclusions in her teeth. The extra finger on the left hand was found to have fused metacarpals that were fused together. Congenital ventricular septal defect and repeated respiratory infections were both noted in her medical records. Chest radiograph showed crowding of the ribs. Mild genu valgum was also observed (Figure 4.7).

Individuals I-2 and II-3 (9-year old boy and 6-year old boy respectively) both had hypoplastic nails, crooked teeth, multiple oral frena, abnormal frenal attachments, and hypoplastic tooth enamel. Bilateral postaxial polydactyly in the feet only was identified in II-2. Surgery had been performed to remove the sixth toe on the left foot as it made it difficult for him to walk. II-3 exhibited partial syndactyly of 4th and 5th toe of the left foot only (Figure 4.7). Individuals II-2 and II-3 lacked any further phenotypic traits associated with the EVC syndrome.

A second female sibling, II-4, had passed very shortly after birth from respiratory distress linked to a possible congenital cardiac condition. Additionally, her hands and feet were found to have bilateral postaxial polydactyly. Parents were first cousins and phenotypically normal. Phenotypic characteristics of the four siblings are summarized in Table 4.5.

### 4.2.2 Genetic Findings

Filtration for pathogenic mutations was performed following the exome sequencing of two affected patients (II-1 and II-2). Variants were filtered according to standard process (Hashmi *et al.*, 2019). The non-synonymous variants in the coding region were selected. Recessive variants that were projected to be harmful and had a frequency of less than 0.01 were screened and examined (Table 4.6).

73 shortlisted variants were carefully analyzed, and a homozygous 27bps deletion variant (c.731_757delTCCTTGACCTTCTTCCTAAAAGAAGT) in the *EVC* gene (NM_153717.2) was identified in both affected individuals. It was considered the most probable pathogenic variant based on literature study and the previously reported involvement of *EVC* gene variants in EvC syndrome.

The inframe deletion of 27 bps in the *EVC* gene results in the replacement of causes 10 amino acids by a single proline residue (p. Leu244_Ser253delinsPro) in the EVC protein. Sanger sequencing data confirmed co-segregation of the variant, as all three affected siblings were homozygous for the variant, whereas their parents were heterozygous (Figure 4.8).

### 4.2.3 In silico Findings

The variant was identified as disease-causing by prediction tools (Table 4.7). The deleted residues of EVC protein were found to be conserved in orthologues (Figure 4.9). The structure of EVC protein was obtained from Alpha-Fold. Mutations were introduced using PyMol. Chimera was used for energy minimization of mutated structure. Analysis of secondary structure using PDBsum Generate, and superimposition of wild-type and mutant 3D structures reveals the loss of two beta-turns in the mutant EVC protein (Figure 4.10).

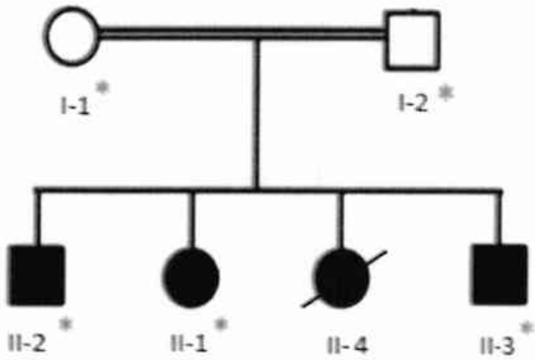


**Figure 4.6 Pedigree of Family-02**

Pedigree of a family segregating EVC Syndrome in an autosomal recessive manner. Asterisks show individuals available for the study

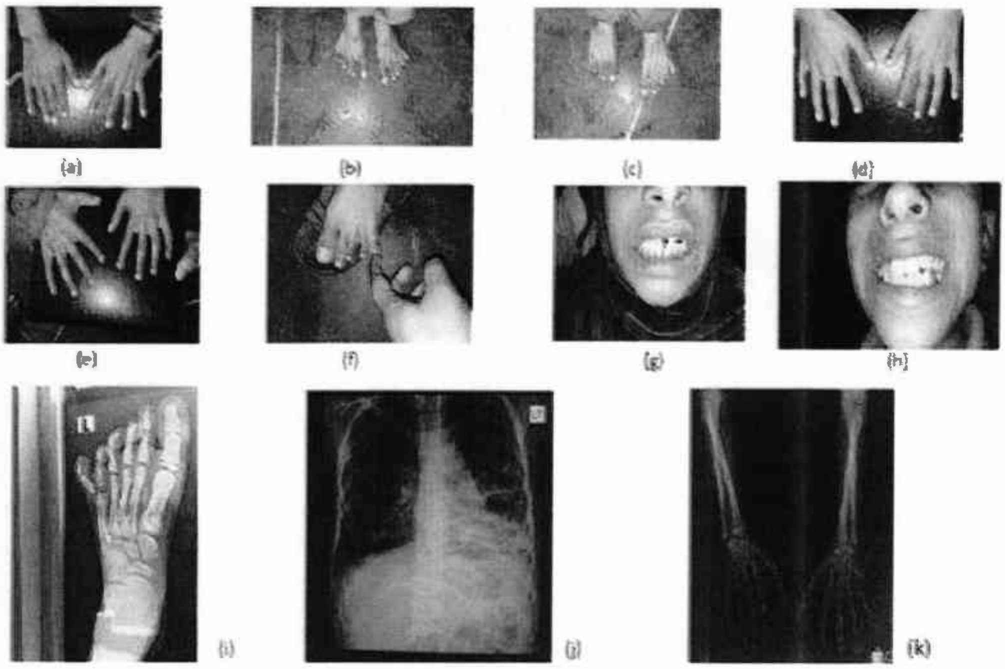

**Figure 4.7 Photographs and radiographs of Family-02**

(a,b) Photograph of hands and feet of individual II-1 showing dysplastic nails and bilateral postaxial polydactyly.

(c, d) Photograph of hand and feet of individual II-2 showing hypoplastic nails and bilateral postaxial polydactyly. 6th toe of right foot was removed by surgery.

(e, f) Photograph of hands and feet showing hypoplastic nails in individual II-3. Partial syndactyly of 4th and 5th toe in individual II-3 is evident.

(g, h) Photograph of teeth showing malocclusions and multiple buccal and labial frena, and abnormal frenal attachments in individual II-1 and II-2.

(i) Feet x-ray of individual II-2 showing bilateral postaxial polydactyly.

(j) Chest X-ray of II-1 showing normal features except for crowding of right upper ribs.

(k) Hand and arm x-ray of II-1 showing bilateral postaxial polydactyly and normal radius and ulna.

**Table 4.5 Comparison of clinical features of affected individuals in Family-02**

| | **II-1** | **II-2** | **II-3** | **II-4** |
|---|---|---|---|---|
| **Age** | 12 yrs old | 9 yrs old | 6 yrs old | Died as a newborn |
| **Sex** | Female | Male | Male | Female |
| **Congenital Heart Defects** | + | - | - | Highly suspected |
| **Postaxial Polydactyly in hands** | Bilateral | - | - | Bilateral |
| **Postaxial Polydactyly in feet** | Bilateral | Bilateral | Unilateral Partial Syndactyly | Bilateral |
| **Capitate-hamitate fusion** | - | - | - | - |
| **Genu valgum** | + | - | - | Unknown |
| **Nail dystrophy** | + | + | + | Unknown |
| **Multiple oral frena** | + | + | + | Unknown |
| **Dental malocclusions** | + | + | + | Unknown |
| **Long narrow chest** | - | - | - | - |

Key: (+) = presence of features; (-) = absence of features

**Table 4.6 Filtration steps used to search for the disease-causing variant after WES in Family-02**

| Filtration Steps | No. of variants detected |
|---|---|
| Total number of variants | 108,067 |
| Variants in coding region | 28,585 |
| Filter for non-synonymous variants | 17,124 |
| Rare variants (less than or equal to 1%) | 2,992 |
| Recessive variants (homozygous or compound heterozygous) | 403 |
| Predicted damaging | 73 |
| Related to the phenotype based on literature study | 1 |

**Table 4.7 Pathogenicity prediction of the shortlisted variant in EVC gene using online tools**

| Software | Score | Prediction | Comments |
|---|---|---|---|
| Mutation Taster | 0.999 | Deleterious | Frameshift<br>NMD<br>Protein features affected |
| SIFT | NA | NA | - |
| PolyPhen-2 | NA | NA | - |
| MutPred2 | 0.57 | Pathogenic | - |
| Provean | -33.84 | Deleterious | - |

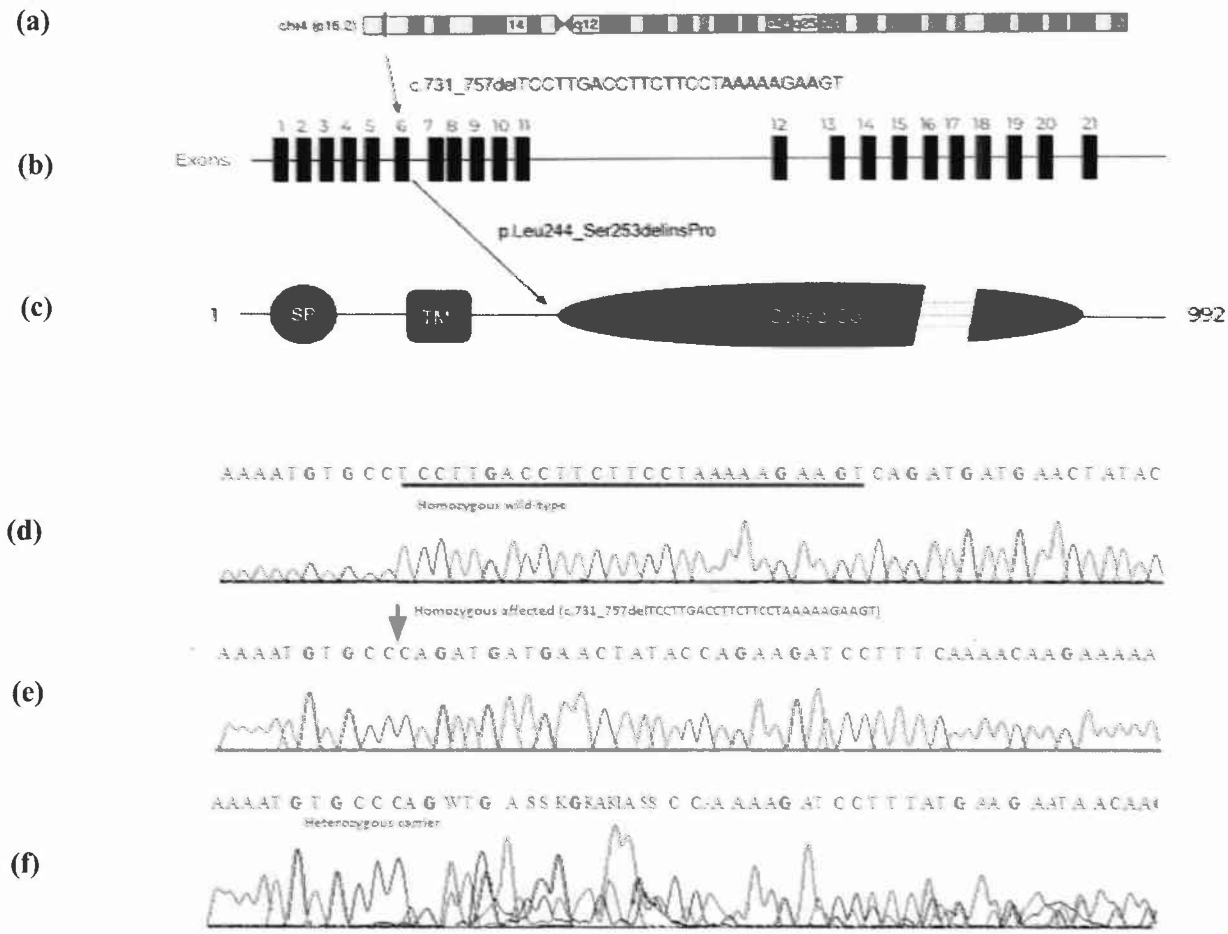


**Figure 4.8 Graphical representation of *EVC* gene and EVC protein, and partial chromatograms of *EVC* gene**

(a) Representation of *EVC* gene at position 4p16.2 on chromosome 4 (Figure taken from UCSC Genome Browser)

(b) Representation of exons in *EVC* gene (NM_153717.2). The mutation lies in the 6$^{th}$ exon.

(c) Representation of the domains in EVC protein (SP=Signal Peptide; TM= Transmembrane domain)

(d) Chromatogram showing partial sequence of the exon 6 of the *EVC* gene in a control individual. A 27bps deletion, identified in this study, is underlined.

(e) Chromatogram showing partial sequence of the exon 6 of the *EVC* gene in an affected individual. Position of a 27bps deletion mutation is marked with arrow.

(f) Chromatogram showing partial sequence of exon 6 of the *EVC* gene in parents of the affected individuals (c).

| | | | | | | | | | | | | | | | | | | | | | | |
|---|---|---|---|---|---|---|---|---|---|---|---|---|---|---|---|---|---|---|---|---|---|---|
| Gaps | | | | | | | | | | | | | | | | | | | | | | |
| Human | F | I | Q | I | F | K | M | C | L | L | D | L | L | P | K | K | K | S | D | D | E | L |
| Rhesus | F | I | Q | I | F | K | M | C | L | L | D | L | L | P | K | K | K | S | D | D | E | L |
| Mouse | F | I | Q | I | L | K | A | C | L | L | D | F | F | P | K | K | K | F | D | D | E | L |
| Dog | F | I | Q | I | F | K | M | C | L | L | D | L | L | P | K | K | K | S | D | D | E | L |
| Elephant | F | I | Q | I | F | K | M | C | L | L | D | L | L | P | K | K | K | S | D | D | E | L |
| Bat | F | I | Q | I | L | K | M | C | L | L | D | L | L | P | K | K | K | S | D | D | E | L |
| Horse | F | I | Q | I | F | K | M | C | L | L | D | L | F | P | K | K | K | S | D | D | E | L |
| Cow | F | I | Q | I | L | K | M | C | L | L | D | L | L | P | K | K | K | S | D | D | E | L |
| Camel | F | I | H | I | F | K | M | C | L | L | D | L | L | P | K | K | K | S | D | D | E | L |
| Sloth | F | I | Q | I | F | K | M | C | L | A | D | | L | P | K | K | K | S | D | D | E | L |

**Figure 4.9 Multiple Sequence Alignment of EVC Protein**

Amino acid sequence comparison of EVC protein showing conservation of the mutated residues across different species. Conserved residues are shown in blue. Unconserved residues are shown in red. Residues deleted in the mutant protein are represented by gray shaded squares in the top row.

(a)

(b)

(c)

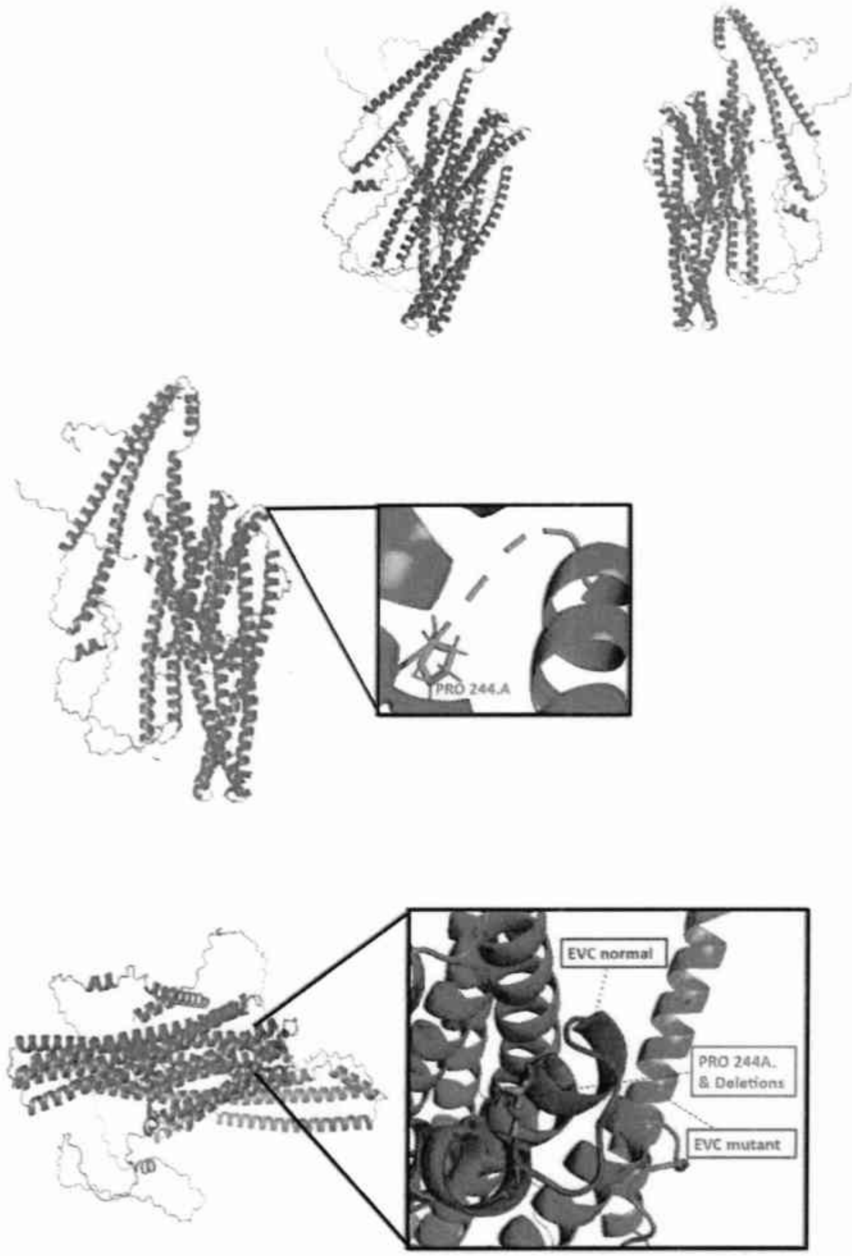


**Figure 4.10 Structural models of wild-type and mutated EVC protein**

(a) Structure of EVC protein (wild-type) on the left in pink color, and mutated EVC protein on the right in blue colour. (b) Zoomed-in panel shoes the deleted residues and inserted Proline residue in the mutated EVC protein at position 244. (c) Superimposition of wild-type (pink colour) and mutated (blue colour) EVC protein structure shows that 2 beta-folds are missing in the mutated protein

## 4.3 Family 3

Family 3 was a consanguineous family collected from Karachi, Sindh Province. It comprised six affected cousins, three of whom were deceased. All affected and unaffected siblings and their parents participated in the study (Figure 4.11).

### 4.3.1 Clinical Findings

The proband III:1 is a 13-year-old boy, born to unaffected, consanguineous parents. His height was measured to be 112cm. According to medical records, he exhibited prenatal and postnatal growth retardation. Birth weight was 1.8 kg. He exhibited normal intelligence but had characteristic features of facial dysmorphism including frontal bossing, hypoplastic midface, prominent mouth and lips, broad forehead and anteverted nares. He was observed to have short neck, short thorax, square shoulders, winged scapulae, and lumbar scoliosis (Figure 4.12).

Radiological findings showed spina bifida occulta, and rib hypoplasia evident by relative thinning of the posterior end of ribs (Figure 4.12). Protruding, fleshy heels and hyper-extendable thumbs were observed. Growth hormone levels were within the normal range.

The other sibling III:4 is a 10-year old girl. Her height was measured to be 90cm. She was also born as a low birth-weight infant and exhibited postnatal growth retardation despite normal blood tests for growth hormones. She exhibited normal intelligence, and also showed facial dysmorphism, similar to her brother. She also had a short neck and thorax, winged scapulae and a protruding chest. Heels were fleshy and protruding (Figure 4.12).

Three male siblings (III:2, III:6 and III:7) had died in utero while in the 2nd trimester due to unknown causes. All three fetuses were diagnosed with severe prenatal growth retardation.

III:8 is a 33-year old male born to unaffected, consanguineous parents with height of 125 cm. He exhibited short neck, short stature, dislocated hips, lumbar scoliosis, high square shoulders, and winged scapulae (Figure 4.12). He exhibited normal intelligence. Characteristic facial dysmorphism was present, but less pronounced than rest of patients. Details of clinical features in all 3M syndrome affected members in this family are given in Table 4.8.

### 4.3.2 Genetic Findings

16 homozygous variants were identified after filtering for non-synonymous, autosomal recessive, and rare (allele frequency ≤ 1%) variants, that were present in the coding region and were predicted to be damaging. On the basis of the functions of the genes in which these 16 candidate variants localized and the previously reported gene association with 3M Syndrome, *CUL7* variant (c.4493T>C) was considered as the most probable candidate (Table 4.9).

It was confirmed through Sanger sequencing that parents (II:1-4) of all patients were heterozygous for the identified variant, whereas the three patients (III:1, III:4 and III:8) carried the homozygous mutation. The variant was absent in the unaffected siblings (III:3, III:5 and III:9) (Figure 4.14).

The variant was absent in the exome-sequencing data of 100 individuals of Pakistani origin. It was also not found in the available population databases, including ExAC and gnomAD. This novel variant (c.4493T>C) in exon 24 of the *CUL7* gene was found to segregate perfectly with 3M Syndrome manifestations in this family, and therefore, considered as the cause of the syndrome in this family. The point mutation (c.4493T>C) in exon 24 of *CUL7* gene results in a modification p.Leu1498Pro at protein level.

**4.3.3 In silico Findings**

The variant was predicted to be disease-causing by several online tools (Table 4.10). Both amino acids Leucine and Proline differs in specific size, charge, and hydrophobicity-value. The wild-type leucine residue is predicted (using the Reprof software) to be located in an α-helix. Proline, if not located at one of the first three positions of α-helix, disrupts the helix. The identified mutation disrupts the helix, producing a significant change in the structure of the protein (Figure 4.13). The wild-type residue is much conserved in orthologues (Figure 4.11). The mutated residue is located in cullin homology domain that is important for binding of other molecules.

The mutant protein structure was modelled by Pymol (16) Fig 3(A and B), and structural superimposition was performed via Chimera 1.14 (18). Structural evaluation and validation of the wild type and mutant proteins was performed via Ramachandran plots created by PROCHECK webserver (19) ) Fig 3(C and D). 3D model of the wild type protein contains 86.3% residues in the favored region, 12.2% amino acids in additionally allowed regions, 1.2% residues in generously allowed regions, and only 0.3% residues in disallowed region. Similarly, 3D structure of mutant *CUL7* protein modelled via Pymol has 86.3% residues in the favored region, 12.2% amino acids in additionally allowed regions, 1.2% residues in generously allowed regions, and only 0.3% residues in disallowed region. Similar Ramachandran plot statistics of normal and mutant protein structures indicates that our structures are good enough to be employed for molecular interaction studies.

Molecular docking studies were performed to calculate and analyze the binding interactions between two molecules. *CUL7* belongs to the family of structurally related proteins Cullins, which share an evolutionarily conserved C-domain. Many members of Cullin family play a significant role in Ubiquitin dependent proteolysis (Sarikas *et al.,* 2011). A published research conducted on *CUL7* (formerly known as KIAA0076) indicates that it interacts with multiple proteins such as *ROC1* (RING finger protein) and Skp1-Fbx29 complex to form an SCF-like complex that plays a significant role in ubiquitination (Dias *et al.,* 2003). In the present study, effect of mutation on the molecular interactions of *CUL7* with *ROC1* was assessed by performing protein-protein docking via ClusPro. Figure 4.16 shows the docked complexes of wild type *CUL7* with *ROC1* protein and mutant *CUL7* with *ROC1*. From the LigPlot+ interaction diagram it is quite clear that the mutant *CUL7* has increased number of interactions with *ROC1* protein (Figure 4.17). The 4493T>C mutation has a significant influence on the protein's normal structure and conformation, which is clearly proved by the differences in the number and position of residues involved in both types of docked complexes. This is due to a change in the interaction site as a result of a mutation that harmed protein-protein interaction. Residues involved in hydrogen bonding between docked complexes are shown in Table 4.11.

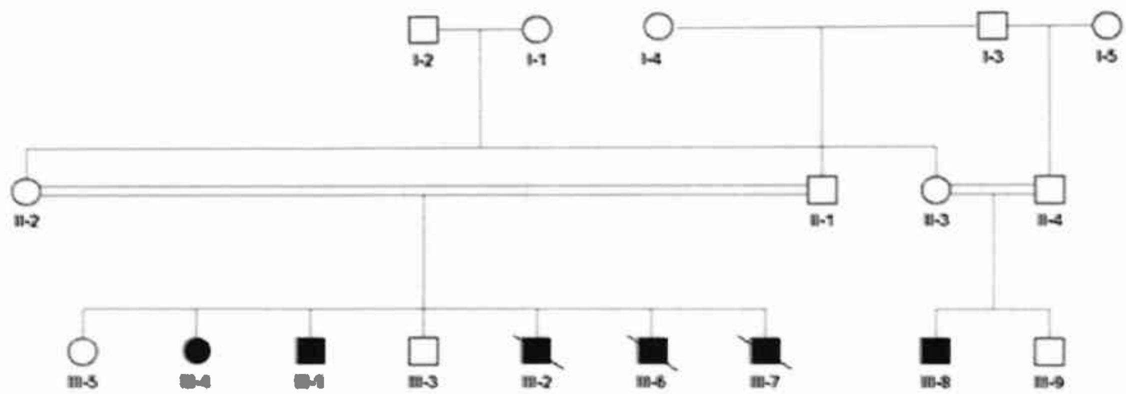


**Figure 4.11 Pedigree of Family-03**

Pedigree of a family segregating 3M Syndrome in an autosomal recessive manner. Asterisks show individuals available for the study.

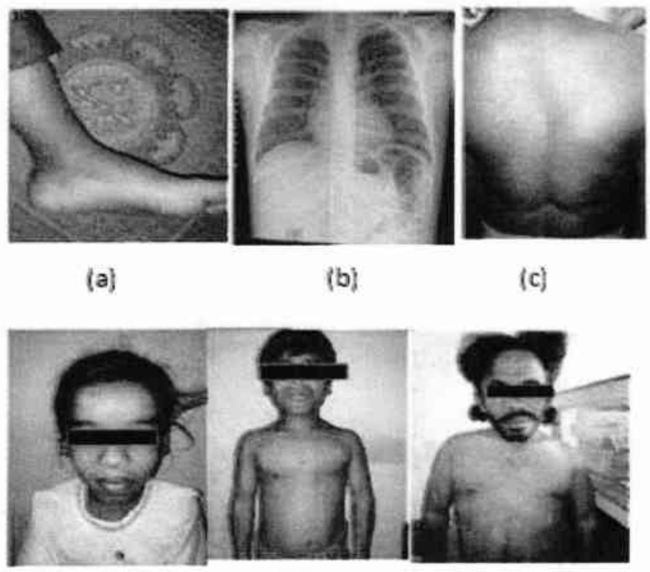

(a) (b) (c)

(d) (e) (f)

**Figure 4.12 Photographs and radiographs of Family-03**

a- Heel photograph of affected individual III-1 showing fleshy, protruding heels
b- Chest X-ray of affected individual III-1 showing posterior thinning of ribs and spina bifida occulta
c- Photograph of affected individual III-8 showing scoliosis- Photograph of affected individual III-4 showing triangular face, frontal bossing, midface hypoplasia, full fleshy lips, fleshy tipped nose and long philtrum
e- Photograph of affected individual III-1 showing dysmorphic facial features including fleshy tipped nose, anteverted nares, fleshy lips, triangular face, dolichocephaly, frontal bossing, midface hypoplasia, and long philtrum
f- Photograph of affected individual III-8 showing dysmorphic facial features: short neck and thorax, square shoulders and winged scapulae

**Table 4.8 Comparison of clinical features of affected individuals in Family-03**

Summary of auxology, radiological and clinical phenotype of three 3-M syndrome individuals reported in this paper. List of clinical features has been taken from Hanson *et al.* (2009).

| 3M Syndrome Features | III-1 | III-4 | III-8 |
|---|---|---|---|
| Gender | M | F | M |
| Age at initial presentation (years) | 13 | 10 | 33 |
| Height SDS at presentation | −5.8 | −7 | −5.2 |
| **Radiological features** | | | |
| Slender long bones | − | − | NA |
| Tall vertebral bodies | − | − | NA |
| **Facial Features** | | | |
| Fleshy tipped nose | + | + | + |
| Anteverted nares | + | - | + |
| Full fleshy lips | + | + | + |
| Triangular face | + | + | + |
| Dolichocephaly | + | - | + |
| Frontal bossing | + | + | + |
| Midface hypoplasia | + | + | + |
| Long philtrum | + | + | - |
| Pointed chin | + | + | + |
| Prominent ears | - | - | - |
| **Other Features** | | | |
| Short neck | - | + | + |
| Winged scapulae | + | + | + |
| Square shoulders | + | + | + |
| Short thorax | + | + | + |
| Transverse chest groove | − | − | − |
| Pectus deformity | + | + | + |
| Hyperlordosis | − | − | − |
| Scoliosis | − | − | + |
| Hypermobility of joints | + | + | NA |
| Fifth finger clinodactyly | − | − | − |
| Prominent heels | + | + | NA |
| Spina bifida occulta | + | NA | NA |
| Developmental dysplasia hip | − | − | + |

(+) = Presence of features ; (-) = Absence of features

**Table 4.9 Filtration steps used to search for the disease-causing variant after Whole Exome Sequencing (WES) in Family-03**

| Filtration Steps | No. of variants detected |
|---|---|
| Total number of variants | 69,317 |
| Variants in coding region | 3,512 |
| Filter for non-synonymous variants | 1,231 |
| Rare variants (less than or equal to 1%) | 430 |
| Recessive variants (homozygous or compound heterozygous) | 21 |
| Predicted damaging | 16 |
| Related to the phenotype based on literature study | 1 |

**Table 4.10 Pathogenicity prediction of the shortlisted variant in *CUL7* gene using online tools.**

| Software | Score | Prediction | Comments |
|---|---|---|---|
| Mutation Taster | 0.995 | Damaging | Splice site affected |
| PhD-SNP | 0.698 | Disease | - |
| mvPPT | 0.833 | Disease-causing | - |
| SNAP | 0.725 | Disease | |
| PolyPhen-2 | 0.999 | Damaging | - |
| Panther | 0.802 | Disease | - |
| Meta-SNP | 0.705 | Disease | |

| | | | | | | | | | | | | | |
|---|---|---|---|---|---|---|---|---|---|---|---|---|---|
| Human Mutated: | L | A | F | S | G | L | S | A | D | M | P | N | Q |
| Human Normal: | L | A | F | S | G | L | S | A | D | M | L | N | Q |
| P troglodytes: | L | A | L | S | G | L | S | A | D | M | L | N | Q |
| M musculus: | Q | A | I | S | E | L | P | P | D | V | L | H | R |
| M mulatta: | L | A | L | S | G | L | S | E | D | M | L | N | E |
| F catus: | L | A | L | S | G | L | S | P | D | M | L | N | Q |

**Figure 4.13 Multiple sequence alignment of CUL7 protein**

Amino acid sequence comparison of CUL7 protein conservation of the mutated residues across different species. Conserved residues are shown in green. Changed residues are shown in red.

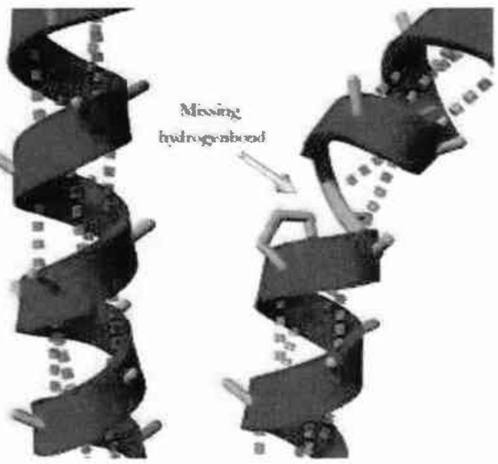


**Figure 4.14 Portion of the structural model of CUL7 7 wild-type and mutated protein**

Portion of the CUL7 protein model- Leucine (on the left, in wild-type protein) is replaced by Proline (on the right, in mutated protein) causing a disruption in the α-helix, due to missing hydrogen bond. Image generated by HOPE software.

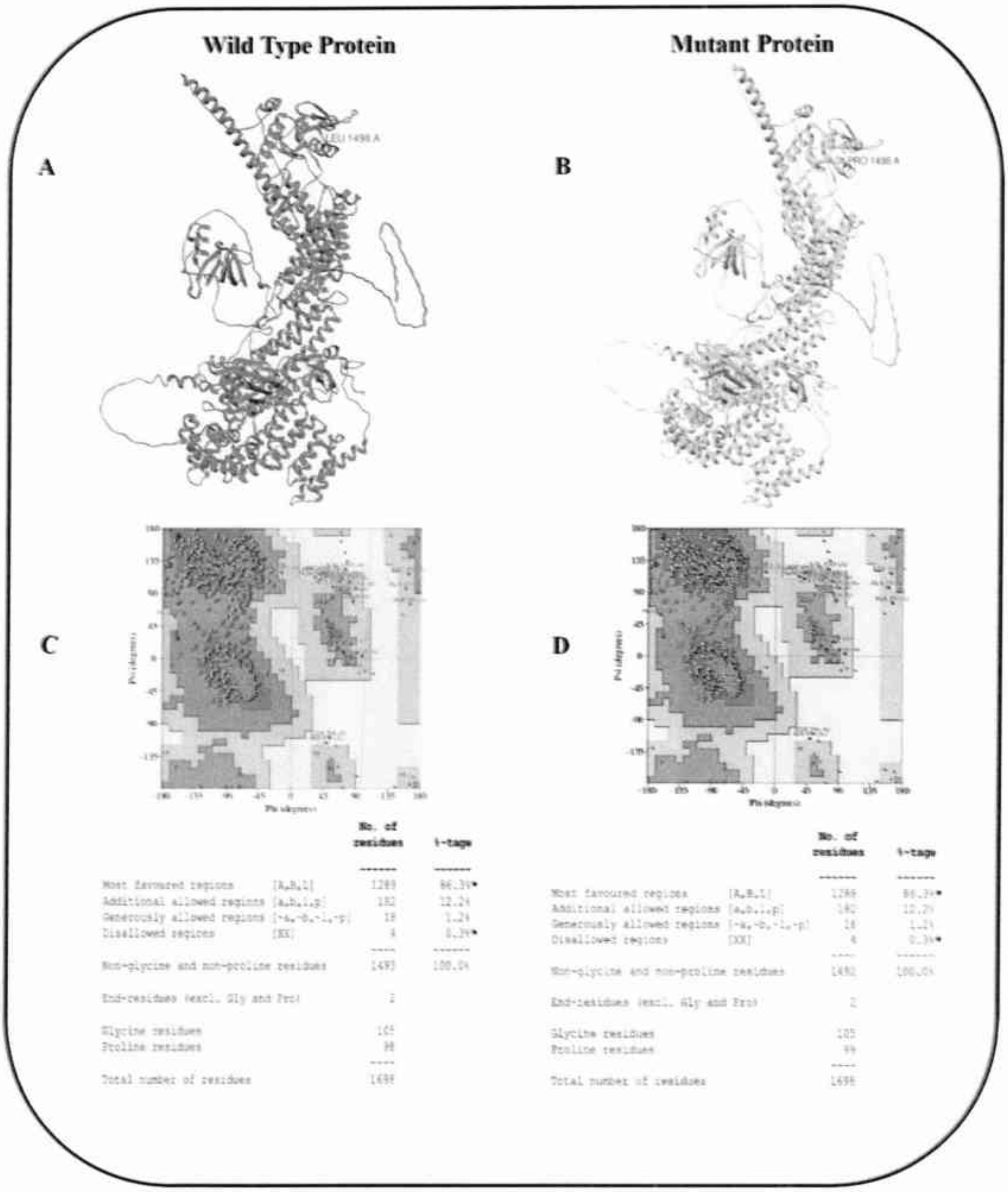


**Figure 4.15 Predicted 3D structures of wild-type and mutant CUL7 L1498P protein generated by Pymol and their validations by Ramachandran plots developed by PROCHECK.**

a- 2D representation of 3D structure of wild-type CUL7 shown in red along with Leu1498 represented in blue color.

b- 2D representation of 3D structure of mutant CUL7 shown in yellow color along with Pro1498 represented in blue color.

c-Ramachandran plot of wild-type CUL7.

d- Ramachandran plot of mutant CUL7.

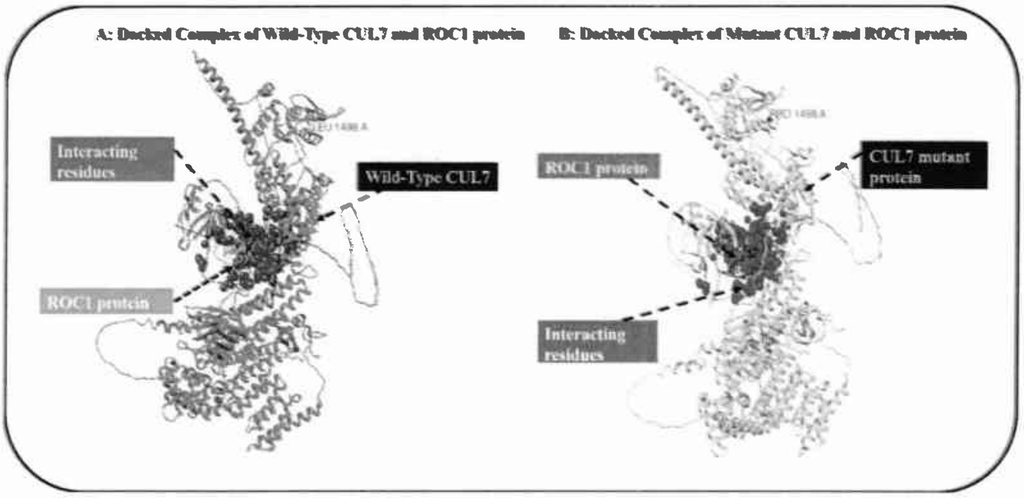


**Figure 4.16 Docked pose of wild-type CUL7 and mutant CUL7 protein with ROC1 protein.**

a- Docked complex of wild-type CUL7 with ROC1 protein. Wild-type CUL7 is shown in red color with Leucine 1498 residue represented in magenta color, ROC1in orange and interacting residues in medium blue color.

b- Docked complex of mutant CUL7 with ROC1 protein. Mutant CUL7 is shown in yellow color with Proline 1498 residue represented in medium blue color, ROC1 in forest green shade and interacting residues in magenta color.

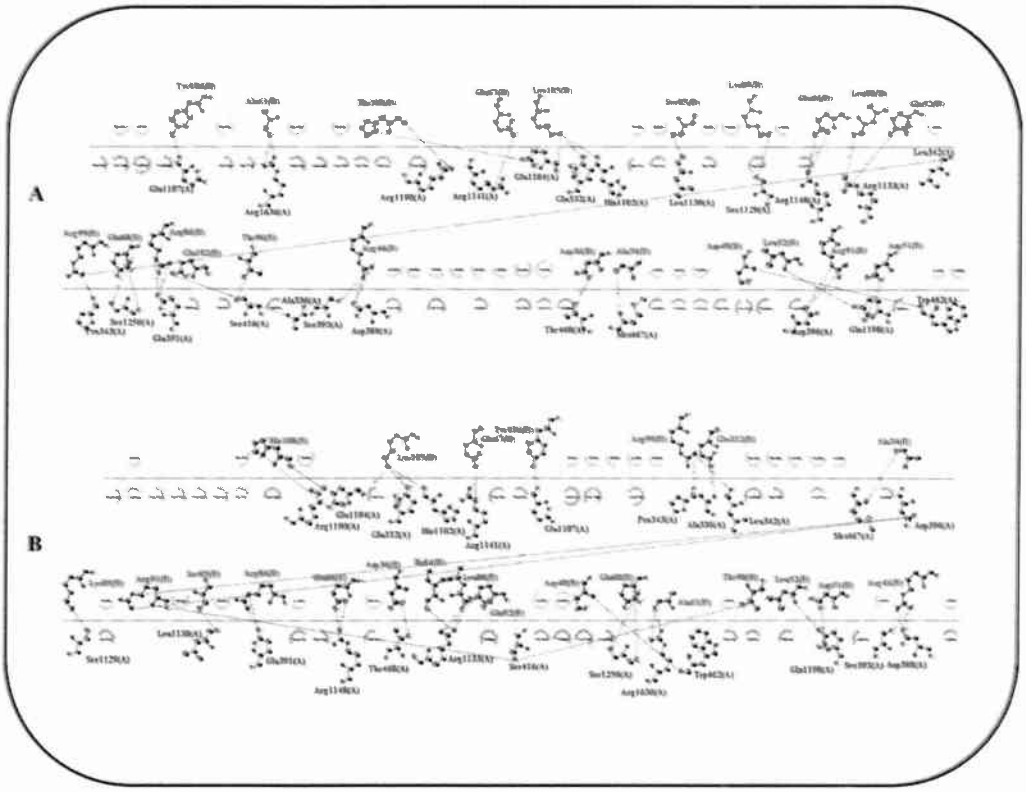

**Figure 4.17 Schematic representation of interacting residues and binding interactions involved in docked complexes.**

a- 2D LigPlot+ interaction diagram of wild-type CUL7 with ROC1 protein. Blue residues represent binding residues of wild-type CUL7, however binding residues of ROC1 are represented in green color.

b- 2D LigPlot+ interaction diagram of wild-type CUL7 with ROC1 protein. Blue residues represent binding residues of wild-type CUL7 and binding residues of ROC1 are represented in green color. Olive green line indicates hydrogen bonding between interacting residues.

**Table 4.11 Hydrogen bonded interactions between CUL7 andROC1 docked complexes**

| Hydrogen bonded interactions between Protein-Protein Docked Complex | | | |
|---|---|---|---|
| **Wild-type CUL7 Residues** | **ROC1 Residues** | **Mutant CUL7 Residues** | **ROC1 Residues** |
| Glu1107, Arg1636, Arg1190, Arg1141, Glu1104, Glu332, His1102, Leu1130, Ser1129, Arg1148, Arg1133, Pro343, Ser1256, Glu391, Ser416, Ala336, Ser393, Asp388, Thr468, Met467, Asp396, Glu1198 | Tyr106, Ala61, His108, Glu67, Lys105, Ser85, Lys89, Glu66, Leu88, Gln92, Arg99, Gln60, Arg86, Glu102, Thr90, Arg46, Asp36, Ala34, Asp40, Leu52, Arg91, Asp51 | Arg1190, Glu1104, Gln332, His1102, Arg1141, Glu1107, Pro343, Ala336, Leu342, Met467, Asp396, Ser1129, Leu1130, Glu391, Arg1148, Thr468, Arg1133, Ser416, Ser1256, Arg1636, Trp462, Gln1198, Ser393, Asp388 | His108, Lys105, Glu67, Tyr106, Arg99, Glu102, Ala34, Lys89, Arg91, Ser85, Arg86, Glu66, Asp36, Ile84, Leu88, Gln92, Asp 40, Gln60, Ala61, Thr90, Leu52, Asp51, Arg46 |

(a)

(b)

(c)

(d)

(e)

(f)

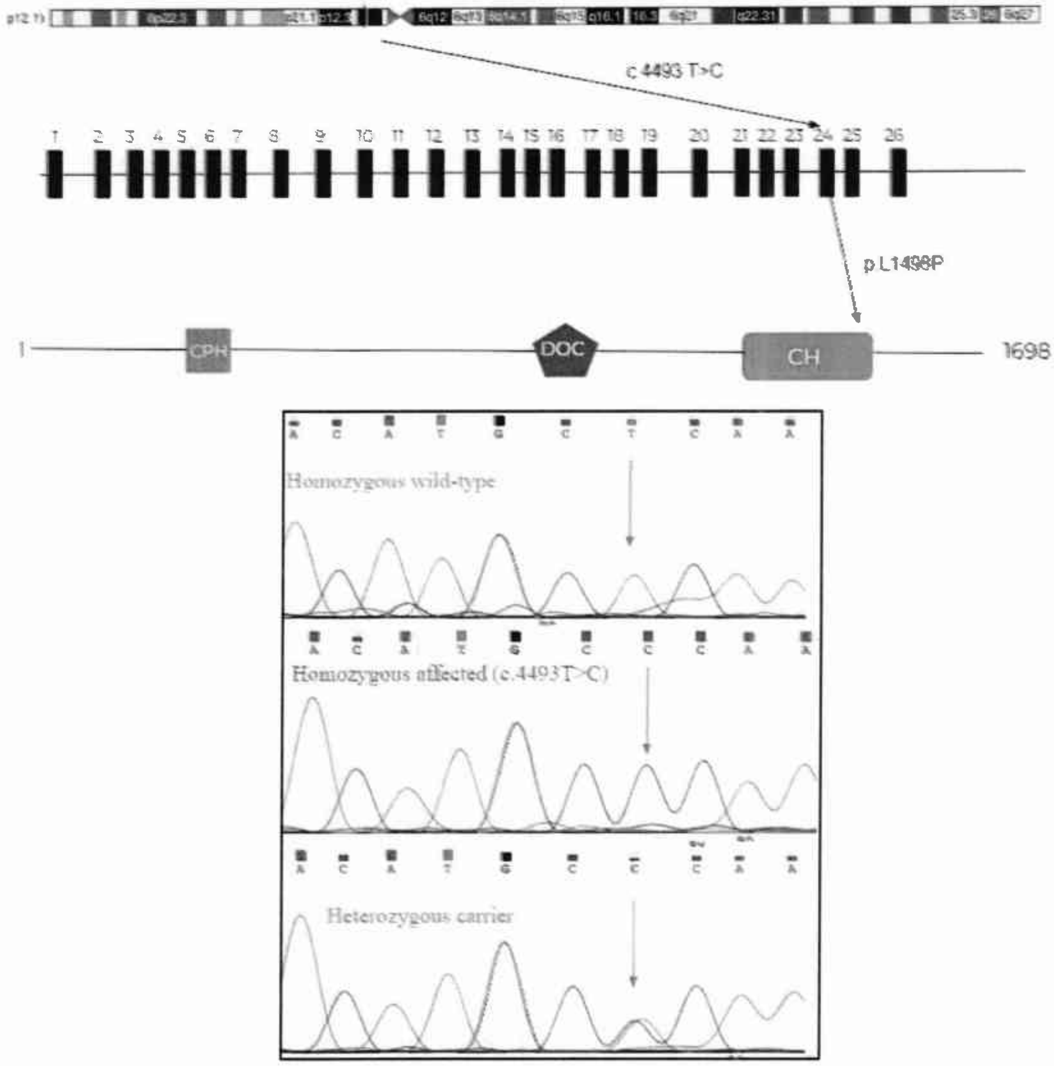


**Figure 4.18 Graphical representation of *CUL7* gene and CUL7 protein, and partial chromatograms of *CUL7* gene**

(a) Representation of *CUL7* gene at position 6p12.1 on chromosome 6 (Figure taken from UCSC Genome Browser)

(b) Representation of exons in *CUL7* gene (NM_014780.5). The mutation lies in the 24th exon.

(c) Representation of the domains in *CUL7* protein (CPH= Conserved Domain in CUL7, PARC and HERC2; DOC= a domain similar to the DOC1 domain of the anaphase-promoting complex/cyclosome but of unknown function; CH= Cullin Homology domain). The mutation lies in the Cullin Homology domain.

(d) Chromatogram showing partial sequence of exon 24 of the *CUL7* gene in homozygous wild-type individual III-9.

(e) Chromatogram showing partial sequence of exon 24 of the *CUL7* gene in homozygous affected individual III-1.

(f) Chromatogram showing partial sequence of exon 24 of the *CUL7* gene in heterozygous parent II-1.

## 4.4 Family 4

Family 4 was collected from Attock, Punjab. It consisted of two affected brothers and an unaffected sister. The parents were deceased. The unaffected sister did not agree to participate in the study. However, one of the affected brother's wife who was also his first cousin, took part in the study (Figure 4.15).

### 4.4.1 Clinical Findings

The proband III-1 was a 40-year old male, with height 48 inches and weight 40kg. He was born as a normal birth-weight infant, but exhibited severe post-natal retardation. He presented with short stature, short neck, winged scapulae, club foot, limited elbow extension, pes planus and protruding abdomen (secondary to lordosis) (Figure 4.16). Dental examination revealed multiple caries and enamel hypoplasia. The proband suffered from severe hearing impairment since early childhood.

Radiographs showed severe kyphoscoliotic deformity of dorsolumbar spine with convexity to left side in dorsal region and convex to right side in lumbar region. Segmentation abnormalities were observed in spine. Abnormal angulation of sacrum, and mild early degenerative changes at the hip joints were observed bilaterally. Bilateral capitate-hamitate coalition was also observed in both hands (Figure 4.16). Tarsal synostosis leading to talipes equniovarus was evident in right foot.

Strikingly similar clinical and radiological abnormalities were observed in the other affected individual III-3. He was 35 years old with height 46 inches. He also presented with short stature, short neck, winged scapulae, joint pain, scoliosis, pes planus, protruding abdomen (secondary to lordosis), hearing impairment and enamel hypoplasia (Table 4.12).

#### 4.4.2 Genetic Findings

Variants obtained after exome sequencing of III-1 were filtered for pathogenic mutations. Variants with a frequency greater than 0.01 in human genetic variation databases were filtered out. Eight potentially pathogenic, homozygous, rare variants in the coding region were shortlisted (Table 4.13). Analysis of the variants led to the identification of a point mutation (c.3243C>A) in exon 21 of *FLNB* gene (NM_001457), resulting in a modification p.Cys1081* at protein level.

Due to previous reports linking FLNB gene variants to the pathology of spondylocarpotarsal synostosis syndrome, the FLNB gene variant (c.3243C>A) found in our family was deemed to be the most likely candidate variant.

Primers were constructed for the variant, and the region surrounding the gene variant was sequenced in affected individuals and an unaffected cousin. Sanger read analysis confirmed that the variant was fully segregating with disease phenotype. (Figure 3). Both patients (III-1 and III-3) were homozygous for this variant; maternal cousin (III-4) was wild-type for this variant (Figure 4.18). Parents were deceased; blood of unaffected sister was not available for analysis.

#### 4.4.3 In silico Analysis

The variant was identified as disease causing by in silico prediction tools (Table 4.14). It is predicted to introduce a premature stop codon, resulting in the formation of a truncated protein with several important conserved repeat domains missing (Figure 4.17, 4.19). The mutated residues were conserved in orthologues (Figure 4.21)

PDBsum generate was employed to predict and compare the change in secondary structure elements of wild-type and mutant FLNB proteins (Laskowski, 2001). From Table 4.15, it is clearly evident that mutant protein has reduced number of sheets, beta hairpins, strands, helices, helic-helic interacs and beta-turns; however, there is an increase in the number of beta bulges and gamma turns along with the formation of a psi-loop which was absent is wild-type protein structure.

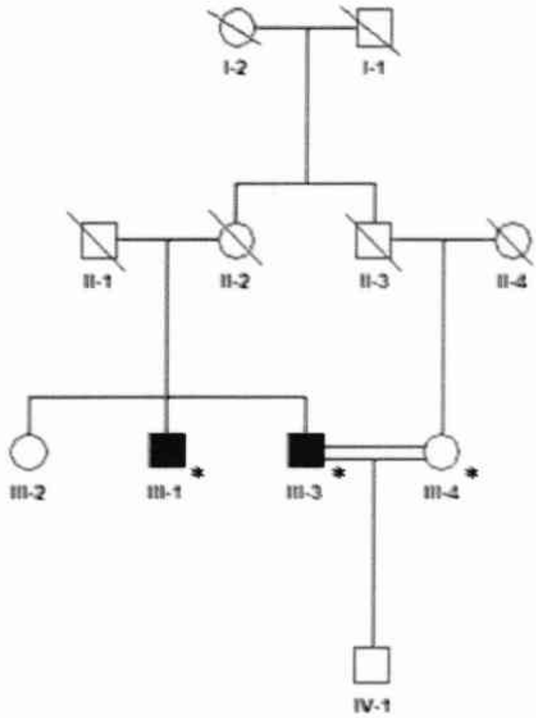


**Figure 4.19 Pedigree of Family -04**

Pedigree of a consanguineous Pakistani family segregating spondylocarpotarsal synostosis syndrome in an autosomal recessive manner. Asterisks represent the individuals whose blood samples were available for study.

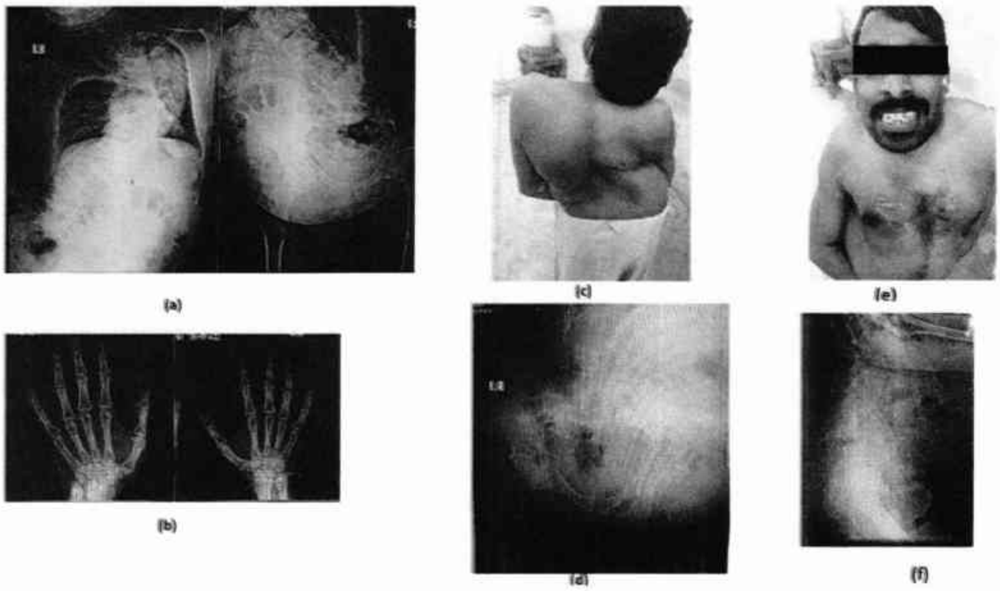

**Figure 4.20 Photographs and radiographs of affected individual III-1 in Family-04**

- a- Radiograph showing short segmentation abnormalities and severe scoliotic deformity
- b- Radiograph of hands showing capitate-hamitate fusion
- c- Photograph showing short stature, scoliosis, lordosis and winged scapulae
- d- Radiograph of pelvis showing scoliotic deformity of lumbar spine, abnormal sacral angulation, and early degenerative changes of hip joints
- e- Photograph showing protruding abdomen
- f- Radiograph of lateral spine showing segmentation abnormalities in spine

**Table 4.12 Comparison of clinical features in affected individuals of Family-04**

| | **Patient III-1** | **Patient III-3** |
|---|---|---|
| Gender | M | M |
| Age | 40 | 35 |
| Dysmorphic facies | - | - |
| Anteverted nares | - | - |
| Tooth enamel hypoplasia | + | + |
| Micrognathia | - | - |
| Hearing loss | + | + |
| Short neck | + | - |
| Short stature | + | + |
| Scoliosis | + | + |
| Abnormal vertebral segmentation | + | + |
| Carpal synostosis | + | + |
| Decreased elbow extension | + | + |
| Tarsal synostosis | + | + |
| Pes planus | + | + |
| Cataracts | - | - |

(+) = presence of features, (-) = absence of features

**Table 4.13 Filtration steps used to search for the disease-causing variant after WES in Family-04**

| Filtration Steps | No. of variants detected |
|---|---|
| Total number of variants | 55,161 |
| Variants in coding region | 7,003 |
| Filter for non-synonymous variants | 2,891 |
| Rare variants (less than or equal to 1%) | 421 |
| Recessive variants (homozygous or compound heterozygous) | 55 |
| Predicted damaging | 8 |
| Related to the phenotype based on literature study | 1 |

**Table 4.14 Pathogenicity prediction of the shortlisted variant in *FLNB* gene using online tools.**

| Software | Score | Prediction | Comments |
|---|---|---|---|
| Mutation Taster | 1 | Deleterious | NMD<br>amino acid sequence changed<br>protein features (might be) affected<br>splice site changes |
| LRT | - | Disease-causing | - |
| GERP | 5.66 | Disease-causing | - |

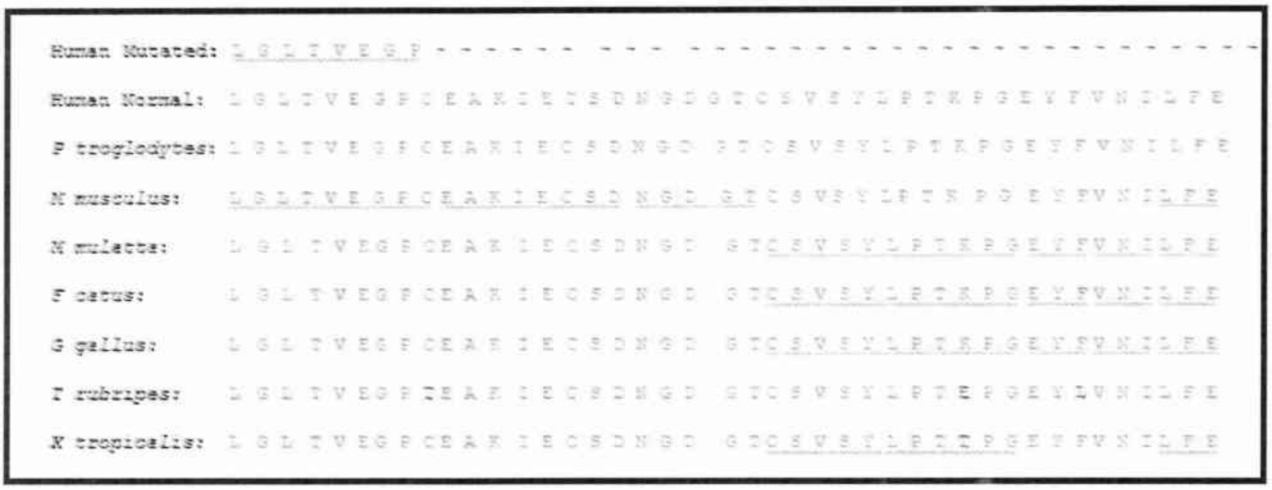


**Figure 4.21 Multiple Sequence Alignment of FLNB Protein**

Amino acid sequence comparison of FLNB protein conservation of the mutated residues across different species. Conserved residues are shown in green. Unconserved residues are shown in red. Red blanks represent that the mutated truncated protein does not contain the corresponding residues.

**Figure 4.22 Structural models of wild-type and mutated FLNB proteins**

Comparison of wild-type FLNB protein model (left side) and mutated FLNB protein model (right side) demonstrates that the predicted mutated protein is truncated

**Table 4.15 List of secondary structure elements in normal and mutant FLNB protein**

| Secondary Structure | Normal FLNB | Mutant FLNB |
|---|---|---|
| **Sheets** | 49 | 20 |
| **Beta Hairpins** | 65 | 42 |
| **Psi loop** | 0 | 1 |
| **Beta bulges** | 25 | 27 |
| **Strands** | 220 | 67 |
| **Helices** | 58 | 9 |
| **Helix-Helix interacs** | 27 | 3 |
| **Beta Turns** | 237 | 143 |
| **Gamma turns** | 26 | 48 |

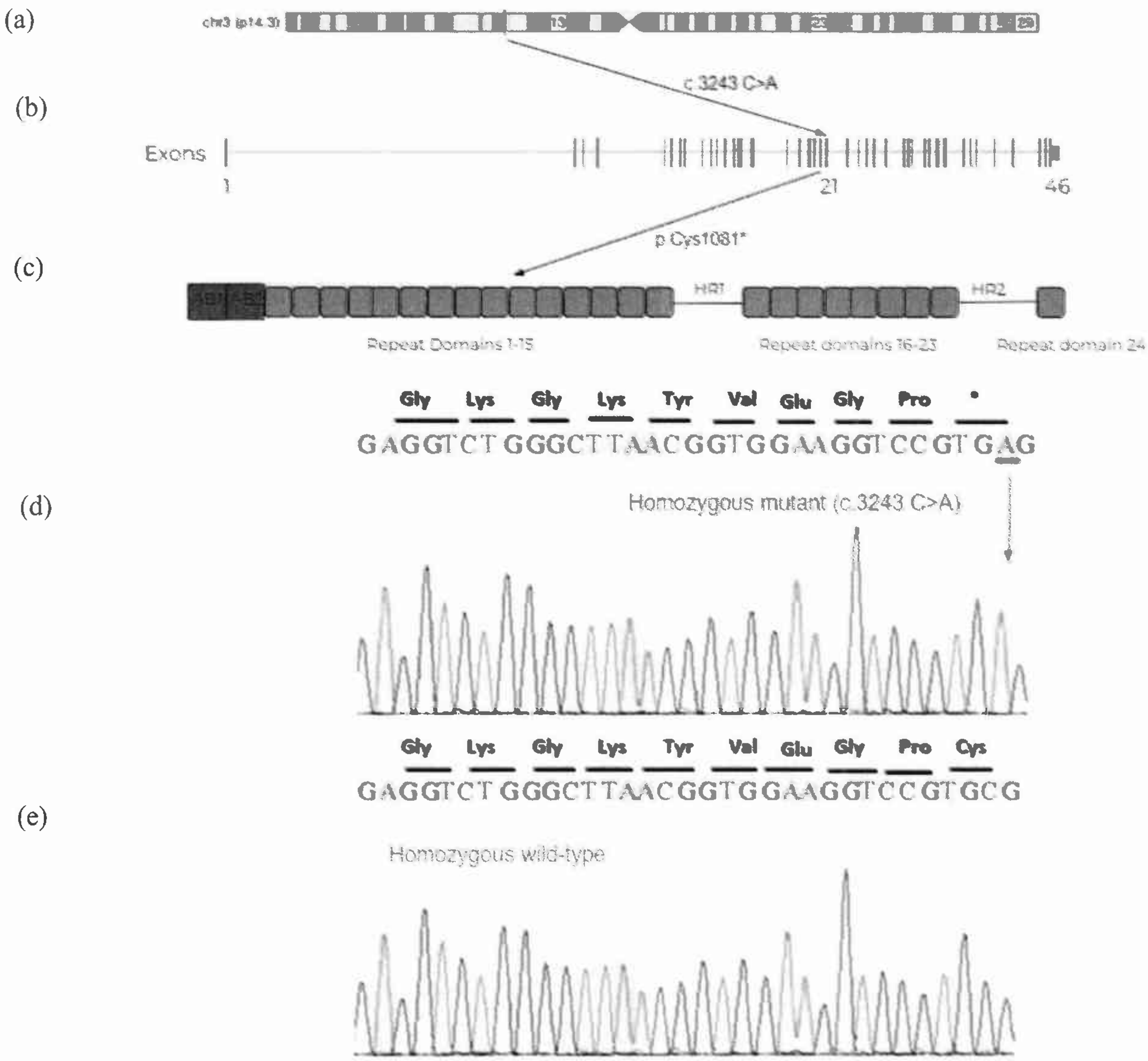


**Figure 4.23 Graphical representation of *FLNB* gene and FLNB protein, and partial chromatograms of *FLNB* gene**

(a) Representation of *FLNB* gene at position 3p14.3 (Fig from UCSC Genome Browser)
(b) Representation of exons in *FLNB* gene (NM_001457). The mutation lies in exon 21.
(c) Representation of the domains in FLNB protein (AB=Actin-Binding Domain; HR= Hinge Region). The mutation lies in the 9$^{th}$ Repeat Domain.
(d) Chromatogram showing partial sequence of exon 21 of the *FLNB* gene in homozygous mutant individual III-1. A red line below A marks homozygous nucleotide substitution.
(e) Chromatogram showing partial wild-type sequence of exon 21 of the *FLNB* gene in individual III-4

## 4.5 Family 5

Family 5 was collected from Narowal, Punjab. Two affected brothers, along with their unaffected sister and parents were recruited for the study (Figure 4.20).

### 4.5.1 Clinical Findings

Affected individuals exhibit symptoms of otopalatodigital syndrome-1 (OPD-1). The proband II-3 was a 33-year old male, with height 51 inches. He exhibited prominent facial dysmorphism including hypertelorism, frontal bossing, down-slanting parpebral fissures and depressed nasal bridge (Figure 4.21). Skull x-rays showed hypoplastic mandibles and maxillary sinuses with significant peri-oral sclerosis. Prominent occiput and cleft palate was also observed. Selective tooth agenesis and impacted teeth were observed in OPG. Chest x-ray showed marked scoliosis with convexity to the right side. Segmentation abnormalities were noted in the dorsal spine (Figure 4.22). Fingernails were short, square and dystrophic. Pectus excavatum, mild scoliosis, narrow pelvis and short stature was observed. Mild mental retardation was also present.

Strikingly similar clinical and radiological abnormalities were observed in the other affected individual II-4. He was 38 years old with height 54 inches. He also presented with facial dysmorphism, short stature, anodontia, scoliosis, and chest deformities (Table 4.16).

### 4.5.2 Genetic and In Silico Findings

Variants obtained after exome sequencing of two affected individuals ((IV-2 and IV-6) were filtered using standard for variant filtration (Hashmi *et al.,* 2019). Non-synonymous variants in the coding region were selected. Variants with a frequency more than 0.01 in genetic variation databases were filtered out. Recessive variants which were predicted deleterious were then selected. (Table 4.17).

16 shortlisted variants were carefully analyzed, a known homozygous point mutation G>A in the *FLNA* gene transcript (ENST00000344736) on chromosome X was identified. This mutation (corresponding to rs137853317) is present on FLNA gene on chromosome X on position 153596246. It causes amino acid substitution R196W in the FLNA protein.

Primers were designed for the variant in the FLNA and the region flanking the variant was Sanger sequenced in all family members. Analysis of the data obtained confirmed that the variant was segregating in accordance with disease phenotype in the family (Figure 4.23). The variant was identified as disease-causing by prediction tools (Table 4.18).

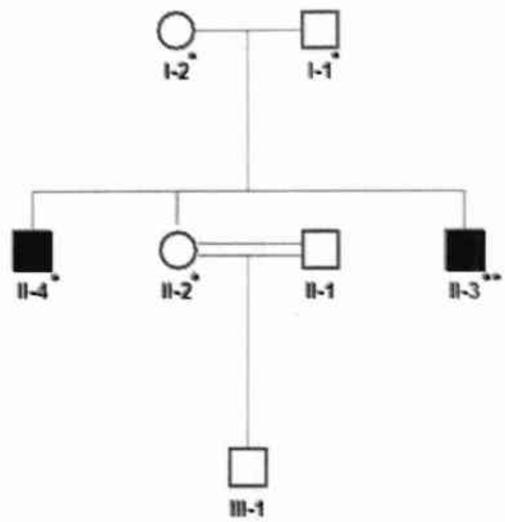


**Figure 4.24 Pedigree of Family-05**

Pedigree of a consanguineous Pakistani family segregating otopalatodigital syndrome-1 in an X-linked recessive manner. Asterisks indicate individuals who participated in the study.

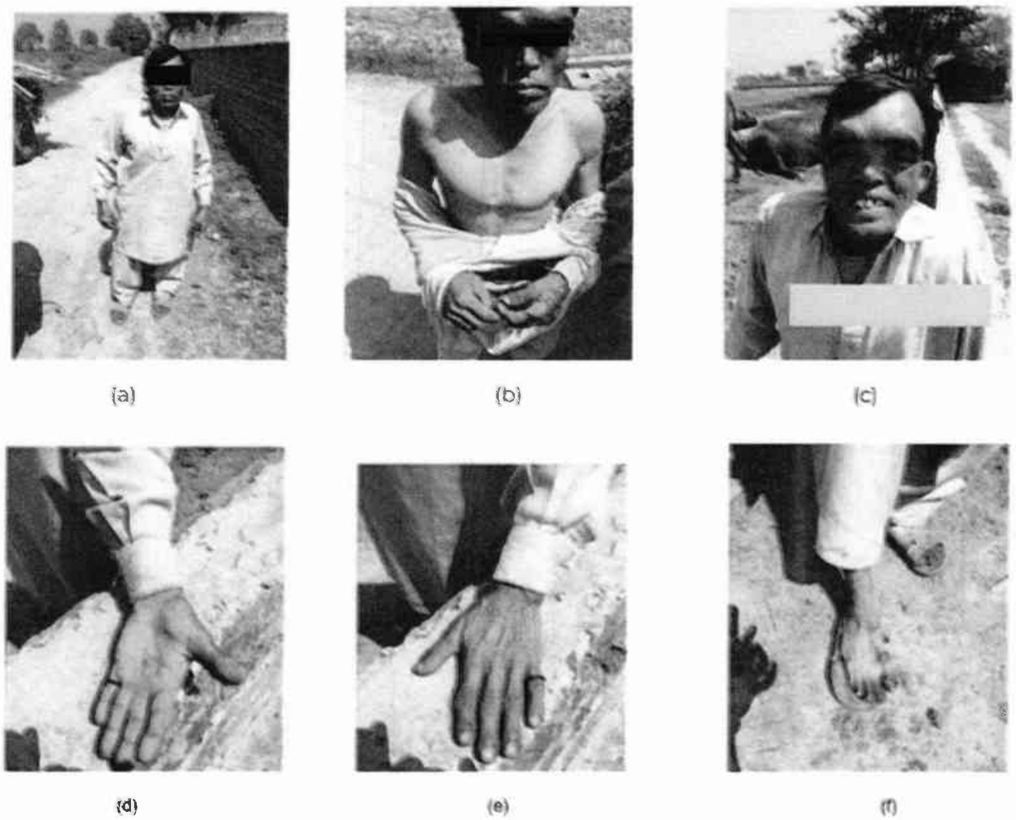


**Figure 4.25 Photographs of affected individual II-4 in Family-05**

(a, b, c)Photographs of individual II-4 showing short stature and distinct facial features. Facial dysmorphism including hypertelorism., prominent occiput, cleft palate and frontal bossing were observed. Pectus excavatum, mild scoliosis, narrow pelvis and short stature can also be seen.

(d, e, f)Photographs of hands and feet of individual II-4 showing short, square, dystrophic nails

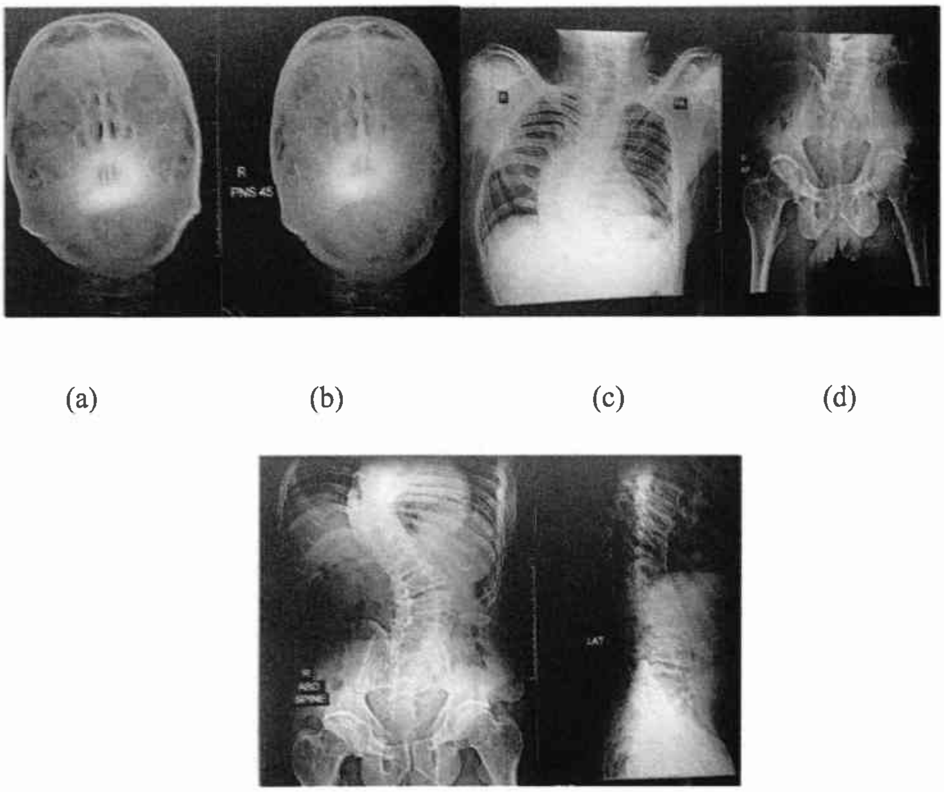

(a) (b) (c) (d)

(e) (f)

**Figure 4.26 Radiographs of affected individual IV-2 in Family-05**

(a, b) Skull x-rays showed hypoplastic mandibles and maxillary sinuses with significant peri-oral sclerosis. Prominent occiput and cleft palate was observed. (c, d, e, f) Chest x-ray showed marked scoliosis with convexity to the right side. Segmentation abnormalities were noted in the dorsal spine.

**Table 4.16 Comparison of clinical features in affected individuals of Family-05**

| | II-3 | II-4 |
|---|---|---|
| Gender | M | M |
| Age | 33 | 38 |
| Hypertelorism | + | + |
| Down-slanting Palpebral Fissures | + | + |
| Cleft Palate | + | + |
| Deafness | - | - |
| Digital anomalies | - | - |
| Chest Deformities | + | + |
| Ophthalmologic Findings | - | - |
| Anodontia | + | + |
| Depressed Nasal Bridge | + | + |
| Short Stature | + | + |
| Mild Mental Retardation | + | + |
| Pectus Excavatum | + | + |

(+) = presence of features; (-) = absence of features

**Table 4.17 Filtration steps used to search for the disease-causing variant after whole exome sequencing (WES) in Family-05**

| Filtration Steps | No. of variants detected |
|---|---|
| Total number of variants | 75,631 |
| Variants in coding region | 21,366 |
| Filter for non-synonymous variants | 9,545 |
| Rare variants (less than or equal to 1%) | 2,688 |
| Recessive variants (homozygous or compound heterozygous) | 439 |
| Predicted damaging | 16 |
| Related to the phenotype based on literature study | 1 |

**Table 4.18 Pathogenicity prediction of the shortlisted variant in *FLNA* gene using online tools.**

| Software | Score | Prediction | Comments |
|---|---|---|---|
| Mutation Taster | 0.99 | Deleterious | Known Disease Mutation |
| Panther | 0.793 | Disease | - |
| PhD-SNP | 0.746 | Disease | - |
| SNAP | 0.715 | Disease | - |

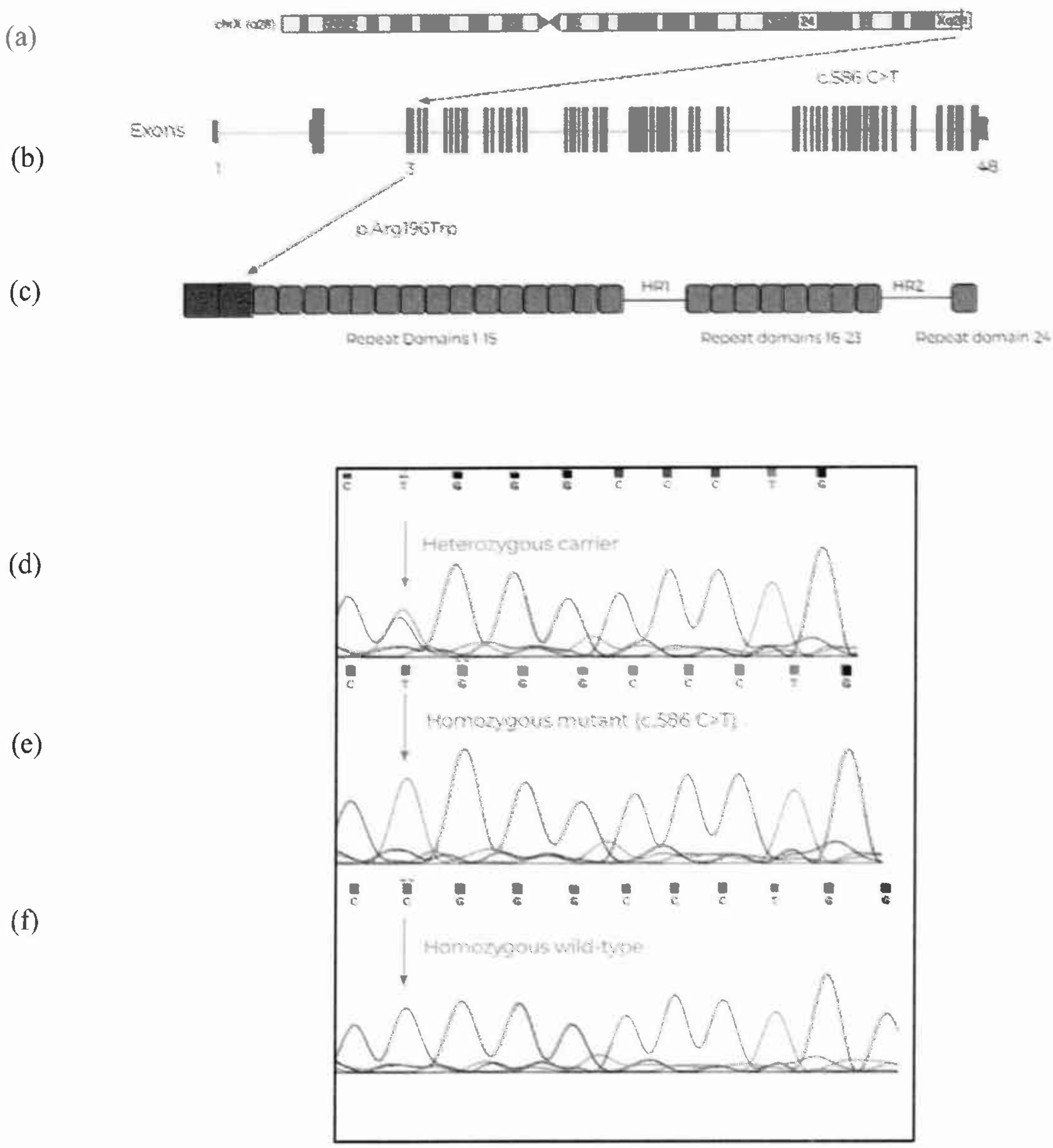


**Figure 4.27 Graphical representation of *FLNA* gene and FLNA protein, and partial chromatograms of *FLNA* gene**

(a) Representation of *FLNA* gene at chromosomal position Xp28 (Figure taken from UCSC Genome Browser)
(b) Representation of exons in *FLNA* gene. The mutation lies in the 3rd exon.
(c) Representation of the domains in FLNA protein (AB=Actin-Binding Domain; HR= Hinge Region). The mutation lies in the 2nd Actin-binding Domain.
(d) Chromatogram showing partial sequence of exon 3 of the *FLNA* gene in heterozygous mutant sequence (of I:2 and II:2).
(e) Chromatogram showing partial sequence of mutated exon 3 of the *FLNA* gene in individual II-4. Arrows mark the point of mutation.
(f) Chromatogram showing wild-type sequence of mutated exon 3 of the FLNA gene in individual I-1.

## 4.6 Family 6

A large family with several affected individuals was recruited from Hasan Abdal, Punjab. However, only two affected and three unaffected individuals consented to give blood (Figure 4.24).

### 4.6.1 Clinical Findings

The proband IV-9 was a 30 year old female with short stature (47 inches). She had a short neck and a broad, bulging chest. Pelvic region was severely displaced, and there was marked scoliosis in the thoracolumbar spine. Radiographic findings confirmed missing ribs and segmentation abnormalities (Figure 4.24). The findings were consistent with the diagnosis of spondylocostal dyostosis.

Individuals III-6, III-8 and III-10 also had markedly similar physical appearance and clinical presentation. They did not consent to radiographic testing or blood sampling.

III-4, the father of the proband had short stature (49 inches). He also had a short neck and bulging chest. Scoliosis and other radiographic anomalies were much milder.

### 4.6.2 Genetic Findings

Variants obtained after exome sequencing of IV:9 were filtered for pathogenic mutations. There were 28,651 variants in the coding region, out of which 13,157 were non-synonymous. Further filtration revealed that there were 3,709 rare variants (where the allele frequency was less than 1 percent in human genetic variation databases (1000 Genome, dbSNP, ExAc, gnomAD). Out of these, 446 variants were consistent with the autosomal recessive mode of inheritance observed in the family. Out of the 446 variants, 10 were predicted to be damaging (Table 4.19). Literature study helped to identify a novel homozygous frameshift deletion (TGGCC)>T, in *DLL3* gene as the most likely pathogenic variant. This mutation (c.1503_1506delGGCC, p.Ala502Argfs*45) is present in exon 7 of the *DLL3* gene on chromosome 19 on position 39998087. *DLL3* mutations have previously been implicated in spondylocostal dyostosis patients.

The variant was absent in 1000 Genomes Database, and Exome Aggregation Consortium (ExAc). Sanger sequencing revealed that IV:9 had a homozygous deletion mutation, while unaffected siblings of the proband were homozygous wild type.

### 4.6.3 In silico Findings

The variant was identified as disease causing through in silico tools (Table 4.20). The frameshift mutation introduces a premature stop codon, and a truncated protein with several important domains missing is produced (Figure 4.25). The missing domains are conserved in *DLL3* orthologues (Figure 4.26).

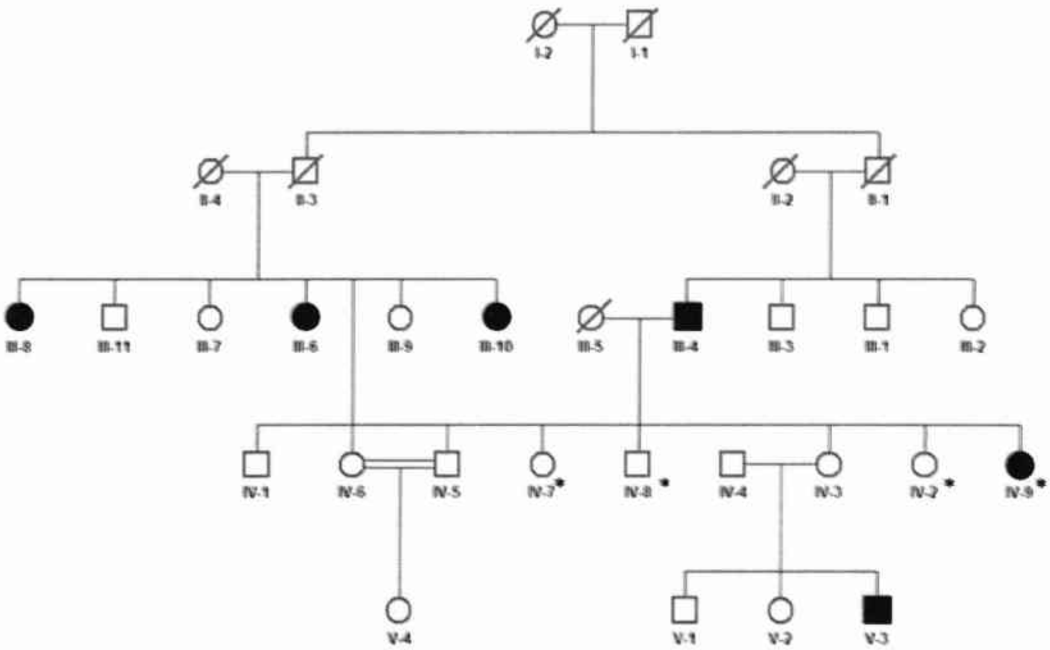

**Figure 4.28 Pedigree of Family-06**

Pedigree of a consanguineous family segregating spondylocostal dyostosis in an autosomal recessive manner. Asterisks represent the individuals available for study.

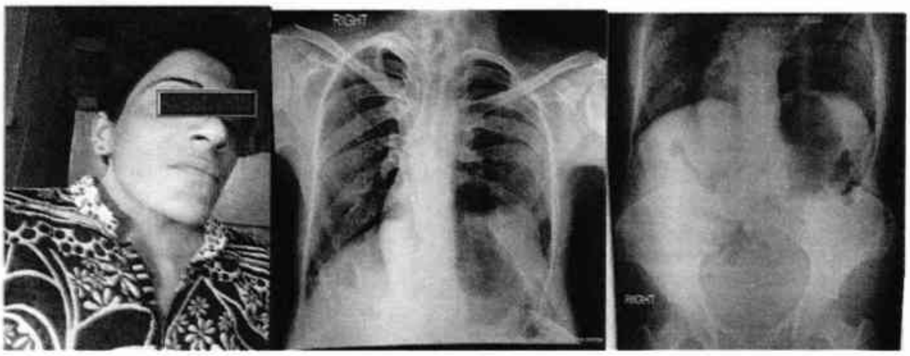

**(a)** **(b)** **(c)**

**Figure 4.29 Photographs and radiographs of Family-06**

a. Photograph of IV-9 showing short neck and broad, bulging chest

b. Pelvic and abdominal X-ray of IV-9 showing displaced pelvic region, scoliosis of thoracolumbar spine, and segmentation abnormalities in dorso-lumbar spine.

c. Chest X-ray of IV-9 showing compressed/missing ribs, scoliosis and segmentation abnormalities in spine.

**Table 4.19 Filtration steps used to search for the disease-causing variant after WES in Family-06**

| Filtration Steps | No. of variants detected |
|---|---|
| Total number of variants | 85,667 |
| Variants in coding region | 28,651 |
| Filter for non-synonymous variants | 13,157 |
| Rare variants (less than or equal to 1%) | 3,709 |
| Recessive variants (homozygous or compound heterozygous) | 446 |
| Predicted damaging | 10 |
| Related to the phenotype based on literature study | 1 |

**Table 4.20 Pathogenicity prediction of the shortlisted variant in *DLL3* gene using online tools.**

| Software | Score | Prediction | Comments |
|---|---|---|---|
| Mutation Taster | 1 | Deleterious | NMD<br>Frameshift<br>protein features (might be) affected<br>splice site changes |
| MutPred | 0.4 | Disease | - |

| | |
|---|---|
| Human Mutated: | Y L L P P A L G L L V R A W P A L R S C N S T C A A V A T P |
| Human Normal: | Y L L P P A L G L L V A A G V A G A A L L L V H V R R P G H |
| *P troglodytes:* | Y L L P P A L G L L V A A G V A G A A L L L V H V R R R G H |
| *M mulatta:* | Y L L P P A L G L L V A A G V A G A A L L L V H V R R R G H |
| *F catus:* | F L L P P A L G L L V A A G L A G T A L L L V H V R R R G P |
| *M musculus:* | F L L P P A L G L L V A A G L A G A A L L V I H V R R R G P |
| *L africana:* | F L L P P A L G L L V A A S F A G A V L W L I H L R R R G S |

**Figure 4.30 Multiple Sequence Alignment of DLL3 Protein**

Amino acid sequence comparison of DLL3 protein conservation of the mutated residues across different species. Conserved residues are shown in green.

**Figure 4.31 Structural models of wild-type and mutated DLL3 protein**

Structure of DLL3 protein (wild-type) on the left in pink color, and mutated, truncated DLL3 protein on the right in blue colour.

(a)
(b)
(c)
(d)

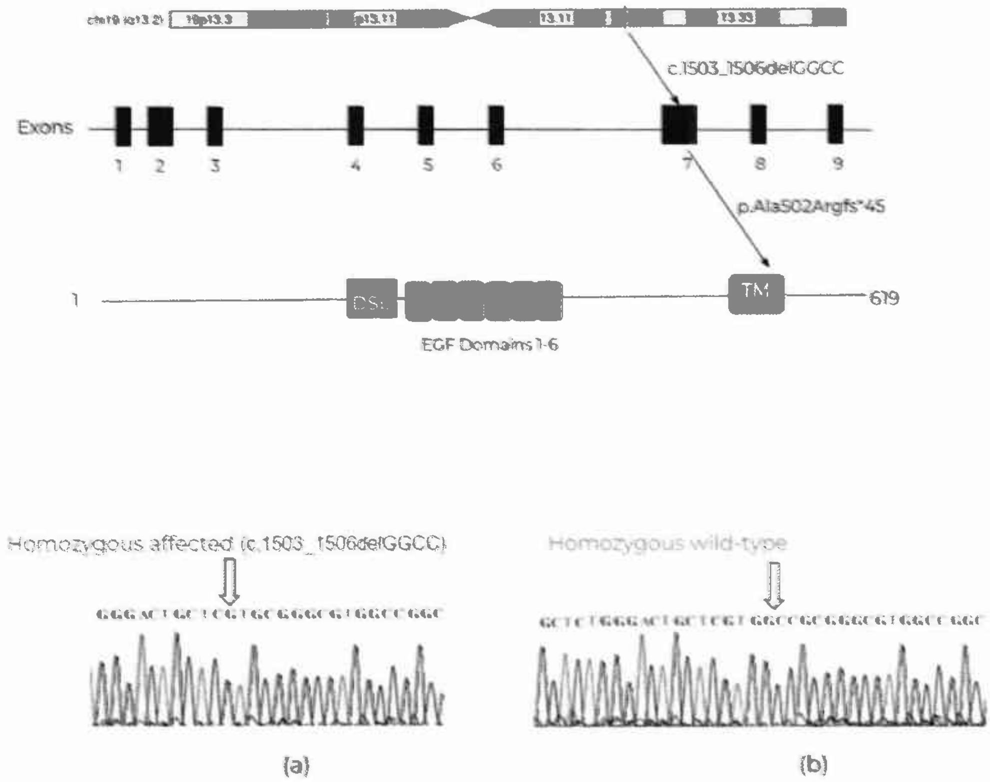


**Figure 4.32 Graphical Representation of *DLL3* gene andDLL3 protein, and partial chromatograms of *DLL3* gene**

(a) Representation of *DLL3* gene at chromosomal position 19q13.2 (Figure taken from UCSC Genome Browser)

(b) Representation of exons in *DLL3* gene. The mutation lies in the 7$^{th}$ exon.

(c) Representation of the domains in DLL3 protein (DSL = Delta/Serrate/LAG-2 domain; TM= Transmembrane domain). The mutation lies in the transmembrane domain.

(d) Chromatogram showing partial sequence of exon 7 of the *DLL3* gene. Sequence of homozygous deletion mutation in affected individuals IV:9 on the left, and homozygous wild type in unaffected individuals IV:2, IV:7 and IV:8 on the right. Mutation site is marked with an arrow.

## 4.7 Family 7

A family with two affected siblings and normal parents was recruited from Chakwal, Punjab (Figure 4.28).

### 4.7.1 Clinical Findings

Two siblings presented with non-syndromic post-axial polydactyly type A2. Both had an extra digit on the ulnar side of the left hand (Figure 4.28). Their parents were phenotypically normal.

### 4.7.2 Genetic and In silico Findings

Variants obtained after exome sequencing of two affected individuals (IV-4 and IV-5) were filtered for pathogenic mutations. Standard procedure was used for variants filtration (Hashmi *et al.,* 2019). Non-synonymous variants in the coding region were selected. Recessive variants which were predicted deleterious, and had a frequency of less than 0.01 in human genetic variation databases were filtered and studied (Table 4.21).

A variant (c.1158G>T, p.Lys386Asn) in the *LMBR1* gene (NM_022458.3) was identified as the most probable pathogenic variant in the family based on the previous reports of involvement of *LMBR1* variants in triphalangeal thumb and polydactyly.

The homozygous variant c.1158G>T in *LMBR1* changes an amino acid Lys to Asn at codon 386 in exon 14. It has not been reported in the large population cohorts (GenomAD). This variant is potentially damaging to the protein structure, function, or protein-protein interaction, according to a variety of lines of computational evidence (Table 4.22). In accordance with the recommendations of the American

College of Medical Genetics/Association for Molecular Pathology (ACMG/AMP), this variant is categorized as having uncertain significance. The mutated residue is highly conserved in orthologues (Figure 4.29).

The data from Sanger sequencing revealed that both parents are heterozygous and both affected siblings are homozygous for the variant (Figure 4.30).

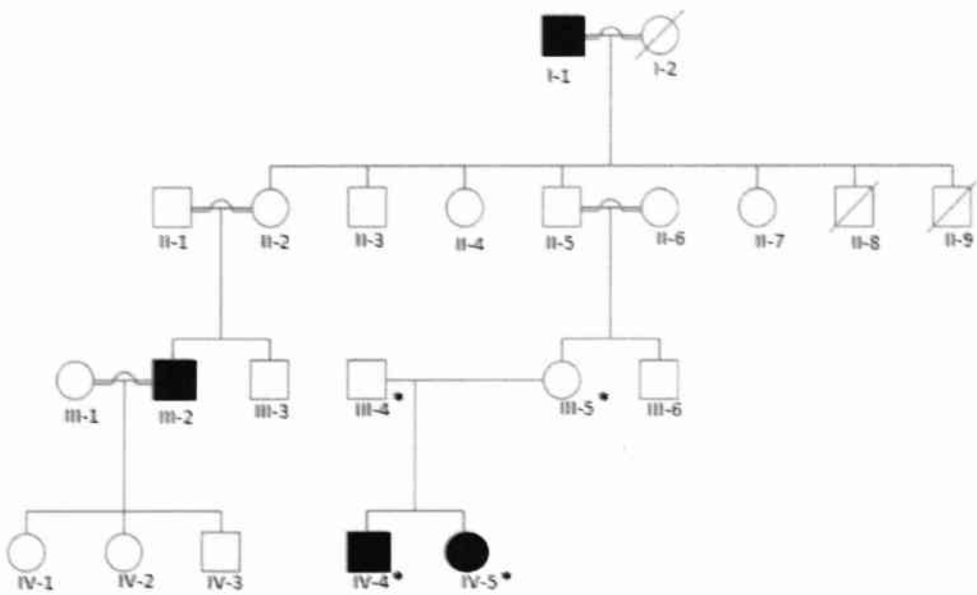


**Figure 4.33 Pedigree of Family-07**

Pedigree of a consanguineous family segregating non-syndromic polydactyly in an autosomal recessive manner. Asterisks mark the family members who participated in the study.

(a) (b)

**Figure 4.34 Photographs of Family-07**

a. Photograph of left hand of IV-4 showing an extra digit

b. Photograph of left hand of IV-5 showing an extra digit

**Table 4.21 Filtration steps used to search for the disease-causing variant after whole-exome sequencing (WES) in Family-07.**

| Filtration Steps | No. of variants detected |
|---|---|
| Total number of variants | 109,998 |
| Variants in coding region | 28,964 |
| Filter for non-synonymous variants | 17,229 |
| Rare variants (less than or equal to 1%) | 2,792 |
| Recessive variants (homozygous or compound heterozygous) | 261 |
| Predicted damaging | 38 |
| Related to the phenotype based on literature study | 1 |

**Table 4.22 Pathogenicity prediction of the shortlisted variant in *LMBR1* gene using online tools.**

| Software | Score | Prediction | Comments |
|---|---|---|---|
| Mutation Taster | - | Benign | - |
| Panther | 0.5 | Possibly damaging | - |
| PolyPhen-2 | 0.684 | Possibly Damaging | - |
| SNAP | 0.550 | Disease | - |

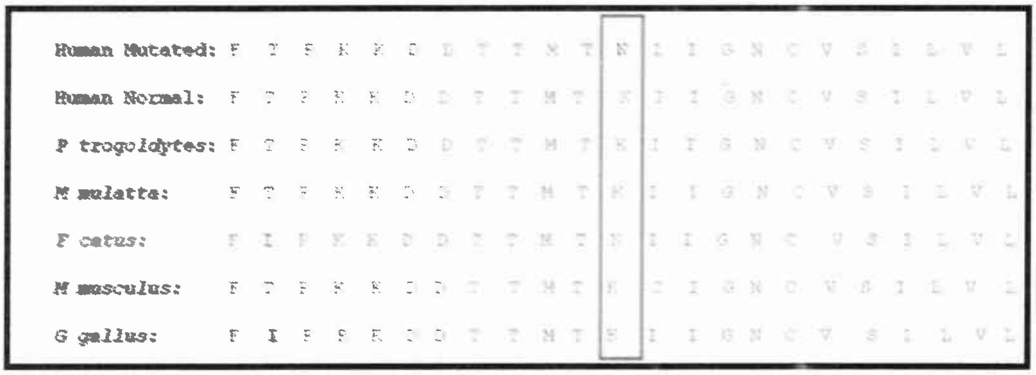


**Figure 4.35 Multiple sequence alignment of LMBR1 protein**

Amino acid sequence comparison of LMBR1 protein conservation of the mutated residues across different species. Conserved residues are shown in green. Lys/Asn at 386 is shown in the rectangle.

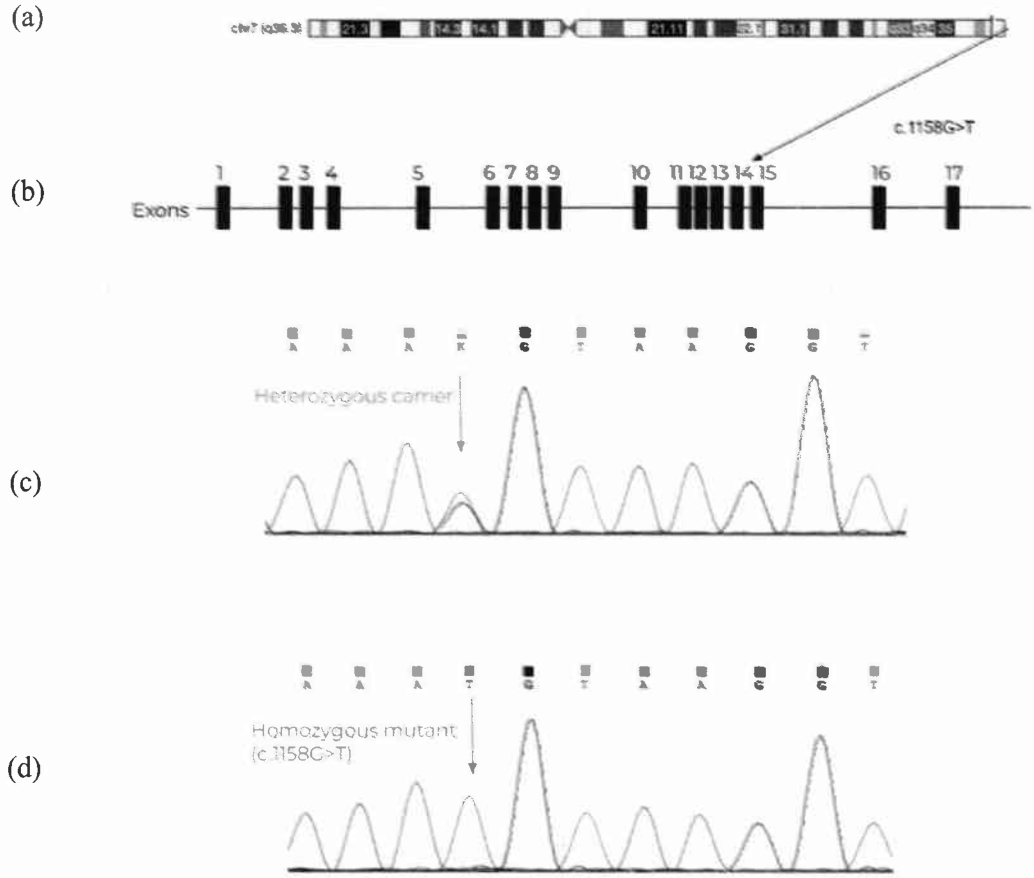


**Figure 4.36 Graphical representation and partial chromatograms of *LMBR1* gene**

(a) Representation of *LMBR1* gene at chromosomal position 7q36.3 (Figure taken from UCSC Genome Browser)

(b) Representation of exons in *LMBR1* gene. The mutation lies in the 14th exon.

(c) Chromatogram showing partial sequence of exon 14 of the *LMBR1* gene in heterozygous parents III:4 and III:5.

(d) Chromatogram showing partial sequence of exon 14 of the *LMBR1* gene in affected individuals IV:4 and IV:5. Mutation site is marked with an arrow.

## 4.8 Family 8

A large family of Karachi, Sindh Province segregating autosomal dominant achondroplasia was selected. All eight siblings and their father were affected (Figure 4.31).

### 4.8.1 Clinical Findings

All affected individuals had childhood-onset short stature, short long bones and distinct facial features including broad jaws and midface hypoplasia (Figure 4.31).

### 4.8.2 Genetic and In silico Analysis

Variants obtained after exome sequencing of two affected individuals (II-7 and II-8) were filtered for pathogenic mutations. Standard procedure was used for variants filtration (Hashmi *et al.,* 2019). Non-synonymous variants in the coding region were selected. Due to dominant mode of inheritance, heterozygous variants which were predicted deleterious, and had a frequency of less than 0.01 in human genetic variation databases were filtered and studied (Table 4.23).

A known heterozygous variant (c.1144G>A, p.Gly382Arg) in the *FGFR3* gene (NM_001163213.1) was identified in the family. The segregation of the variant was confirmed using Sanger Sequencing (Figure 4.32)

Amino acid changes identical to known pathogenic variant has been previously reported in autosomal dominant achondroplasia with established evidence (ClinVar ID:16327). The variant is located in a well-established functional domain and/or exonic hotspot where frequently reported pathogenic variants are present. Multiple in silico tools predict it to be pathogenic (Table 4.24).

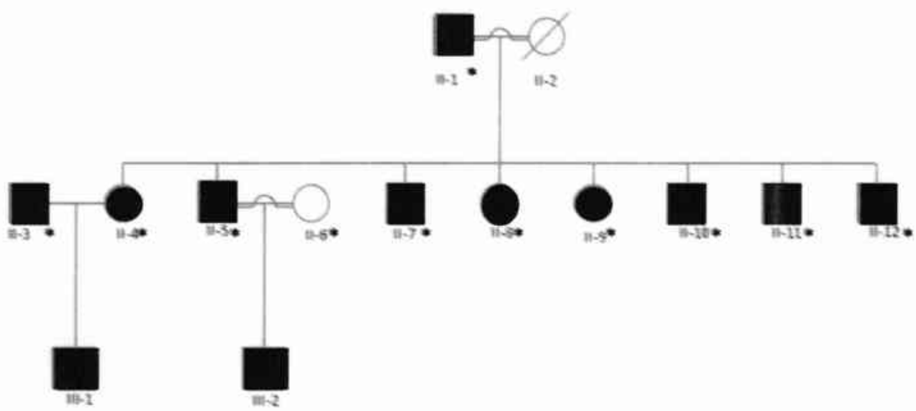


**Figure 4.37 Pedigree of Family-08**

Pedigree of a consanguineous Pakistani family segregating autosomal dominant achondroplasia. Asterisks mark the individuals who participated in the study.

**(b)** **(c)**

**Figure 4.38 Photographs of Family-08**

Photographs of individuals II:3 and II:4 showing distinct facial features including broad jaws and midface hypoplasia.

**Table 4.23 Filtration steps used to search for the disease-causing variant after whole exome sequencing (WES) in Family-08**

| Filtration Steps | No. of variants detected |
|---|---|
| Total number of variants | 108,067 |
| Variants in coding region | 28,585 |
| Filter for non-synonymous variants | 17,124 |
| Rare variants (less than or equal to 1%) | 2,992 |
| Recessive variants (homozygous or compound heterozygous) | 403 |
| Predicted damaging | 73 |
| Related to the phenotype based on literature study | 1 |

**Table 4.24 Pathogenicity prediction of the shortlisted variant in *FGFR3* gene using online tools.**

| Software | Score | Prediction | Comments |
|---|---|---|---|
| Mutation Taster | 0.99 | Pathogenic | - |
| Panther | 0.774 | Pathogenic | - |
| PhD-SNP | 0.921 | Pathogenic | - |
| SNAP | 0.550 | Pathogenic | - |

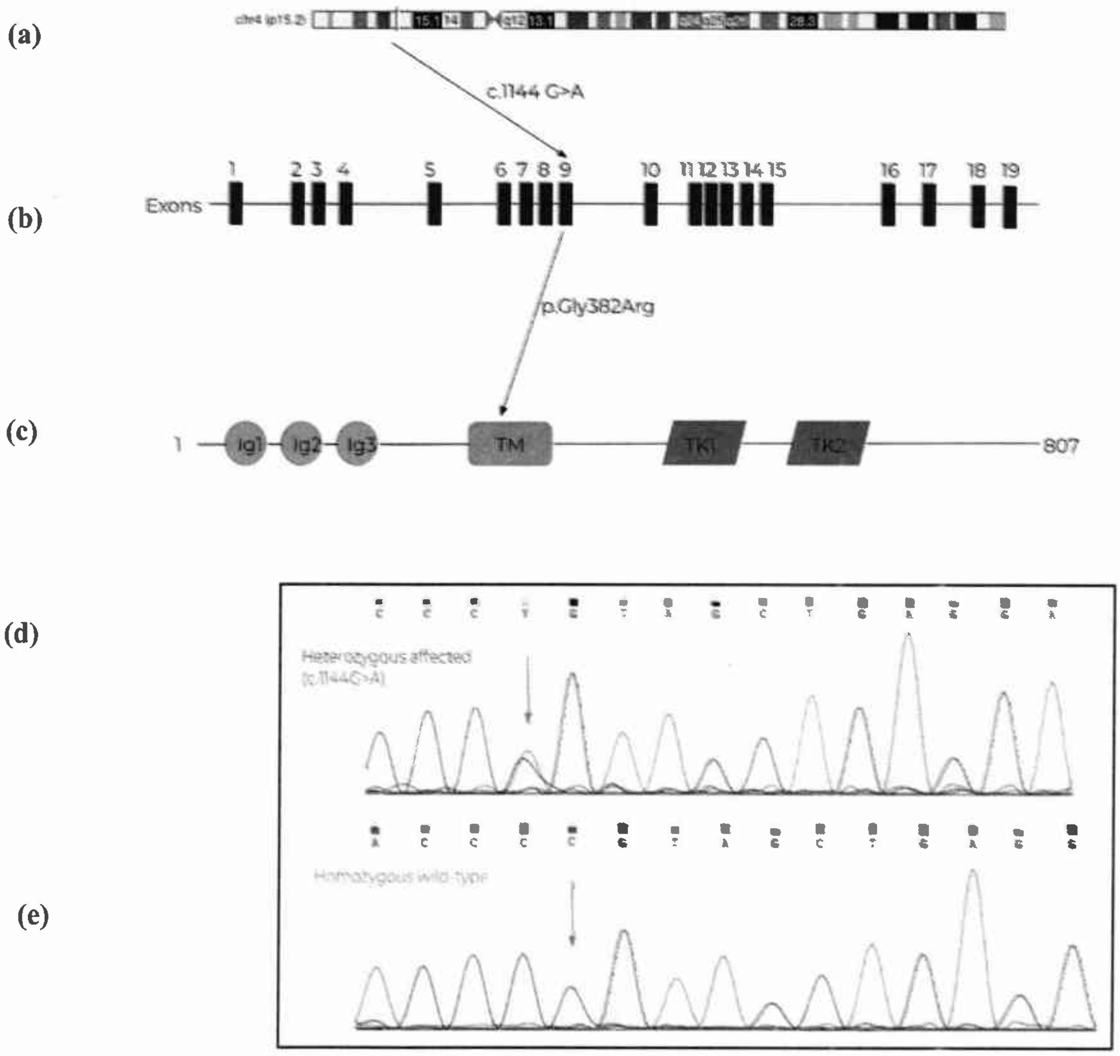


**Figure 4.39 Graphical representation of *FGFR3* gene and FGFR3 protein, and partial chromatograms of *FGFR3* gene**

(a) Representation of *FGFR3* gene at chromosomal position 4p15.2 (Figure taken from UCSC Genome Browser)

(b) Representation of exons in *FGFR3* gene. The mutation lies in the 9$^{th}$ exon.

(c) Representation of the domains in FGFR3 protein (Ig= Immunoglobulin like domain, TM= Transmembrane domain, TK=Tyrosine Kinase). The mutation lies in the transmembrane domain.

(d)Chromatogram showing partial sequence of exon 9 of the *FGFR3* gene in affected individuals (I:1, II:3, II:4, II:5, II:7 and II:8) with heterozygous dominant mutation

(e) Chromatogram showing partial sequence of wild-type individual II:6.

Arrows mark the point of interest.

# DISCUSSION

After clinical and genetic characterization, novel pathogenic variants were discovered in six families, whereas known pathogenic variants were identified in two families. In Family-01, we identify a novel pathogenic variant in DCC, as the cause of horizontal gaze palsy with progressive scoliosis-2 (HGPPS-2). In Family-02, we show that a novel variant in EVC causes EVC Syndrome with notable intra-familial phenotypic variations. The study on Family-03 shows that novel pathogenic variants in CUL7 cause 3M syndrome. In Family-04, we describe a novel mutation in FLNB causing spondylocarpotarsal synostosis syndrome in two brothers. In Family-06, we discovered a novel variant in DLL3 causing spondylocostal dyostosis. In Family-07, a novel variant in LMBR1 is believed to cause postaxial polydactyly. Finally, in Family-05 (otopalatodigital syndrome 2) and Family-08 (Autosomal dominant achondroplasia), we uncovered known mutations in *FLNA* and *FGFR3* gene respectively.

**Novel homozygous *DCC* mutations identified in HGPPS-2**

Horizontal Gaze Palsy with Progressive Scoliosis-2 with Impaired Intellectual Development (HGPPS-2) is an autosomal recessive disorder, characterized by childhood-onset progressive scoliosis and horizontal gaze palsy. Neurological symptoms include intellectual disability, absent hippocampal commissure, agenesis of the corpus callosum and delayed psychomotor development. It is reminiscent of the HGPPS phenotype caused by recessive mutation in *ROBO2* (Marsh *et al.,* 2019).

Jamuar *et al.* (2017) reported three HGPPS-2 patients from 2 unrelated consanguineous families. They identified two homozygous intragenic deletions (p.(Pro11Thrfs*15) and p.(Val263Alafs*36)) in the *DCC* gene, both resulting in premature termination and functional null alleles. The deletion in the first family was found by a combination of homozygosity mapping and CNV analysis; the deletion in the second family was found by targeted sequencing of the *DCC* gene. The pattern of inheritance in both the families was autosomal recessive (Jamuar *et al.*, 2017).

Family 1 in this study also has characteristic features of HGPPS-2. A comparison of clinical and radiological features present in patients in current study and previously reported patients having loss-of-function *DCC* mutations and HGPPS-2 phenotype is given in the Table 4.2.

We identified a novel biallelic *DCC* mutation in the affected members of the family. The identified autosomal recessive frameshift mutation (c.2399dupA, p.(Asn800Lysfs*11)) is a loss-of-function mutation resulted in premature truncation of the DCC protein. The mutation lies in a conserved region in the third firbronectin-3 domain. It results in the formation of a predicted protein that lacks the remaining fibronectin domains, transmembrane domain and intracellular Neogenin-C domain.

A netrin-1 receptor protein is encoded by the gene *DCC* (deleted in colorectal cancer). Belonging to the immunoglobulin superfamily of cell adhesion molecules, it is a single-pass transmembrane glycoprotein. The cytoplasmic tail of DCC protein interacts with the tyrosine kinases Src and focal adhesion kinase PTK2 to facilitate axon attraction. It has been proven that DCC contributes to the formation of the central nervous system (Keino-Masu, *et al.*, 1996; Srour, *et al.*, 2009).

Previous research has demonstrated the significance of *DCC* for forebrain and brainstem midline crossing in the human CNS (Jamuar *et al.,* 2017). It is believed that an imbalanced activation of the paraspinal muscles may be the cause of scoliosis. Spinal interneuronal circuit defects may cause the imbalance. Previous research has shown that Netrin-1 and *DCC*-deficient mice have impaired spinal interneuronal circuit function (Barallobre *et al.,* 2000). According to studies from mice with *DCC* mutations, alterations in the axon-guidance system can also result in spinal cord miswiring. There may not be adequate muscle innervations to give the spine the required biomechanical support if the two sides are not properly coordinated. Tracts in the hindbrain are vital in controlling conjugate horizontal eye movements, and midline axon guidance defects in them may cause horizontal gaze palsy in DSBS (Chan *et al.,* 2006; Renier *et al.,* 2010).

Congenital mirror motions and/or corpus callosum agenesis have previously been linked to heterozygous truncating variations in the DCC gene (Marsh *et al.*, 2017, Bierhals *et al.*, 2018; Vosberg, *et al.*, 2019). The heterozygous parents in this study have normal phenotypes; radiographic information on the parents was not available.

To comprehend the full developmental ramifications and phenotypic variability of biallelic mutations in the *DCC* gene, additional research is required. A better understanding of *DCC* mutations can help guide prenatal genetic testing and counselling of Pakistani families with a history of similar defects.

It is important to note that the *DCC* gene sequence variant (p.(Asn800Lysfs*11)), found in the family described here, is a novel and the first account of a mutation linked to HGPPS-2 in the Pakistani community (Zaka *et al.,* 2020).

**Novel homozygous EVC mutations identified in EVC Syndrome**

Ellis-van Creveld syndrome, often known as EvC Syndrome (OMIM #225500), is an autosomal recessive chondroectodermal dysplasia characterised by extra-skeletal traits such ectodermal and congenital cardiac problems as well as skeletal ones (Nguyen *et al.*, 2016). Most frequently, mutations in the *EVC* and *EVC2* genes are to blame for this syndrome (Tompson *et al.*, 2007). The bulk of the mutations introduce an early termination codon, which is likely to result in protein truncation and subsequent loss of function. Only 2.6 kb separates the *EVC* and *EVC2* genes from one another on chromosome 4p16.2 (Umm-e-Kalsoom *et al.*, 2010; D'Asdia *et al.*, 2013; Aziz *et al.*, 2016).

On chr4p16.2, the *EVC* gene spans a 103 kb area and codes for a 992 amino acid protein. The *EVC* gene product plays a role in skeletogenesis, ectodermal and mesodermal differentiation signalling, and control (Caparrós-Martin *et al.,* 2013; Valencia *et al.,* 2009). Additionally, a function in cardiogenesis has been suggested (Liu *et al.*, 2018; Ruiz Perez *et al.*, 2009).

A protein complex is formed at the base of the cilia by the direct interaction of the *EVC* and *EVC2* genes. The EVC/EVC2 complex has been demonstrated to be involved in the transduction of Sonic hedgehog signalling (Ruiz-Perez & Goodship, 2009; Louie *et al.,* 2020).

In cases of EvC syndrome, more than 80 *EVC* gene mutations have been described (Umair *et al.,* 2017; Umair *et al.,* 2019). Premature termination codons are generated by the bulk of the mutations. There have been very few in-frame deletions or missense mutations described (Tompson *et al.* 2007; Huang *et al.,* 2019).

In the present study, in Family 2, through exome sequencing, a homozygous 27 bp disruptive inframe deletion mutation has been identified. The 27bps deletion variation (c.731-757delTCCTTGACCTTCTTCCTAAAAGAAGT), which results in the deletion of 10 amino acids and the addition of a new proline residue in the EVC protein, is anticipated to maintain the integrity of the reading frame. It leads to the loss of 2 beta-turns in a beta-sheet. Loss of EVC/EVC2 interaction or formation of the unstable complex might lead to the EVC phenotype in this family (Zaka *et al.,* 2021).

Important characteristics of the reported family include incomplete penetrance and variable expressivity within individuals with the same genotype. Clinical heterogeneity within and across families is well-documented in the literature (Ulucan *et al.,* 2008; Ahluwalia *et al.,* 2009; Kousi & Katsanis, 2015). Our family stands out in demonstrating the varying expressivity of the EvC phenotype caused by pathogenic homozygous deletion mutations of the *EVC* gene in patients from the same family, when the diagnosis has been supported by genetic testing. The unstable association of the EVC/EVC2 complex and, as a result, the varied transduction of downstream Sonic hedgehog signalling may be the cause of the varying expressivity of phenotypic traits in these patients. The fact that the female affected participants in this study have more severe clinical characteristics than the male affected individuals is another crucial finding. While a female affected person (II-I) demonstrates several important phenotypic traits (polydactyly, genu valgum, short stature, cardiac abnormalities) of the syndrome, two affected males (II-2 and II-3) only displayed polydactyly/syndactyly, nail and dental phenotypic characteristics of EvC syndrome. Nail hypoplasia in all three siblings was less severe than it was in people with normal EvC syndrome. Dental abnormalities in all three siblings appeared as numerous oral frenula, malocclusion and enamel hypoplasia. For the individual (II-4) who passed away at the neonatal stage due to unidentified respiratory difficulties, complete clinical information and blood samples were not available. She had bilateral postaxial polydactyly similar to individual II-1. Her death may have been brought on by congenital heart defects and respiratory problems brought on by a narrow thorax, which are frequently cited as the leading cause of mortality in EvC infants (Akar *et al.,* 2002).

It is also interesting to note that a homozygous missense mutation in the *EVC* gene caused an unusually mild phenotype in a Turkish family (Ulucan *et al.,* 2008), suggesting a milder clinical manifestation in patients with restricted EVC protein activity (Rudnik-Schöneborn *et al.,* 2010). Discovery of a mild clinical subtype of EvC syndrome, by Piceci-Sparascio *et al.* (2020), resulting from hypomorphic *EVC* gene mutations is also noteworthy.

There are notable differences in phenotype and expressivity among polydactyly syndromes, including EvC syndrome, according to a number of genetic, molecular, and embryological investigations (Talamillo *et al.,* 2005; Lange & Muller, 2017). Several factors, including variations in modifier genes, incomplete penetrance, environmental impacts, and epigenetic factors, may contribute to the development of the differential phenotypes (Umair *et al.,* 2018). Additional research would bring responses to unanswered issues regarding the variable penetrance and expressivity of mutations, resulting in variable phenotypes between individuals with same genotype (Ahluwalia *et al.,* 2009; Kousi & Katansis, 2015).

The findings of this study have significance for clinical care and genetic counselling and widen the mutation spectrum of *EVC*. Family 2 presented in this study is noteworthy for revealing the heterogeneous expressivity of the EvC phenotype within the same family as a result of the homozygous deletion mutation in the *EVC* gene. The hypomorphic character of the mutation or the existence of additional modifiers could be the reason of the varied expressivity (Cooper *et al.*, 2013).

### *CUL7* mutations in 3M Syndrome

3M Syndrome is primarily characterized by prenatal and postnatal growth retardation. It also presents with other minor anomalies such as characteristic facial features and fleshy, prominent heels (Clayton *et al.*, 2012).

Mutations in three genes *CUL7*, *OBSL1* and *CCDC8* are known to cause 3M syndrome. It is hypothesized that all *CUL7* gene mutations result in disruption of the ubiquitination pathway, by preventing the cullin-7 protein from assembling the various components of the E3 ubiquitin ligase complex. All the genes associated with 3M syndrome are thought to produce proteins that help regulate other proteins involved in growth hormone response of the body (Sarikas *et al.*, 2008). 3M Syndrome can, therefore, be considered as a manifestation of the impaired response to growth hormones in the body. The exact relationship between *CUL7* gene mutations and the manifestations of 3M syndrome are not clear (Li *et al.*, 2014).

In *CUL7*, knockout mice models, intra-uterine placental and fetal growth and development is significantly restricted; and perinatal lethality attributed to respiratory distress is high (Arai *et al.*, 2003; Tsutsumi *et al.*, 2005). Knockout mice models highlight the importance of *CUL7* in growth regulation. Skeletal changes associated with prenatal and postnatal growth retardation in 3M syndrome suggest the involvement of *CUL7* in the endochondral ossification process (Sarikas *et al.*, 2008).

We identified a novel *CUL7* mutation (c.4493 T>C, p.Leu149Pro) in Family 3 in this study. The point mutation lies in the 24$^{th}$ exon of the *CUL7* gene. The mutated residue lies in the functionally important Cullin homology domain. The mutated Leucine residue is highly conserved in orthologues. When it is replaced by Proline, it causes a disruption in the alpha-helix, due to missing hydrogen bond.

Radiological features (such as slender long bones and tall vertebral bodies) common in 3M Syndrome patients were not present in our family. Characteristic facial features and prominent, fleshy heels were present. The intra-uterine death of three siblings in our family supports previous reports of intra-uterine deaths of 3M syndrome fetuses, though the finding is not conclusive, as genetic data of fetuses was not available. It is important to mention that the novel sequence variant (c.4493T>C; p.Leu1498Pro) in the *CUL7* gene, identified in this family, is only the third report of a *CUL7* mutation implicated in 3M Syndrome in the Pakistani population. Future studies are needed to shed more light on the developmental consequences of pathogenic, homozygous mutations in *CUL7* gene.

In silico studies also support the fact that L1498P variant in CUL7 is pathogenic variant, and it alters interactions between proteins involved in ubiquitination pathways.

### Novel *FLNB* mutation identified in Spondylocarpotarsal Synostosis Syndrome

Short height, fused vertebrae, and fused carpal and tarsal bones are characteristics of the Spondylocarpotarsal Synostosis Syndrome (SCT).

Clinodactyly, brachydactyly, decreased joint mobility, cleft palate, and dysmorphic facial characteristics are further skeletal defects observed in patients. Hypoplastic dental enamel and mixed hearing loss may also be seen in SCT individuals. (Yang *et al.,* 2017; Mangaraj *et al.,* 2017).

SCT can be passed from generation to generation by a *MYH3* variation or primarily through biallelic loss-of-function alleles of *FLNB* (Yang *et al.,* 2017; Mangaraj *et al.,* 2017). There are just 20 known families with members who have FLNB-related SCT (Salian *et al.,* 2018).

*FLNB* encodes filamin B, a 280 kDa multifunctional cytoplasmic protein. It is a member of the same protein family as filamins A and C. The modular design of the three filamins is strikingly similar to one another: 24 filamin repeat domains are preceded by two calponin homology domains (CHD), and interrupted by two tiny hinge regions (Figure 5.1). Calponin homology domains are the actin-binding domains (ABD). The filamins participate in multicellular processes like cell division and motility as well as signal transduction, small solute transport, communication between the intracellular and external environment, and supplying structure to the cell. Filamins control the structure and function of the cytoskeleton by organising actin into three-dimensional networks. Filamin B is an important component of cartilage growth and condensation of developing vertebrae (Mangaraj *et al.*, 2017).

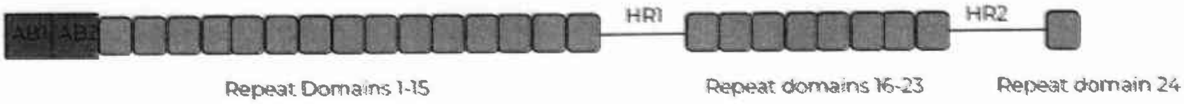


**Figure 5.1 Graphical representation of FLNB protein**

(AB = Actin-binding; HR = Hinge Region)

The *FLNB* variant c.3243C>A found in Family 3 introduces premature stop codon that affects the 9th repeat domain and, if translated, results in a shortened protein.

The truncation of *FLNB* in its repeat domains or the loss of function of protein have both been implicated in the development of SCT in the past. Previous research has demonstrated that variations in the actin-binding domain and repeat domain, specifically repeat regions 2, 3, 5, 6, 13, 14, 17, 19, 20, 22, and 24, are often responsible for SCT (Salian *et al.,* 2018). The fate of most frameshift *FLNB* variants has been found to be nonsense-mediated mRNA degradation. Hence, they result in complete absence of filamin B protein (Yang *et al.*, 2017).

The majority of affected individuals have short height, a short neck, scoliosis, and carpal fusion, whereas other disease manifestations are more diverse. Many of the clinical characteristics connected with SCT were present in the individuals in the current investigation. They had short necks and trunks, short statures, a modest form of facial dysmorphism, and gradual hearing loss. Along with these characteristics, there was scoliosis, lordosis, vertebral fusion, and synostosis of the carpal and tarsal bones. There was also capitate hamate synostosis. Patients in this study also had club foot, cleft palate, and enamel hypoplasia, which are less common SCT features.

Despite being a widely expressed intracellular protein, the discovery that a variety of *FLNB* mutations led to a number of unique skeletal dysplasias revealed a crucial function for filamin B in skeletal growth and development. It is still unclear how exactly these mutations cause disease. (Krakow *et al.,* 2004).

39 genetically defined autosomal recessive SCT patients from 18 families (including those given here) carrying 20 biallelic *FLNB* mutations have been identified thus far (Table 5.1). Most of these variants are nonsense or frameshift variants encoding a premature stop codon.

**Table 5.1 Mutations reported in *FLNB* gene in SCT Syndrome**

| **Exon** | **Variant** | **Reported by** |
|---|---|---|
| 1 | c.28G>T | Salian *et al*., 2018 |
| 2 | c.429delinsCT | Salian *et al*., 2018 |
| 7 | c.1204delG | Salian *et al*., 2018 |
| 7 | c.1243C>T | Salian *et al*., 2018 |
| 9-12 | c.1346-1372_1941+389del | Fukushima *et al*., 2012 |
| 10 | c.1493delA | Salian *et al*., 2018 |
| 10 | c.1592dup | Salian *et al*., 2018 |
| 13 | c.1945C>T | Krakow *et al*., 2004 |
| 16 | c.2452C>T | Krakow *et al*., 2004 |

| | | |
|---|---|---|
| 20 | c.2911dupG | Yasin *et al.*, 2021 |
| 21-24 | c.3127-353_4223-1836del | Fukushima *et al.*, 2012 |
| 21 | c.3243C>A | Present study |
| 27 | c.4671G>A | Farrington-Rock *et al.*, 2007 |
| 28 | c.4819C > T | Krakow *et al.*, 2004 |
| 33 | c.5548G > T | Farrington-Rock *et al.*, 2007 |
| 36 | c.6010C > T | Mitter *et al.*, 2008 |
| 38 | c.6317delC | Salian *et al.*, 2018 |
| 39 | c.6408delC | Krakow *et al.*, 2004 |
| 43 | c.7029 T > G | Krakow *et al.*, 2004 |
| 45 | c.7621dupG | Yang *et al.*, 2017 |

**Known *FLNA* variant identified in Otopalatodigital syndrome 1**

This is the first report of otopalatodgital syndrome in a Pakistani family. A rare collection of X-linked abnormalities known as otopalatodigital spectrum disorder (OPDSD) is brought on by mutations in the filamin A (*FLNA*) gene (Robertson *et al.*, 2007). It is made up of four clinically similar conditions: frontometaphyseal dysplasia (FMD), OMIM 302620; otopalatodigital syndrome type I (OPD type I); otopalatodigital syndrome type II (OPD type II); and Melnick-Needles syndrome (MNS), OMIM 309350. (Robertson *et al.,* 2007; Robertson *et al.,* 2019). Skeletal dysplasia of varying degree affecting both the axial and appendicular skeleton, together with several other skeletal defects, is the defining feature of these diseases (Robertson *et al.*, 2019). The mildest version of the spectrum in boys is OPD1. FMD is more severe, and the majority of OPD2 and MNS patients pass away in utero or in the first few weeks after birth. The phenotypic severity is relatively quite unpredictable in females (Robertson *et al.*, 2003).

The cytoskeletal protein filamin A is encoded by the *FLNA* gene. It is ubiquitously expressed in cells and necessary for membrane integrity as well as for signal transduction and the regulation of the actin cytoskeleton. Modulation of cell shape and migration relies heavily on remodelling of the cytoskeleton. Filamin A controls the remodelling and integrity of the actin cytoskeleton through its interaction with transmembrane receptor complexes, integrins and second messengers (Clark *et al.*, 2009).

Otopalatodigital syndromes are caused by *FLNA* gene mutations (Table 5.2), which are typically gain-of-functions alterations caused by missense mutations or minor deletions that do not change the reading frame (Robertson *et al.*, 2003; Clark *et al.*, 2009). The N-terminal acting binding domain of filament A binds F-actin (ABD). Two highly conserved calponin homology domains, CH1 and CH2, make up the ABD (Clark *et al.*, 2009). It has been observed that the mutations causing OPD type I are grouped near each other in the second calponin homology domain (CH2 domain) of the FLNA protein (Robertson *et al.*, 2003). CH2 domain is a functionally important domain, and mutations in this region are expected to change the activity of the protein, and disrupt the interaction of FLNA with F-actin. This leads to disturbance in signal transduction and cytoskeleton instability (Clark *et al.*, 2009).

The mutation in patients in Family 5 is in the second CH2 domain at amino acid position 196, and converts Arg to Trp. This mutation has been previously reported as a cause of both OPD1 and OPD2 (Robertson *et al.*, 2003; Kondoh *et al.*, 2007). The clinical characteristics of patients in this study are consistent with phenotypes described in OPD type I patients previously (Table 5.3).

Genotype-phenotype link between OPD I and OPD II is not usually obvious, according to prior reports. Both OPD I and II patients have been known to have filamin A mutations in the actin-binding domain (Robertson, 2005). An Arg196Trp substitution in filamin A was found in patients in a Japanese family having an OPD type 2 phenotype. Two other patients have been reported to have a mutation at the same position in *FLNA* as the patient in this study. However, one patient was classified as having OPD I since they only had cleft palates and deformed digits-—not short height or bowed bones (Robertson *et al.*, 2003). Another patient was identified as having OPD II due to a 586C to G mutation that resulted in an Arg196Gly substitution in filamin A (Robertson *et al.*, 2003). The patient's family had four other occurrences of OPD II, all with severe symptoms and deaths occurring between 21 days and 3.5 months after delivery, according to the original report by Andre *et al.* (1981). Therefore, in the three OPD patients with a mutation at 586C in FLNA, the phenotype-genotype connection was not discernible. A family with both OPD I and II individuals has also been observed (Horn *et al.*, 1995).

Even though OPD I and II are caused by similar or even identical *FLNA* mutations, their phenotypes are significantly distinct from one another. The pathophysiology of OPD-spectrum illnesses may involve one or more additional factors. Clarifying the molecular mechanisms underlying OPD-spectrum disorders will necessitate further study.

Clinical signs of OPD2 include abnormally moulded, bowed bones, brain anomalies in the posterior fossa, omphalocele, and heart problems (Fitch *et al.*, 1983; Verloes *et al.*, 2000). Compared to males with OPD2, males with OPD1 have a cleft palate and milder limb and bone abnormalities (Taybi, 1962; Dudding *et al.*, 1967). Female carriers of mutations causing both OPD1 and OPD2 often exhibit a milder phenotypic spectrum. Cardiac defects and omphalocoele (that are characteristic of OPD-2) were absent in this family. The heterozygous carrier females in this family appeared to be phenotypically normal, and did not display any of the phenotypic characteristics of OPD-1 and OPD-2.

**Table 5.2 Mutations reported in *FLNA* gene in OPD Spectrum disorders**

| Protein change | Domain | Reference |
|---|---|---|
| p.Gln170Pro | CH2 | Robertson *et al.*, 2003 |
| p.Leu172Phe | CH2 | Robertson *et al.*, 2003 |
| p.Asn187Ser | CH2 | Moutton *et al.*, 2016 |
| p.Arg196Gly/Trp | CH2 | Robertson *et al.*, 2003/ Kondoh *et al.*, 2007 |
| p.Cys205Arg | CH2 | Sankararaman *et al.*, 2013 |
| p.Pro207Leu | CH2 | Robertson *et al.*, 2003, Moutton *et al.*, 2016 |
| p.Glu245Lys | CH2 | Robertson *et al.*, 2006 |
| p.Asp253Glu | CH2 | Robertson *et al.*, 2006 |
| p.Glu254Lys | CH2 | Robertson *et al.*, 2003 |
| p.Ala273Pro | Repeat domains | Robertson *et al.*, 2003 |
| p.Asp1142Val | Repeat domains | Moutton *et al.*, 2016 |
| p.Pro1156Leu | Repeat domains | Fennell *et al.*, 2015 |
| p.Asp1159Ala | Repeat domains | Robertson *et al.*, 2006 |
| p.Ser1186Leu | Repeat domains | Robertson *et al.*, 2006 |
| p.Pro1223Leu | Repeat domains | Robertson *et al.*, 2006 |
| p.Val1249Ala | Repeat domains | Robertson *et al.*, 2006 |
| p.Ile1620del | Repeat domains | Robertson *et al.*, 2003 |
| p.Cys1723Trp | Repeat domains | Fennell *et al.*, 2015 |
| p.His1840Arg | Repeat domains | Moutton *et al.*, 2016 |

**Table 5.3 Comparison of clinical features of families with R196W mutation in FLNA protein**

| | Robertson *et al.*, (2003) | Kondoh *et al.*, (2007) | Present study |
|---|---|---|---|
| Sex of proband | M | M | M |
| Diagnosis | OPD1 | OPD2 | OPD1 |
| Number of affected individuals in family | 1 | 1 | 2 |
| Number of carrier females tested | 1 | 0 | 2 |
| Omphalocele | - | + | - |
| Perinatal death | - | - | - |
| Short stature | - | + | + |
| Bowed bones | - | + | - |
| Abnormal digits | + | + | - |
| Cleft palate | + | + | + |
| Hearing Impairment | - | + | - |
| Congenital Heart Defects | - | + | - |
| Characteristic Facial Features | NR | + | + |
| Ophthalmologic Findings | - | + | - |
| DNA | c.586C>T | c.586C>T | c.586C>T |
| Exon | 3 | 3 | 3 |
| Protein | R196W | R196W | R196W |

**Novel *DLL3* mutation identified in Spondylocostal Dyostosis**

Reduced stature caused by axial skeletal abnormalities characterizes the group of vertebral malsegmentation diseases known as spondylocostal dysostosis (SD, MIM 277300). Multiple hemivertebrae, rib fusions, deletions, and a non-progressive kyphoscoliosis are characteristics of SD. It results from mutations in DLL3 and other Notch signalling pathway genes (Turnpenny *et al.*, 2007).

There are eight coding exons in the *DLL3* gene. There are 24 known pathogenic mutations in *DLL3* that cause spondylocostal dyostosis (Table 5.4). Some of these variants include frameshift, nonsense, missense, and splicing site variants (Turnpenny *et al.,* 2007). Ethnic origin of spondylocostal dyostosis families with *DLL3* mutations reported in literature is presented in Table 5.5. The majority of the pathogenic variations in *DLL3* that have been found so far are projected to cause misfolded proteins, truncated proteins, or no protein at all due to nonsense-mediated decay (Bulman *et al.,* 2000, Bonafé *et al.,* 2003, Turnpenny *et al.,* 2003).

The human *DLL3* transcript produces a 618 amino acid protein (NP 058637.1) that is made up of a transmembrane domain (TM), six epidermal growth factor-like domains, and the delta-serrate-lag2 region (DSL) (Serth *et al*., 2015).

The DLL3 protein aids in the regulation of the Notch pathway, which is essential for the formation of vertebrae. Specifically, early somite segmentation is mediated by the DLL3 protein and the Notch pathway. Despite the fact that the precise process governing somite segmentation is still unknown, it appears to call on the activity of many Notch pathway proteins, including the NOTCH1 protein, to be switched on and off in a particular manner (Saga *et al.,* 2001). The NOTCH1 protein is sequestered or marked for degradation when the DLL3 protein attaches to it. (Bulman *et al.,* 2000)

*DLL3* is thought to play a significant part in the cell-signaling mechanisms that lead to the establishment of somite boundaries in animal models (Dunwoodie *et al.,* 2002, Kusumi *et al.,* 2004).

*DLL3* is modified in the X-ray-induced mouse mutant pudgy (pu), which has a variety of vertebrocostal defects that are comparable to SD symptoms (Kusumi et al., 1993). The first mutations in a human Delta homologue were found by Turnpenny *et al.* (1999), highlighting the significance of the Notch signalling cascade and its components in mammalian axial skeleton patterning.
The mutation in Family 6lies in a conserved region in the transmembrane domain, and is predicted to result in a truncated protein, lacking the intracellular domain. The clinical and radiographic abnormalities in the proband, such as short stature, scoliosis, missing ribs and segmentation abnormalities were consistent with those reported previously in spondylocostal dyostosis patients.

**Table 5.4 Mutations reported in *DLL3* in spondylocostal dyostosis**

| **Mutation** | **Domain** | **Reported by** |
|---|---|---|
| **Protein Truncating Mutations** | | |
| 215del128 | N-terminus | Turnpenny *et al.*, 2007 |
| 395delG | N-terminus | Turnpenny *et al.*, 2003 |
| 602delG | DSL | Turnpenny *et al.*, 2003 |
| 603ins5 | DSL | Bulman *et al.*, 2000 |
| 614ins13 | DSL | Turnpenny *et al.*, 2003 |
| 615delC | DSL | Bonafe *et al.*, 2003 |
| C207X | DSL | Turnpenny *et al.*, 2003 |
| 712C > T | EGF1 | Bonafe *et al.*, 2003 |
| 868del11 | EGF2 | Turnpenny *et al.*, 2003 |
| 945delAT | EGF3 | Bulman *et al.*, 2000 |
| 948delTG | EGF3 | Turnpenny *et al.*, 2003 |
| Q360X | EGF4 | Turnpenny *et al.*, 2007 |
| C362X | EGF4 | Turnpenny *et al.*, 2003 |
| 1256ins18 | EGF5 | Turnpenny *et al.*, 2003 |
| 1285-1301dup17 | EGF5 | Bonafe *et al.*, 2003 |
| 1365del17 | EGF6 | Turnpenny *et al.*, 2003 |
| 1418delC | C-terminus pre TM | Turnpenny *et al.*, 2003 |
| 1440delG | TM | Whittock *et al.*, 2004 |
| 1503delGGCC | TM | |
| **Missense Mutations** | | |
| C309Y | EGF2 | Sparrow *et al.*, 2002 |

| | | |
|---|---|---|
| C309R | EGF2 | Turnpenny *et al.*, 2007 |
| G325S | EGF2 | Turnpenny *et al.*, 2007 |
| G385D | EGF4 | Bulman *et al.*, 2000 |
| G404C | EGF4 | Turnpenny *et al.*, 2007 |
| G504D | TM | Whittock *et al.*, 2004 |

**Table 5.5 Ethnic origin of spondylocostal dyostosis families with *DLL3* mutations reported in literature**

| **Ethnic Origin** | **Number of families** |
|---|---|
| Pakistan | 7 |
| Middle East | 4 |
| Turkey | 5 |
| Northern Europe | 9 |
| Northern Europe - Turkey | 1 |
| Southern Europe | 1 |

## Novel *LMBR1* mutation identified in Polydactyly

In Family 7, a novel variant in exon 14 has been identified. The family has two affected siblings, presenting with non-syndromic postaxial polydactyly type A on the ulnar side of the left hand only. A conserved Lysine residue is changed to Alanine.

Polydactyly is one of several abnormal limb and digit phenotypes that *LMBR1* has frequently been linked to. Given that the open reading frame suggests a protein with nine predicted transmembrane domains and a coiled-coil domain, this protein is hypothesized to be a receptor protein in the plasma membrane. (Ianakiev *et al.,* 2000; Clark *et al.,* 2000)

Within an intron of this gene is a highly conserved, cis-acting regulatory module for the sonic hedgehog gene. Therefore, interruption of this genic area can change the expression of sonic hedgehog and impact limb patterning, although it is unknown if this gene has a direct role in limb development. Acheiropody and preaxial polydactyly are linked to chromosomal rearrangements and deletions and mutations in this genic region, which most likely appears to be a result of altered sonic hedgehog expression.

An autosomal recessive developmental condition called acheiropodia causes bilateral congenital amputations of the upper and lower extremities as well as hand and foot aplasia. The gene is located on chromosome 7q36. The acheiropodia phenotype suggests that the *LMBR1* gene likely contributes significantly to limb development (Ianakiev *et al.,* 2000). The 7q36 area was also linked to syndactyly type IV (SD4) and triphalangeal thumb-polysyndactyly syndrome (TPTPS), however pathogenic mutations in ZRS have not yet been confirmed. (Sun *et al.*, 2008)

**Known *FGFR3* mutation identified in Achondroplasia**

In Family 8, a large family segregating autosomal dominant achondroplasia, we have identified a known heterozygous variant (c.1144G>A, p.Gly382Arg) in the *FGFR3* gene (NM_001163213.1). This is the single nucleotide in the human genome that has been shown to be the most mutable so far. For an autosomal dominant disease, the homogeneity of the mutations in achondroplasia is unparalleled. This may also explain the relatively uniform phenotype of the disorder (Bellus *et al.,* 1995). All affected individuals have the classic phenotypic appearance of achondroplasia including childhood-onset short stature, short long bones and distinct facial features including macrocephaly, frontal bossing, broad jaws and midface hypoplasia.

Though most cases of achondroplasia are sporadic, this condition is inherited as an autosomal dominant characteristic. A gain-of-function mutation in the fibroblast growth factor receptor 3 (*FGFR3*) leads to achondroplasia (ACH). *FGFR3* gene lies on chromosome 4p16.3. The missense mutation p.Gly382Arg lies in a CpG doublet of the transmembrane domain of the FGFR3 protein. Numerous examples of achondroplasia have been described, and many of these cases are caused by recurrent mutations of a single amino acid in the transmembrane region of FGFR3 protein (Rousseau *et al.,* 1994; Shiang *et al.,* 1994).

Three extracellular immunoglobulin-like domains, a transmembrane hydrophobic domain, and a cytoplasmic tyrosine kinase domain make up the FGFR3 protein. The extracellular domains of the receptor bind the ligand and start a signalling cascade that regulates cell mitogenesis and differentiation. The formation of bones is governed by *FGFR3*, which binds both basic and acidic fibroblast growth hormone ligands. (Richette *et al.*, 2008)

By interacting with fibroblast growth factors, the extracellular component sets off a cascade of downstream signals that have an impact on mitogenesis and differentiation. Mutations in this gene are also responsible for cranial synostosis and a number of skeletal dysplasias (Xue *et al.*, 2014).

Lee *et al.*, (2017) generated an ACH mouse model by replacing the mouse *FGFR3*gene with human FGFR3$^{G380R}$ (FGFR3$^{ACH}$) cDNA. The phenotypes seen in ACH patients, are also seen in homozygous and heterozygous mice expressing human FGFR3$^{G380R}$. The mouse model provides a method for evaluating prospective treatments for skeletal dysplasias brought on by over activation of human FGFR3 as well as for more research into the underlying molecular pathways (Lee *et al.*, 2017).

**Conclusion**

The processes of bone formation and remodeling depend on complex networks, and genetic research on skeletal abnormalities has highlighted the signalling pathways involved. The majority of skeletal dysplasias are caused by monogenic mutations, thus they offer a great opportunity to learn more about the individual genes involved in skeletal development. The specifics of how these genes and their products interact in intricate networks are still being uncovered.

In this research consanguineous families with skeletal dysplasia were clinically and genetically characterized. The genetic analyses for all the families under study are based on WES technology. The data analysis presented here provided the evidence for the involvement of eight candidate genes (*DCC*, *EVC*, *FLNB*, *DLL*, *CUL7*, *FGFR3*, *FLNA* and *LMBR3)* in developing distinct forms of bone deformities. We have identified novel mutations in six genes (*DCC*, *EVC*, *FLNB*, *DLL*, *CUL7* and *LMBR3*) and also uncovered known mutations in *FGFR3* and *FLNA* genes (Table 5.6).

It is evident that whole genome sequencing (WGS) and whole exome sequencing (WES) can help us to quickly and accurately identify the causal variant for almost all Mendelian disorders—not just skeletal dysplasias. Technological advancements are rapidly altering the field of clinical genetics. The WGS strategy is presently the preferred one as it gradually becomes more cost-effective. An increase in the number of correctly identified genetic diagnoses will be possible by the development of new annotation and prediction tools that gather and interpret the data. The bioinformatic pipelines will be further improved with close cooperation between doctors, molecular biologists, and bioinformaticians. From the WGS data, we already have knowledge about structural abnormalities and sequence variants. It offers details on structural abnormalities and sequence variants together with evolutionary conservation, allele frequency, and in silico prediction tools to evaluate the variants in relation to the disease phenotype. Proteomics will also be important to determine whether genomic variants truly alter splicing and will contribute to genotype-phenotype correlations. Long-read sequencing is also an emerging RNA-sequencing technique.

We now know more about the pathophysiology of skeletal dysplasias and the functions of these genes in healthy skeletal development because of genetic research on monogenic illnesses. New research paints a picture of a complex network and identifies potential new medication targets for illnesses like osteoporosis, scoliosis, and arthritis as well as rare bone ailments that share the same or related pathogenetic pathways. The detailed mapping of genetic pathways, the description of the pathophysiological mechanisms behind skeletal illnesses, and the search for opportunities to create novel therapeutic approaches are some of the major areas for the future.

This research has provided selected families with their clinical and genetic diagnosis and shed light on the genetic basis for several of the skeletal dysplasias. The data presented here is valuable addition to genetic research and highly instrumental from both academic and community point of view. The novel clinical features and novel variants identified in the families allow a better understanding of underlying disease-associated pathways. It also aids the families in better understanding of genetic counselling based on the experimental evidence. In the future, this research will benefit experimental efforts to create and improve skeletal dysplasia treatments. Functional studies are needed to further elucidate the pathways involved in disease mechanisms. RNA level experiments and RT-PCR studies would also strengthen the findings.

**Table 5.6 Summary of pathogenic mutations identified in this thesis**

| Family | Gene | Mutation | Disease | Inheritance | Nature of Mutation |
|---|---|---|---|---|---|
| 01 | *DCC* | 16:c.2399dupA, p.(Asn800Lysfs*11) | HGPPS2 | AR | Novel mutation in novel gene (Zaka *et al.*, 2020) |
| 02 | *EVC* | 4:c.731_757delTCCTTGACCTTCTTCC TAAAAAGAAGT, p.Leu244_Ser253delinsPro | EvC Syndrome | AR | Novel mutation in known gene (Zaka *et al.*, 2021) |
| 03 | *CUL7* | 6:c.4493T>C, p.Leu1498Pro | 3M Syndrome | AR | Novel mutation in known gene |
| 04 | *FLNB* | 3:c.3243C>A, p.Cys1081* | SCT Synostosis Syndrome | AR | Novel mutation in known gene |
| 05 | *FLNA* | X:c.586C>T, p.Arg196Trp | OPD-1 | XR | Known mutation |
| 06 | *DLL3* | 19:c.1503_1506delGGCC, p.Ala502Argfs*45 | Spondylocostal Dyostosis | AR | Novel mutation in known gene |
| 07 | *LMBR1* | 7:c.1158G>T, p.Lys386Asn | Polydactyly | AR | Novel mutation in known gene |
| 08 | *FGFR3* | 4:c.1144G>A, p.Gly382Arg | Achondroplasia | AD | Known mutation |

# REFERENCES

Adams SL, Cohen AJ, Lassová L. Integration of signaling pathways regulating chondrocyte differentiation during endochondral bone formation. Journal of cellular physiology. 2007 Dec; 213(3):635-41.

Adzhubei I, Schmidt S, Peshkin L, Ramensky V, Gerasimova A, Bork P, Sunyaev S. PolyPhen-2: prediction of functional effects of human nsSNPs. Nature Methods. 2010 Apr; 7(4): 248–249.

Al-Fardan A, Al-Qattan MM. Wide-spread cone-shaped epiphyses in two Saudi siblings with Ellis-van Creveld syndrome. International journal of surgery case reports. 2017 Jan 1;39:212-7.

Almeida MR, Campos-Xavier AB, Medeira A, Cordeiro I, Sousa AB, Lima M, Soares G, Rocha M, Saraiva J, Ramos L, Sousa S. Clinical and molecular diagnosis of the skeletal dysplasias associated with mutations in the gene encoding fibroblast growth factor receptor 3 (FGFR3) in Portugal. Clinical genetics. 2009 Feb;75(2):150-6.

Assir MZ, Waseem T. Spondylocarpotarsal synostosis with hydromyelia, mega cisterna magna, and pachydermoperiostosis. Clinical Dysmorphology. 2012 Jul 1;21(3):144-7.

Aziz A, Raza SI, Ali S, Ahmad W. Novel homozygous mutations in the EVC and EVC2 genes in two consanguineous families segregating autosomal recessive Ellis–van Creveld syndrome. Clinical Dysmorphology. 2016 Jan 1;25(1):1-6.

Barbosa-Buck CO, Orioli IM, da Graça Dutra M, Lopez-Camelo J, Castilla EE, Cavalcanti DP. Clinical epidemiology of skeletal dysplasias in South America. American Journal of Medical Genetics Part A. 2012 May;158(5):1038-45.

Basit S, Naqvi SK, Wasif N, Ali G, Ansar M, Ahmad W. A novel insertion mutation in the cartilage-derived morphogenetic protein-1 (CDMP1) gene underlies Grebe-type chondrodysplasia in a consanguineous Pakistani family. BMC medical genetics. 2008 Dec;9(1):1-6.

Baujat G, Le Merrer M. Ellis-van Creveld syndrome. Orphanet journal of rare diseases. 2007 Dec;2(1):1-5.

Baumann G, Maheshwari H. The Dwarfs of Sindh: severe growth hormone (GH) deficiency caused by a mutation in the GH-releasing hormone receptor gene. Acta Paediatrica. 1997 Nov;86(S423):33-8.

Bennett RL. The practical guide to the genetic family history. John Wiley & Sons; 2011 Sep 20.

Bi W, Deng JM, Zhang Z, Behringer RR, De Crombrugghe B. Sox9 is required for cartilage formation. Nature genetics. 1999 May;22(1):85-9.

Bierhals T, Korenke GC, Baethmann M, Marín LL, Staudt M, Kutsche K. Novel DCC variants in congenital mirror movements and evaluation of disease-associated missense variants. European journal of medical genetics. 2018 Jun 1;61(6):329-34.

Bin JM, Han D, Sun KL, Croteau LP, Dumontier E, Cloutier JF, Kania A, Kennedy TE. Complete loss of netrin-1 results in embryonic lethality and severe axon guidance defects without increased neural cell death. Cell reports. 2015 Aug 18;12(7):1099-106.

Bitgood MJ, McMahon AP. Hedgehog and Bmp Genes are coexpressed at many diverse sites of cell–cell interaction in the mouse embryo. Developmental biology. 1995 Nov 1;172(1):126-38.

Blottner D, Salanova M, Püttmann B, Schiffl G, Felsenberg D, Buehring B, Rittweger J. Human skeletal muscle structure and function preserved by vibration muscle exercise following 55 days of bed rest. European journal of applied physiology. 2006 Jun;97(3):261-71.

Bonafe L, Cormier-Daire V, Hall C, Lachman R, Mortier G, Mundlos S, Nishimura G, Sangiorgi L, Savarirayan R, Sillence D, Spranger J. Nosology and classification of genetic skeletal disorders: 2015 revision. American journal of medical genetics Part A. 2015 Dec;167(12):2869-92.

Boycott KM, Vanstone MR, Bulman DE, MacKenzie AE. Rare-disease genetics in the era of next-generation sequencing: discovery to translation. Nature Reviews Genetics. 2013 Oct;14(10):681-91.

Brewster TG, Lachman RS, Kushner DC, Holmes LB, Isler RJ, Rimoin DL, Opitz JM, Reynolds JF. Oto-palato-digital syndrome, type II—an X-linked skeletal dysplasia. American journal of medical genetics. 1985 Feb;20(2):249-54.

Bulman MP, Kusumi K, Frayling TM, McKeown C, Garrett C, Lander ES, Krumlauf R, Hattersley AT, Ellard S, Turnpenny PD. Mutations in the human delta homologue, DLL3, cause axial skeletal defects in spondylocostal dysostosis. Nature genetics. 2000 Apr;24(4):438-41.

Caparrós-Martín JA, Valencia M, Reytor E, Pacheco M, Fernandez M, Perez-Aytes A, Gean E, Lapunzina P, Peters H, Goodship JA, Ruiz-Perez VL. The ciliary Evc/Evc2 complex interacts with Smo and controls Hedgehog pathway activity in chondrocytes by regulating Sufu/Gli3 dissociation and Gli3 trafficking in primary cilia. Human molecular genetics. 2013 Jan 1;22(1):124-39.

Carlson RV, Boyd KM, Webb DJ. The revision of the Declaration of Helsinki: past, present and future. British journal of clinical pharmacology. 2004 Jun;57(6):695-713.

Cassart M. Suspected fetal skeletal malformations or bone diseases: how to explore. Pediatric radiology. 2010 Jun;40(6):1046-51.

Castroviejo IP, Rodriguez-Costa T, Castillo F. Spondylo-thoracic dysplasia in three sisters. Developmental Medicine & Child Neurology. 1973 Jun;15(3):348-54.

Chen JH, Cao JL, Chu YL, Wang ZL, Yang ZT, Wang HL. T-2 toxin-induced apoptosis involving Fas, p53, Bcl-xL, Bcl-2, Bax and caspase-3 signaling pathways in human chondrocytes. Journal of Zhejiang University Science B. 2008 Jun;9(6):455-63.

Chen Y, Xue K, Zhang X, Zheng Z, Liu K. Exosomes derived from mature chondrocytes facilitate subcutaneous stable ectopic chondrogenesis of cartilage progenitor cells. Stem Cell Research & Therapy. 2018 Dec;9(1):1-4.

Clark RM, Marker PC, Kingsley DM. A novel candidate gene for mouse and human preaxial polydactyly with altered expression in limbs of Hemimelic extra-toes mutant mice. Genomics. 2000 Jul 1;67(1):19-27.

Clarke NF. Skeletal muscle disease due to mutations in tropomyosin, troponin and cofilin. InThe Sarcomere and Skeletal Muscle Disease 2008 (pp. 40-54). Springer, New York, NY.

Costantini A, Muurinen MH, Mäkitie O. New gene discoveries in skeletal diseases with short stature. Endocrine Connections. 2021 May 1;10(5):R160-74.

D'Asdia MC, Torrente I, Consoli F, Ferese R, Magliozzi M, Bernardini L, Guida V, Digilio MC, Marino B, Dallapiccola B, De Luca A. Novel and recurrent EVC and EVC2 mutations in Ellis-van Creveld syndrome and Weyers acrofacial dyostosis. European journal of medical genetics. 2013 Feb 1;56(2):80-7.

de Crombrugghe B, Lefebvre V, Nakashima K. Regulatory mechanisms in the pathways of cartilage and bone formation. Current opinion in cell biology. 2001 Dec 1;13(6):721-8.

Dighe M, Fligner C, Cheng E, Warren B, Dubinsky T. Fetal skeletal dysplasia: an approach to diagnosis with illustrative cases. Radiographics. 2008 Jul;28(4):1061-77.

Du X, Wang QR, Chan E, Merchant M, Liu J, French D, Ashkenazi A, Qing J. FGFR3 Stimulates Stearoyl CoA Desaturase 1 Activity to Promote Bladder Tumor Growth. Cancer research. 2012 Nov 15;72(22):5843-55.

Duynstee ML, Verwoerd-Verhoef HL, Verwoerd CD, Van Osch GJ. The dual role of perichondrium in cartilage wound healing. Plastic and Reconstructive Surgery. 2002 Sep 1;110(4):1073-9.

Erlebacher A, Filvaroff EH, Gitelman SE, Derynck R. Toward a molecular understanding of skeletal development. Cell. 1995 Feb 10;80(3):371-8.

Escamilla MA, DeMille MC, Benavides E, Roche E, Almasy L, Pittman S, Hauser J, Lew DF, Freimer NB, Whittle MR. A minimalist approach to gene mapping: locating the gene for acheiropodia, by homozygosity analysis. The American Journal of Human Genetics. 2000 Jun 1;66(6):1995-2000.

Farrington-Rock C, Kirilova V, Dillard-Telm L, Borowsky AD, Chalk S, Rock MJ, Cohn DH, Krakow D. Disruption of the Flnb gene in mice phenocopies the human disease spondylocarpotarsal synostosis syndrome. Human molecular genetics. 2008 Mar 1;17(5):631-41.

Fazeli A, Dickinson SL, Hermiston ML, Tighe RV, Steen RG, Small CG, Stoeckli ET, Keino-Masu K, Masu M, Rayburn H, Simons J. Phenotype of mice lacking functional deleted in colorectal cancer (Dec) gene. Nature. 1997 Apr;386(6627):796-804.

Fearon ER, Cho KR, Nigro JM, Kern SE, Simons JW, Ruppert JM, Hamilton SR, Preisinger AC, Thomas G, Kinzler KW, Vogelstein B. Identification of a chromosome 18q gene that is altered in colorectal cancers. Science. 1990 Jan 5;247(4938):49-56.

Fei Y, Gronowicz G, M Hurley M. Fibroblast growth factor-2, bone homeostasis and fracture repair. Current pharmaceutical design. 2013 Jun 1;19(19):3354-63.

Florencio-Silva R, Sasso GR, Sasso-Cerri E, Simões MJ, Cerri PS. Biology of bone tissue: structure, function, and factors that influence bone cells. BioMed research international. 2015 Oct;2015.

Foldynova-Trantirkova S, Wilcox WR, Krejci P. Sixteen years and counting: the current understanding of fibroblast growth factor receptor 3 (FGFR3) signaling in skeletal dysplasias. Human mutation. 2012 Jan;33(1):29-41.

Fox JW, Lamperti ED, Ekşioğlu YZ, Hong SE, Feng Y, Graham DA, Scheffer IE, Dobyns WB, Hirsch BA, Radtke RA, Berkovic SF. Mutations in filamin 1 prevent migration of cerebral cortical neurons in human periventricular heterotopia. Neuron. 1998 Dec 1;21(6):1315-25.

Geister KA, Camper SA. Advances in skeletal dysplasia genetics. Annual Review of Genomics and Human Genetics. 2015;16:199.

Gerber HP, Vu TH, Ryan AM, Kowalski J, Werb Z, Ferrara N. VEGF couples hypertrophic cartilage remodeling, ossification and angiogenesis during endochondral bone formation. Nature medicine. 1999 Jun;5(6):623-8.

Gurnett CA, Bowcock AM, Dietz FR, Morcuende JA, Murray JC, Dobbs MB. Two novel point mutations in the long-range SHH enhancer in three families with triphalangeal thumb and preaxial polydactyly. American journal of medical genetics Part A. 2007 Jan 1;143(1):27-32.

Hanson D, Murray PG, Sud A, Temtamy SA, Aglan M, Superti-Furga A, Holder SE, Urquhart J, Hilton E, Manson FD, Scambler P. The primordial growth disorder 3-M syndrome connects ubiquitination to the cytoskeletal adaptor OBSL1. The American Journal of Human Genetics. 2009 Jun 12;84(6):801-6.

Harada D, Yamanaka Y, Ueda K, Tanaka H, Seino Y. FGFR3-related dwarfism and cell signaling. Journal of bone and mineral metabolism. 2009 Jan;27(1):9-15.

Hecht JT, Francomano CA, Horton WA, Annegers JF. Mortality in achondroplasia. American journal of human genetics. 1987 Sep;41(3):454.

Helms, J.A., Schneider, R.A., 2003. Cranial skeletal biology. Nature May 15;423(6937):326-31.

Hidalgo-Bravo, A., Pompa-Mera, E.N., Kofman-Alfaro, S., Gonzalez-Bonilla, C.R. and Zenteno, J.C. A novel filamin A D203Y mutation in a female patient with otopalatodigital type 1 syndrome and extremely skewed X chromosome inactivation. American Journal of Medical Genetics Part A. 2005 July:136(2): 190-193.

Hodges E, Xuan Z, Balija V, Kramer M, Molla MN, Smith SW, Middle CM, Rodesch MJ, Albert TJ, Hannon GJ, McCombie WR. Genome-wide in situ exon capture for selective resequencing. Nature genetics. 2007 Dec;39(12):1522-7.

Huber C, Delezoide AL, Guimiot F, Baumann C, Malan V, Le Merrer M, Da Silva DB, Bonneau D, Chatelain P, Chu C, Clark R. A large-scale mutation search reveals genetic heterogeneity in 3M syndrome. European journal of human genetics. 2009 Mar;17(3):395-400.

Huber C, Dias-Santagata D, Glaser A, O'Sullivan J, Brauner R, Wu K, Xu X, Pearce K, Wang R, Uzielli ML, Dagoneau N. Identification of mutations in CUL7 in 3-M syndrome. Nature genetics. 2005 Oct;37(10):1119-24.

Hurst JA, Firth HV, Smithson S. Skeletal dysplasias. InSeminars in Fetal and Neonatal Medicine 2005 Jun 1 (Vol. 10, No. 3, pp. 233-241). WB Saunders.

Hussain R, Bittles AH. The prevalence and demographic characteristics of consanguineous marriages in Pakistan. Journal of biosocial science. 1998 Apr;30(2):261-75.

Ibarra-Ramirez M, Campos-Acevedo LD, Lugo-Trampe J, Martínez-Garza LE, Martinez-Glez V, Valencia-Benitez M, Lapunzina P, Ruiz-Peréz V. Phenotypic Variation in patients with homozygous c. 1678G> T mutation in EVC Gene: report of two mexican families with ellis-van creveld syndrome. The American Journal of Case Reports. 2017;18:1325.

Issack PS, Helfet DL, Lane JM. Role of Wnt signaling in bone remodeling and repair. HSS Journal®. 2008 Feb;4(1):66-70.

Iyama KI, Ninomiya Y, Olsen BR, Linsenmayer TF, Trelstad RL, Hayashi M. Spatiotemporal pattern of type X collagen gene expression and collagen deposition in embryonic chick vertebrae undergoing endochondral ossification. The Anatomical Record. 1991 Apr;229(4):462-72.

Jamuar SS, Schmitz-Abe K, D'Gama AM, Drottar M, Chan WM, Peeva M, Servattalab S, Lam AT, Delgado MR, Clegg NJ, Zayed ZA. Biallelic mutations in human DCC cause developmental split-brain syndrome. Nature genetics. 2017 Apr;49(4):606-12.

Jarcho S, Levin PM. Hereditary malformations of the vertebral bodies. Bull Johns Hopkins Hosp 1938, 62: 216-226.

Johnson JN, Hartman TK, Krych EH, Seferian EG, Ouellette Y. Tracheomalacia in siblings with otopalatodigital syndrome. American Journal of Medical Genetics Part A. 2008 May 15;146(10):1347-9.

Jumper J, Evans R, Pritzel A, Green T, Figurnov M, Ronneberger O, Tunyasuvunakool K, Bates R, Žídek A, Potapenko A, Bridgland A. Highly accurate protein structure prediction with AlphaFold. Nature. 2021 Aug;596(7873):583-9.

Karner CM, Long F. Wnt signaling and cellular metabolism in osteoblasts. Cellular and Molecular Life Sciences. 2017 May;74(9):1649-57.

Karsenty G, Wagner EF. Reaching a genetic and molecular understanding of skeletal development. Developmental cell. 2002 Apr 1;2(4):389-406.

Khan S, Ali RH, Abbasi S, Nawaz M, Muhammad N, Ahmad W. Novel mutations in natriuretic peptide receptor-2 gene underlie acromesomelic dysplasia, type maroteaux. BMC medical genetics. 2012 Dec;13(1):1-8.

Kim SJ, Lee SM, Choi JM, Jang JH, Kim HG, Kim JT, Cho JH, Sohn YB. Genetic analysis using a next generation sequencing-based gene panel in patients with skeletal dysplasia: a single-center experience. Frontiers in Genetics. 2021:737.

Kini U, Nandeesh BN. Physiology of bone formation, remodeling, and metabolism. InRadionuclide and hybrid bone imaging 2012 (pp. 29-57). Springer, Berlin, Heidelberg.

Knudsen TB, Kochhar DM. The role of morphogenetic cell death during abnormal limb-bud outgrowth in mice heterozygous for the dominant mutation Hemimelia-extra toe (Hmx).Development. 1981. 65 (Supplement): 289–307.

Koosha E, Eames BF. Two Modulators of Skeletal Development: BMPs and Proteoglycans. Journal of Developmental Biology. 2022 Apr 6;10(2):15.

Koziel L, Kunath M, Kelly OG, Vortkamp A. Ext1-dependent heparan sulfate regulates the range of Ihh signaling during endochondral ossification. Developmental cell. 2004 Jun 1;6(6):801-13.

Krakow D, Robertson SP, King LM, Morgan T, Sebald ET, Bertolotto C, Wachsmann-Hogiu S, Acuna D, Shapiro SS, Takafuta T, Aftimos S. Mutations in the gene encoding filamin B disrupt vertebral segmentation, joint formation and skeletogenesis. Nature genetics. 2004 Apr;36(4):405-10.

Ku CS, Wu M, Cooper DN, Naidoo N, Pawitan Y, Pang B, Iacopetta B, Soong R. Exome versus transcriptome sequencing in identifying coding region variants. Expert review of molecular diagnostics. 2012 Apr 1;12(3):241-51.

Langer Jr LO, Moe JH. A recessive form of congenital scoliosis different from spondylothoracic dysplasia. Birth defects original article series. 1975;11(6):83-6.

Laurin M, Canoville A, Germain D. Bone microanatomy and lifestyle: a descriptive approach. Comptes Rendus Palevol. 2011 Jul 1;10(5-6):381-402.

Lefebvre V, Bhattaram P. Vertebrate skeletogenesis. Current topics in developmental biology. 2010 Jan 1;90:291-317.

Lettice LA, Heaney SJ, Purdie LA, Li L, de Beer P, Oostra BA, Goode D, Elgar G, Hill RE, de Graaff E. A long-range Shh enhancer regulates expression in the developing limb and fin and is associated with preaxial polydactyly. Human molecular genetics. 2003 Jul 15;12(14):1725-35.

Li H, Durbin R. Fast and accurate short read alignment with Burrows–Wheeler transform. bioinformatics. 2009 Jul 15;25(14):1754-60.

Liu F, Liu X, Xu Z, Yuan P, Zhou Q, Jin J, Yan X, Xu Z, Cao Q, Yu J, Cheng Y. Molecular mechanisms of Ellis van Creveld gene variations in ventricular septal defect. Molecular Medicine Reports. 2018 Jan 1;17(1):1527-36.

Llambi F, Causeret F, Bloch-Gallego E, Mehlen P. Netrin-1 acts as a survival factor via its receptors UNC5H and DCC. The EMBO journal. 2001 Jun 1;20(11):2715-22.

Long F, Ornitz DM. Development of the endochondral skeleton. Cold Spring Harbor perspectives in biology. 2013 Jan 1;5(1):a008334.

Louie KA, Mishina Y, Zhang H. Molecular and cellular pathogenesis of Ellis-van Creveld syndrome: lessons from targeted and natural mutations in animal models. Journal of developmental biology. 2020 Oct 9;8(4):25.

Mackie EJ, Tatarczuch L, Mirams M. Thematic Review: The Skeleton: A Multi-Functional Complex Organ. The Growth Plate Chondrocyte and Endochondral Ossification. Journal of Endocrinology. 2011;211:109-21.

Maestrini E, Patrosso C, Mancini M, Rivella S, Rocchi M, Repetto M, Villa A, Frattini A, Zoppe M, Vezzoni P, Toniolo D. Mapping of two genes encoding isoforms of the actin binding protein ABP-280, a dystrophin like protein, to Xq28 and to chromosome 7. Human molecular genetics. 1993 Jun 1;2(6):761-6.

Maksimova N, Hara K, Miyashia A, Nikolaeva I, Shiga A, Nogovicina A, Sukhomyasova A, Argunov V, Shvedova A, Ikeuchi T, Nishizawa M. Clinical, molecular and histopathological features of short stature syndrome with novel CUL7 mutation in Yakuts: new population isolate in Asia. Journal of Medical Genetics. 2007 Dec 1;44(12):772-8.

Malik S. Polydactyly: phenotypes, genetics and classification. Clinical Genetics. 2014 Mar;85(3):203-12.

Mariani FV, Martin GR. Deciphering skeletal patterning: clues from the limb. Nature. 2003 May;423(6937):319-25.

Marie PJ, Miraoui H, Sévère N. FGF/FGFR signaling in bone formation: progress and perspectives. Growth Factors. 2012 Apr 1;30(2):117-23.

Marsh AP, Héron D, Edwards TJ, Quartier A, Galea C, Nava C, Rastetter A, Moutard ML, Anderson V, Bitoun P, Bunt J. Mutations in DCC cause isolated agenesis of the corpus callosum with incomplete penetrance. Nature genetics. 2017 Apr;49(4):511-4.

McGinnis W, Krumlauf R. Homeobox genes and axial patterning. Cell. 1992 Jan 24;68(2):283-302.

Miller JD, McKusick VA, Malvaux P, Temtamy S, Salinas C. The 3-M syndrome: a heritable low birthweight dwarfism. Birth defects original article series. 1975;11(5):39-47.

Miraoui H, Oudina K, Petite H, Tanimoto Y, Moriyama K, Marie PJ. Fibroblast growth factor receptor 2 promotes osteogenic differentiation in mesenchymal cells via ERK1/2 and protein kinase C signaling. Journal of Biological Chemistry. 2009 Feb 20;284(8):4897-904.

Mortier GR, Cohn DH, Cormier-Daire V, Hall C, Krakow D, Mundlos S, Nishimura G, Robertson S, Sangiorgi L, Savarirayan R, Sillence D. Nosology and classification of genetic skeletal disorders: 2019 revision. American Journal of Medical Genetics Part A. 2019 Dec;179(12):2393-419.

Mortier GR. The diagnosis of skeletal dysplasias: a multidisciplinary approach. European journal of radiology. 2001 Dec 1;40(3):161-7.

Mumtaz S, Riaz HF, Touseef M, Basit S, Haque MF, Malik S. Recurrent mutation in CDMP1 in a family with Grebe chondrodysplasia: broadening the phenotypic manifestation of syndrome in Pakistani population. Pakistan Journal of Medical Sciences. 2015 Nov;31(6):1542.

Murakami S, Balmes G, McKinney S, Zhang Z, Givol D, de Crombrugghe B. Constitutive activation of MEK1 in chondrocytes causes Stat1-independent achondroplasia-like dwarfism and rescues the Fgfr3-

deficient mouse phenotype. Genes & development. 2004 Feb 1;18(3):290-305.

Naski MC, Wang Q, Xu J, Ornitz DM. Graded activation of fibroblast growth factor receptor 3 by mutations causing achondroplasia and thanatophoric dysplasia. Nature genetics. 1996 Jun;13(2):233-7.

Nguyen TQ, Saitoh M, Trinh HT, Doan NM, Mizuno Y, Seki M, Sato Y, Ogawa S, Mizuguchi M. Truncation and microdeletion of EVC/EVC2 with missense mutation of EFCAB7 in Ellis-van Creveld syndrome. Congenital anomalies. 2016 Sep;56(5):209-16.

Ogata T, Matsuo N, Nishimura G, Hajikano H. Oto-palato-digital syndrome, type II: Evidence for defective intramembranous ossification. American journal of medical genetics. 1990 Jun;36(2):226-31.

Orioli IM, Castilla EE, Scarano G, Mastroiacovo P. Effect of paternal age in achondroplasia, thanatophoric dysplasia, and osteogenesis imperfecta. American journal of medical genetics. 1995 Nov 6;59(2):209-17.

Ornitz DM. FGF signaling in the developing endochondral skeleton. Cytokine & growth factor reviews. 2005 Apr 1;16(2):205-13.

Parla J, Kramer M, McCombie WR. High-throughput sequencing. InMicrobial forensics 2011 Jan 1 (pp. 461-478). Academic Press.

Parnell SE, Phillips GS. Neonatal skeletal dysplasias. Pediatric radiology. 2012 Jan;42(1):150-7.

Pauli RM. Achondroplasia: a comprehensive clinical review. Orphanet journal of rare diseases. 2019 Dec;14(1):1-49.

Penton AL, Leonard LD, Spinner NB. Notch signaling in human development and disease. InSeminars in cell & developmental biology 2012 Jun 1 (Vol. 23, No. 4, pp. 450-457). Academic Press.

Pérez-Andreu J, Ray VG, Arribas JM, Sánchez SJ. Ellis-van Creveld syndrome in adulthood: extending the clinical spectrum. Singapore medical journal. 2015 Jun;56(6):e110.

Rao MS, Sahu D, Kareem H, Devasia T, Shetty KK. Adult Survival in Ellis-van Creveld Syndrome with Common Atrium–A Rare Case Report. Journal of clinical and diagnostic research: JCDR. 2017 Aug;11(8):OD12.

Rimoin DL, Cohn D, Krakow D, Wilcox W, Lachman RS, Alanay Y. The skeletal dysplasias: clinical–molecular correlations. Annals of the New York Academy of Sciences. 2007 Nov;1117(1):302-9.

Robertson SP, Twigg SR, Sutherland-Smith AJ, Biancalana V, Gorlin RJ, Horn D, Kenwrick SJ, Kim CA, Morava E, Newbury-Ecob R, Ørstavik KH. Localized mutations in the gene encoding the cytoskeletal protein filamin A cause diverse malformations in humans. Nature genetics. 2003 Apr;33(4):487-91.

Rousseau F, Bonaventure J, Legeai-Mallet L, Pelet A, Rozet JM, Maroteaux P, Merrer ML, Munnich A. Mutations in the gene encoding fibroblast growth factor receptor-3 in achondroplasia. Nature. 1994 Sep;371(6494):252-4.

Ruiz-Perez VL, Goodship JA. Ellis–van Creveld syndrome and Weyers acrodental dysostosis are caused by cilia-mediated diminished response to hedgehog ligands. InAmerican Journal of Medical Genetics Part C: Seminars in Medical Genetics 2009 Nov 15 (Vol. 151, No. 4, pp. 341-351). Hoboken: Wiley Subscription Services, Inc., A Wiley Company.

Saga Y, Takeda H. The making of the somite: molecular events in vertebrate segmentation. Nature Reviews Genetics. 2001 Nov;2(11):835-45.

Sambrook J, Fritsch EF, Maniatis T. Molecular cloning: a laboratory manual. Cold spring harbor laboratory press; 1989.

Sarikas A, Xu X, Field LJ, Pan ZQ. The cullin7 E3 ubiquitin ligase: a novel player in growth control. Cell cycle. 2008 Oct 15;7(20):3154-61.

Savarirayan R, Rimoin DL. The skeletal dysplasias. Best practice & research Clinical endocrinology & metabolism. 2002 Sep 1;16(3):547-60.

Schkrohowsky JG, Hoernschemeyer DG, Carson BS, Ain MC. Early presentation of spinal stenosis in achondroplasia. Journal of Pediatric Orthopaedics. 2007 Mar 1;27(2):119-22.

Schuster SC. Next-generation sequencing transforms today's biology. Nature methods. 2008 Jan;5(1):16-8.

Semerci CN, Demirkan F, Özdemir M, Biskin E, Akin B, Bagci H, Akarsu NA. Homozygous feature of isolated triphalangeal thumb–preaxial polydactyly linked to 7q36: no phenotypic difference between homozygotes and heterozygotes. Clinical genetics. 2009 Jul;76(1):85-90.

Shiang R, Thompson LM, Zhu YZ, Church DM, Fielder TJ, Bocian M, Winokur ST, Wasmuth JJ. Mutations in the transmembrane domain of FGFR3 cause the most common genetic form of dwarfism, achondroplasia. Cell. 1994 Jul 29;78(2):335-42.

Shiang R, Thompson LM, Zhu YZ, Church DM, Fielder TJ, Bocian M, Winokur ST, Wasmuth JJ. Mutations in the transmembrane domain of FGFR3 cause the most common genetic form of dwarfism, achondroplasia. Cell. 1994 Jul 29;78(2):335-42.

Sim NL, Kumar P, Hu J, Henikoff S, Schneider G, Ng PC. SIFT web server: predicting effects of amino acid substitutions on proteins. Nucleic acids research. 2012 Jul 1;40(W1):W452-7.

Srour M, Rivière JB, Pham JM, Dubé MP, Girard S, Morin S, Dion PA, Asselin G, Rochefort D, Hince P, Diab S. Mutations in DCC cause congenital mirror movements. Science. 2010 Apr 30;328(5978):592-.

Stefanova M, Meinecke P, Gal A, Bolz H. A novel 9 bp deletion in the filamin a gene causes an otopalatodigital-spectrum disorder with a variable, intermediate phenotype. American Journal of Medical Genetics Part A. 2005 Feb 1;132(4):386-90.

Tang H, Zhang Q, Xiang J, Yin L, Wang J, Wang T. Whole exome sequencing aids the diagnosis of fetal skeletal dysplasia. Frontiers in Genetics. 2021 Mar 10;12:599863.

Temtamy SA, Aglan MS, Ashour AM, Ramzy MI, Hosny LA, Mostafa MI. 3-M syndrome: a report of three Egyptian cases with review of the literature. Clinical dysmorphology. 2006 Apr 1;15(2):55-64.

Tompson SW, Ruiz-Perez VL, Blair HJ, Barton S, Navarro V, Robson JL, Wright MJ, Goodship JA. Sequencing EVC and EVC2 identifies mutations in two-thirds of Ellis–van Creveld syndrome patients. Human genetics. 2007 Jan;120(5):663-70.

Trujillo-Tiebas MJ, Fenollar-Cortés M, Lorda-Sánchez I, Díaz-Recasens J, Carrillo Redondo A, Ramos-Corrales C, Ayuso C. Prenatal diagnosis of skeletal dysplasia due to FGFR3 gene mutations: a 9-year experience. Journal of assisted reproduction and genetics. 2009 Aug;26(8):455-60.

Tsutsumi T, Kuwabara H, Arai T, Xiao Y, DeCaprio JA. Disruption of the Fbxw8 gene results in pre-and postnatal growth retardation in mice. Molecular and cellular biology. 2008 Jan 15;28(2):743-51.

Turner DJ, Keane TM, Sudbery I, Adams DJ. Next-generation sequencing of vertebrate experimental organisms. Mammalian genome. 2009 Jun;20(6):327-38.

Turnpenny PD, Bulman MP, Frayling TM, Abu-Nasra TK, Garrett C, Hattersley AT, Ellard S. A gene for autosomal recessive spondylocostal dysostosis maps to 19q13. 1-q13. 3. The American Journal of Human Genetics. 1999 Jul 1;65(1):175-82.

Ullah A, Umair M, Muhammad D, Bilal M, Lee K, Leal SM, Ahmad W. A novel homozygous variant in BMPR1B underlies acromesomelic dysplasia Hunter–Thompson type. Annals of human genetics. 2018 May;82(3):129-34.

Umair M, Ahamd F, Bilal M, Asiri A, Younus M, Khan A. A comprehensive review of genetic skeletal disorders reported from Pakistan: a brief commentary. Meta Gene. 2019 Jun 1;20:100559.

Umair M, Khan S, Ahmad W. Homozygous sequence variants in the NPR2 gene underlying Acromesomelic dysplasia Maroteaux type (AMDM) in consanguineous families. Annals of Human Genetics. 2015 Jul;79(4):238-44.

Umair M, Shah K, Alhaddad B, Haack TB, Graf E, Strom TM, Meitinger T, Ahmad W. Exome sequencing revealed a splice site variant in the IQCE gene underlying post-axial polydactyly type A restricted to lower limb. European Journal of Human Genetics. 2017 Aug;25(8):960-5.

Umair M, Wasif N, Albalawi AM, Ramzan K, Alfadhel M, Ahmad W, Basit S. Exome sequencing revealed a novel loss-of-function variant in the GLI3 transcriptional activator 2 domain underlies nonsyndromic postaxial polydactyly. Molecular Genetics & Genomic Medicine. 2019 Jul;7(7):e00627.

Umlauf D, Frank S, Pap T, Bertrand J. Cartilage biology, pathology, and repair. Cellular and molecular life sciences. 2010 Dec;67(24):4197-211.

Unger S, Bonafé L, Gouze E. Current care and investigational therapies in achondroplasia. Current osteoporosis reports. 2017 Apr;15(2):53-60.

Vajo Z, Francomano CA, Wilkin DJ. The molecular and genetic basis of fibroblast growth factor receptor 3 disorders: the achondroplasia family of skeletal dysplasias, Muenke craniosynostosis, and Crouzon syndrome with acanthosis nigricans. Endocrine reviews. 2000 Feb 1;21(1):23-39.

Valencia M, Lapunzina P, Lim D, Zannolli R, Bartholdi D, Wollnik B, Al-Ajlouni O, Eid SS, Cox H, Buoni S, Hayek J. Widening the mutation spectrum of EVC and EVC2: ectopic expression of Weyer variants in NIH 3T3 fibroblasts disrupts Hedgehog signaling. Human mutation. 2009 Dec;30(12):1667-75.

Van der Wal G, Otten BJ, Brunner HG, Van der Burgt I. 3-M syndrome: description of six new patients with review of the literature. Clinical dysmorphology. 2001 Oct 1;10(4):241-52.

Vassy JL, Christensen KD, Schonman EF, Blout CL, Robinson JO, Krier JB, Diamond PM, Lebo M, Machini K, Azzariti DR, Dukhovny D. The impact of whole-genome sequencing on the primary care and outcomes of healthy adult patients: a pilot randomized trial. Annals of internal medicine. 2017 Aug 1;167(3):159-69.

Vortkamp A, Lee K, Lanske B, Segre GV, Kronenberg HM, Tabin CJ. Regulation of rate of cartilage differentiation by Indian hedgehog and PTH-related protein. Science. 1996 Aug 2;273(5275):613-22.

Vosberg DE, Beaulé V, Torres Berrío A, Cooke D, Chalupa A, Jaworska N, Cox SM, Larcher K, Zhang Y, Allard D, Durand F. Neural function in DCC mutation carriers with and without mirror movements. Annals of neurology. 2019 Mar;85(3):433-42.

Waller DK, Correa A, Vo TM, Wang Y, Hobbs C, Langlois PH, Pearson K, Romitti PA, Shaw GM, Hecht JT. The population-based prevalence of achondroplasia and thanatophoric dysplasia in selected regions of the US. American Journal of Medical Genetics Part A. 2008 Sep 15;146(18):2385-9.

Wang S, Zhang Z, Zhao J, Zhang X, Sun X, Xia L, Chang Q, Ye D, Jiang X. Vertical alveolar ridge augmentation with β-tricalcium phosphate and autologous osteoblasts in canine mandible. Biomaterials. 2009 May 1;30(13):2489-98.

Warman ML, Cormier-Daire V, Hall C, Krakow D, Lachman R, LeMerrer M, Mortier G, Mundlos S, Nishimura G, Rimoin DL, Robertson S. Nosology and classification of genetic skeletal disorders: 2010 revision. American journal of medical genetics Part A. 2011 May;155(5):943-68.

Wilkie AO. Bad bones, absent smell, selfish testes: the pleiotropic consequences of human FGF receptor mutations. Cytokine & growth factor reviews. 2005 Apr 1;16(2):187-203.

Wilkin DJ, Szabo JK, Cameron R, Henderson S, Bellus GA, Mack ML, Kaitila I, Loughlin J, Munnich A, Sykes B, Bonaventure J. Mutations in fibroblast growth-factor receptor 3 in sporadic cases of achondroplasia occur exclusively on the paternally derived chromosome. The American Journal of Human Genetics. 1998 Sep 1;63(3):711-6.

Williams ME, Lu X, McKenna WL, Washington R, Boyette A, Strickland P, Dillon A, Kaprielian Z, Tessier-Lavigne M, Hinck L. UNC5A promotes neuronal apoptosis during spinal cord development independent of netrin-1. Nature neuroscience. 2006 Aug;9(8):996-8.

Xu C, Yang X, Zhou H, Li Y, Xing C, Zhou T, Zhong D, Lian C, Yan M, Chen T, Liao Z. A novel ZRS variant causes preaxial polydactyly type I by increased sonic hedgehog expression in the developing limb bud. Genetics in medicine. 2020 Jan;22(1):189-98.

Xue Y, Sun A, Mekikian PB, Martin J, Rimoin DL, Lachman RS, Wilcox WR. FGFR3 mutation frequency in 324 cases from the International Skeletal Dysplasia Registry. Molecular genetics & genomic medicine. 2014 Nov;2(6):497-503.

Yasin S, Makitie O, Naz S. Spondylocarpotarsal synostosis syndrome due to a novel loss of function FLNB variant: a case report. BMC Musculoskeletal Disorders. 2021 Dec;22(1):1-6.

Zaka A, Shahzad S, Rao HZ, Hashim Y and Basit S. A novel homozygous frameshift mutation in the DCC gene in a Pakistani family with autosomal recessive horizontal gaze palsy with progressive scoliosis-2 with impaired intellectual development. American Journal of Medical Genetics Part A. 2020; 185(2), pp.355-361.

Zelzer E, Olsen BR. The genetic basis for skeletal diseases. Nature. 2003 May;423(6937):343-8.

Zenker M, Nährlich L, Sticht H, Reis A, Horn D. Genotype–epigenotype–phenotype correlations in females with frontometaphyseal dysplasia. American Journal of Medical Genetics Part A. 2006 May 15;140(10):1069-73.

# APPENDIX-1

## List of Mutations before the last filtration step in Family 1

**Supplementary Table 1:** Filtered homozygous recessive candidate variants from Patient IV:1

| | Gene | Ref | Alt | Amino Acid Substitution | Variant | Chr:Position (Hg19) | Average Allele Frequency | | Pathogenicity predictions | |
|---|---|---|---|---|---|---|---|---|---|---|
| | | | | | | | 1000 Genomes | ESP6500 | SIFT | Polyphen2 |
| *Missense* | FOXD6 | C | T | p.Pro386Ser | rs12092825 | 1:41,848,060 | NA | NA | NA | NA |
| | SAA1 | T | C | p.Val75Ala | rs1136747 | 11:18,290,874 | NA | NA | DAMAGING | DAMAGING |
| | MUC19 | G | T | p.Gly6927Cys | rs12822472 | 12:40,884,533 | NA | NA | NA | NA |
| | PRSS41 | C | G | p.Leu141Val | rs61747736 | 16:2,849,411 | 0.0017971 | NA | NA | NA |
| | PKD1 | C | T | p.Val3297Met | NA | 16:2,149,896 | NA | NA | DAMAGING | DAMAGING |
| | LOC400863 | C | T | p.Ser126Phe | rs768424 | 21:35,334,666 | NA | NA | NA | NA |
| | SYN2 | A | C | p.Thr36Pro | rs74213196 | 3:12,046,131 | NA | NA | NA | NA |
| | SYN2 | G | C | p.Ala34Pro | rs74900608 | 3:12,046,125 | NA | G:0.0058 | NA | NA |
| | MUC3A | T | C | p.Leu456Ser | rs79714278 | 7:100,550,786 | NA | NA | NA | NA |
| | MUC3A | A | C | p.Arg449Ser | NA | 7:100,550,766 | NA | NA | NA | NA |
| | CTAGE15 | A | G | p.Glu421Gly | rs62484910 | 7:143,270,172 | NA | NA | NA | NA |
| Frameshift | AIM1L | AGCAC | A | p.Gly536fs | NA | 1:26,671,538 | NA | NA | NA | NA |
| | AIM1L | GGGGCCCTTCAGGACCTCTTTCCAGGTGC | G | p.Leu524fs | NA | 1:26,671,544 | NA | NA | NA | NA |
| | AIM1L | GAAATGAGGCATCA | G | p.Pro538fs | NA | 1:26,671,522 | NA | NA | NA | NA |
| | OR2T35 | TCAGCACG | T | p.Cys203fs | rs143310547 | 1:248,801,944 | NA | NA | NA | NA |
| | OR2T35 | T | TCA | p.Ile320fs | rs370874870 | 1:248,801,602 | NA | NA | NA | NA |
| | MMP12 | G | GT | p.Thr211fs | rs5794199 | 11:102,738,793 | NA | NA | NA | NA |
| | VPS11 | T | TC | p.Tyr75fs | rs370939658 | 11:118,938,939 | NA | NA | NA | NA |
| | FAM186A | C | CCTGCTGAG | p.Gln1585fs | NA | 12:50,745,863 | NA | T:0.00126 | NA | NA |
| | FAM186A | T | TGA | p.Gln1585fs | NA | 12:50,745,861 | NA | NA | NA | NA |
| | MUC19 | TA | T | p.Lys5212fs | rs112524759 | 12:40,882,387 | NA | NA | NA | NA |
| | SLAIN1 | T | TGG | p.Leu75fs | rs201380414 | 13:78,272,267 | NA | NA | NA | NA |
| | RAI1 | AGC | A | p.Gln279fs | rs35068024 | 17:17,697,098 | NA | NA | NA | NA |
| | RAI1 | AG | A | p.Gln280fs | rs34083643 | 17:17,697,101 | NA | NA | NA | NA |
| | SARM1 | A | AGC | p.Gly182fs | rs374054341 | 17:26,708,296 | NA | NA | NA | NA |
| | SARM1 | GGT | G | p.Gly182fs | NA | 17:26,708,302 | NA | A:0.00143 | NA | NA |
| | **DCC** | **T** | **TA** | **p.Asn890fs** | **NA** | **18:50,912,450** | **NA** | **NA** | **NA** | **NA** |
| | UHRF1 | G | GC | p.Gly673fs | rs397767650 | 19:4,954,679 | NA | NA | NA | NA |
| | PRR21 | CCGTGGGTG | C | p.Phe111fs | NA | 2:240,982,059 | NA | NA | NA | NA |
| | MAML3 | GC | G | p.Gln502fs | rs373804083 | 4:140,811,083 | NA | G:0.00175 | NA | NA |
| | MAML3 | TGCTGCTGCTGC | T | p.Gln498fs | rs58287721 | 4:140,811,085 | NA | NA | NA | NA |
| | DCHS2 | TTTTG | T | p.Asn1365fs | rs140019361 | 4:155,244,401 | NA | NA | NA | NA |
| | ZNF595 | G | GA | p.Asp639fs | rs397952018 | 4:87,313 | 0.0091853 | NA | NA | NA |
| | NOP16 | C | CGT | p.Arg196fs | rs386358673 | 5:175,811,094 | NA | NA | NA | NA |
| | GRIFIN | G | GC | p.Ala58fs | rs397976651 | 7:2,516,392 | NA | G:0.0006 | NA | NA |
| Splice site | KRTAP4-1 | ACGGCAGCAGCTGGACATACCACAGCTGG | A | p.Cys83_Arg8 | rs71155126 | 17:39,340,795 | NA | NA | NA | NA |
| | SLC6A6 | CT | C | NA | rs67559364 | 3:14,444,329 | NA | G:0.0010 | NA | NA |
| | ZNF595 | TC | T | NA | rs67594632 | 4:86,034 | NA | NA | NA | NA |

## List of Mutations before the last filtration step in Family 2

| | Gene | Ref | ALT | AA Substitute | Variant | Chr position | 1000Gp | ESP6500 | SIFT | Polyphen |
|---|---|---|---|---|---|---|---|---|---|---|
| 1 | | | | | | | | | | |
| 2 | | | | | | | | | | |
| 3 | AFAP1L2 | C | CCCG | p.Leu110dup | rs7492817! | 116,085,784 | . | | | |
| 4 | AGAP3 | GTCT | G | p.Val31_Cys32delins | | 150,783,919 | . | | | |
| 5 | AR | T | TGCA | p.Gln80dup | rs3032358 | 66,765,158 | . | | | |
| 6 | C1orf177 | GC | G | p.Arg306fs | | 55,279,635 | . | | | |
| 7 | C20orf96 | T | TA | | rs3835237 | 271,225 | . | | | |
| 8 | CDCA2 | G | T | p.Gly569Val | rs1158295E | 25,360,923 | 0.000599 | T:0.001744 | D;D | D;D;D |
| 9 | CDCP2 | T | TGGG | p.Pro408dup | | 54,605,318 | . | | | |
| 10 | CRIPAK | G | GTGCCCATGTGGAGTGCCCGCCTGC | p.Cys27fs | | 1,388,350 | . | | | |
| 11 | CTAGE5 | GTA | G | | rs5487238 | 39,784,004 | . | | | |
| 12 | DCHS2 | TTTTG | T | p.Asn1365fs | rs1400193E | 155,244,401 | . | | | |
| 13 | DGKK | A | AG | p.Leu1021fs | rs11415534 | 50,121,146 | . | A:0.00000 | | |
| 14 | EVC | CTCCTTGACCTTCTTCCTAAAAAGAAGT | C | p.Leu244_Ser253de | rs5298188 | 5,743,470 | 0.000799 | | | |
| 15 | FDFT1 | GTCCCAC | G | p.His76_Ser77del | rs71711801 | 11,666,218 | . | | | |
| 16 | GOLGA8H | T | C | p.Cys488Arg | rs1995297( | 30,906,066 | . | | | |
| 17 | GRIFIN | G | GC | p.Ala58fs | rs3979766 | 2,515,382 | . | G:0.00063 | | |
| 18 | HOMEZ | ACAT | A | p.Asp545del | rs1480055: | 23,744,800 | . | | | |
| 19 | HRNR | C | CAG | p.Gly2765fs | | 152,185,812 | . | | | |
| 20 | IQSEC1 | GC | G | | rs3979887 | 12,942,850 | . | GC:0.0013! | | |
| 21 | KDM6B | T | TACCACC | p.Pro263_Pro264du | rs6146244: | 7,750,177 | . | | | |
| 22 | KRTAP4-1 | ACGGCAGCAGCTGGACATACCACAGCTGGGGTGGCAGG | A | p.Cys83_Arg85del | rs71155126 | 39,340,795 | . | | | |
| 23 | KRTAP5-1 | ACCACAGCCACCCTTGGATCCCCCACAAGAG | A | p.Ser111_Gly120del | | 1,606,120 | . | ACCACAG | | |
| 24 | KRTAP5-2 | ACCCCCACAGGAGCCACAGCCCCCCTTGGAG | A | p.Ser94_Gly103del | rs5950644 | 1,619,172 | . | | | |
| 25 | KRTAP5-5 | A | AGGCTGTGGCTCC | p.Gly43_Gly46dup | rs7102576: | 1,651,199 | . | | | |
| 26 | LOC40086 | C | T | p.Ser126Phe | rs766424 | 35,334,666 | . | | | |
| 27 | LOC44115! | A | G | p.Thr720Ala | rs2653988 | 66,014,572 | . | | | |
| 28 | MAFA | ATGG | A | p.His208del | rs14181687 | 144,511,953 | . | | | |
| 29 | MAP1A | C | T | p.Ala2527Val | rs5443296 | 43,821,251 | 0.0002 | | D;D;D | D |
| 30 | MAP3K4 | CCTG | C | p.Ala1199del | rs11380138 | 161,519,350 | . | | | |
| 31 | MIR205HG | TAGCAGCAGCAGC | T | p.Ala94_Ala97del | rs3842530 | 209,605,636 | . | | | |

## List of Mutations before the last filtration step in Family 3

| 1 | chr | Position | Ref | Alt | GeneName | AminoAcid_St | DBSNP150_ID | SIFT4G2.4_Prediction | SNPType | Splice_Sit | Polyphen2 | MutationTaster |
|---|---|---|---|---|---|---|---|---|---|---|---|---|
| 2 | chr11 | 1651393 | CCTGTGG( | C | KRTAPS-5 | NA | NA | NA | NONFRAM | No | NA | NA |
| 3 | chr13 | 99404851 | A | G | SLC15A1 | M1T | NA | DELETERIOUS | START_LO | No | B | 0.999976 |
| 4 | chr19 | 6760707 | G | A | SH2D3A | R121* | rs149620409 | NA | STOP_GAI | No | NA | 1;1 |
| 5 | chr19 | 13002352 | C | G | GCDH | S48W | rs578242746 | NA | NONSYNO | No | NA | NA |
| 6 | chr19 | 54724605 | A | AATAAC | LILRB3 | NA | NA | NA | FRAMESHI | No | NA | NA |
| 7 | chr19 | 54778579 | A | AGAG | LILRB2 | NA | rs771433769 | NA | NONFRAM | No | NA | NA |
| 8 | chr19 | 54778581 | GTT | G | LILRB2 | NA | rs781576541 | NA | FRAMESHI | No | NA | NA |
| 9 | chr19 | 54778586 | CT | C | LILRB2 | NA | rs745907042 | NA | FRAMESHI | No | NA | NA |
| 10 | chr2 | 1.14E+08 | CA | C | IL36B | NA | rs758127645 | NA | FRAMESHI | Yes | NA | NA |
| 11 | chr2 | 10095007 | AGT | A | GRHL1 | NA | rs762229274 | NA | FRAMESHI | No | NA | NA |
| 12 | chr2 | 1.7E+08 | C | G | SPC25 | D38H | rs781700632 | DELETERIOUS | NONSYNO | No | P | 0.995182 |
| 13 | chr6 | 43006378 | A | G | CUL7 | L1498P | NA | DELETERIOUS | NONSYNO | No | D | 0.99991 |
| 14 | chr6 | 75899061 | G | A | COL12A1 | T232M | rs200443479 | DELETERIOUS | NONSYNO | No | D | 0.954324 |
| 15 | chr6 | 90384235 | G | C | MDN1 | P4279A | rs530285469 | NA | NONSYNO | No | D | 1;1 |
| 16 | chr6 | 90500003 | C | T | MDN1 | V325M | rs537168884 | NA | NONSYNO | No | D | 0.781295 |
| 17 | chrX | 1.07E+08 | TTCCCTTT | T | COL4A6 | NA | rs775824038 | NA | NONFRAM | No | NA | NA |

## List of Mutations before the last filtration step in Family 4

| 1 | Chr | Position | Ref | Alt | Transcript | GeneId | GeneNam | GeneDesc | AminoAci | DBSNP15 | GERP | SIFT4G2.4 | SNPType | SIFT4G2.4 | Splice_Sit | AverageA | Eur_AF_1 |
|---|---|---|---|---|---|---|---|---|---|---|---|---|---|---|---|---|---|
| 2 | chr16 | 2.1E+07 | T | C | ENST0000 | ENSG000C | DNAH3 | dynein axc | Y73C | rs5491237 | NA | NA | NONSYNC | NA | No | NA | NA |
| 3 | chr16 | 8.4E+07 | A | C | ENST0000 | ENSG000C | ATP2C2 | ATPase se | K474N | rs3767186 | NA | DELETERI | NONSYNC | 0.035 | No | 0.0012 | NA |
| 4 | chr17 | 4E+07 | G | A | ENST0000 | ENSG000C | KRT33A | keratin 33 | R293* | rs5432785 | NA | NA | STOP_GAI | NA | Yes | 0.0002 | NA |
| 5 | chr17 | 3.8E+07 | G | T | ENST0000 | ENSG000C | ERBB2 | erb-b2 rec | M1I | rs5468868 | NA | DELETERI | START_LO | 0 | No | 0.001 | NA |
| 6 | chr17 | 7.1E+07 | T | C | ENST0000 | ENSG000C | SDK2 | sidekick ce | I765V | rs7460909 | NA | DELETERI | NONSYNC | 0.02 | No | NA | NA |
| 7 | chr20 | 3.2E+07 | G | A | ENST0000 | ENSG000C | E2F1 | E2F transc | S37F | NA | NA | DELETERI | NONSYNC | 0.014 | No | NA | NA |
| 8 | chr3 | 5.8E+07 | C | A | ENST0000 | ENSG000C | FLNB | filamin B | [illegible] | NA | NA | NA | STOP_GAI | NA | No | NA | NA |
| 9 | chr6 | 1.4E+08 | C | T | ENST0000 | ENSG000C | KIAA1244 | NA | R862C | rs7594596 | NA | DELETERI | NONSYNC | 0 | No | NA | NA |

## List of Mutations before the last filtration step in Family 5

| 1 | Chr | Position | Ref | Alt | Transcript | GeneId | GeneNam | GeneDesc | AminoAci | DBSNP151 | GERP | SIFT4G2.4 | SNPType | SIFT4G2.4 | Splice_Sit | AverageA | Eur_AF |
|---|---|---|---|---|---|---|---|---|---|---|---|---|---|---|---|---|---|
| 2 | chr1 | 166028176 | C | A | ENST0000 | ENSG000( | AL626787 | NA | V98L | rs577435E | NA | NA | NONSYNC | NA | No | 0.0004 | NA |
| 3 | chr1 | 231557634 | TGGC | T | ENST0000 | ENSG000( | EGLN1 | egl-9 fami | NA | NA | NA | NA | NONFRAN | NA | No | NA | NA |
| 4 | chr10 | 85965589 | A | G | ENST0000 | ENSG000( | CDHR1 | cadherin r | D49G | rs5749201 | NA | DELETERI | NONSYNC | 0.006 | No | 0.0006 | NA |
| 5 | chr10 | 89487160 | C | T | ENST0000 | ENSG000( | PAPSS2 | 3'-phosph | R329* | rs1219089 | NA | NA | STOP_GAI | NA | No | 0.0002 | NA |
| 6 | chr10 | 133954073 | A | ACTTGGA( | ENST0000 | ENSG000( | JAKMIP3 | Janus kina | NA | NA | NA | NA | NONFRAN | NA | No | NA | NA |
| 7 | chr11 | 59245747 | T | TACGG | ENST0000 | ENSG000( | OR4D10 | olfactory | NA | NA | NA | NA | FRAMESH | NA | No | NA | NA |
| 8 | chr19 | 49207114 | G | A | ENST0000 | ENSG000( | FUT2 | fucosyltra | G301R | rs144269( | NA | DELETERI | NONSYNC | 0.038 | No | 0.0014 | NA |
| 9 | chr2 | 114257704 | AC | A | ENST0000 | ENSG000( | FOXD4L1 | forkhead | NA | rs572529 | NA | NA | FRAMESH | NA | No | 0.0022 | NA |
| 10 | chr5 | 482203 | T | C | ENST0000 | ENSG000( | SLC9A3 | solute car | N476D | NA | NA | DELETERI | NONSYNC | 0.029 | No | NA | NA |
| 11 | chr5 | 149324212 | C | T | ENST0000 | ENSG000( | PDE6A | phosphod | V9M | rs7559224 | NA | DELETERI | NONSYNC | 0.004 | No | NA | NA |
| 12 | chr7 | 5428497 | G | A | ENST0000 | ENSG000( | TNRC18 | trinucleot | R320C | rs7548493 | 1962.4 | DELETERI | NONSYNC | 0.02 | No | NA | NA |
| 13 | chr7 | 77229988 | G | A | ENST0000 | ENSG000( | PTPN12 | protein ty | R187H | rs368515E | NA | DELETERI | NONSYNC | 0.006 | No | NA | NA |
| 14 | chr8 | 86574748 | TCTC | T | ENST0000 | ENSG000( | REXO1L1 | REX1, RN/ | NA | NA | NA | NA | NONFRAN | NA | No | NA | NA |
| 15 | chr9 | 46390575 | GACACAC | G | ENST0000 | ENSG000( | FAM27D1 | family wit | NA | rs782132E | NA | NA | FRAMESH | NA | No | NA | NA |
| 16 | chrX | 44091744 | C | T | ENST0000 | ENSG000( | EFHC2 | EF-hand d | E535K | rs7747557 | NA | DELETERI | NONSYNC | 0.046 | No | NA | NA |
| 17 | chrX | 153596246 | G | A | ENST0000 | ENSG000( | FLNA | filamin A | R196W | rs1378533 | NA | DELETERI | NONSYNC | 0.004 | No | NA | NA |

## List of Mutations before the last filtration step in Family 6

| 1 | Chr | Position | Ref | Alt | Transcript | GeneId | GeneNam | GeneDesc | AminoAci | DBSNP15( | GERP | SIFT4G2_4 | SNPType | SIFT4G2_4 | Splice_Sit | AverageA | Eur_AF_1 |
|---|---|---|---|---|---|---|---|---|---|---|---|---|---|---|---|---|---|
| 2 | chr1 | 1.8E+08 | C | T | ENST0000 | ENSG000C | TNN | tenascin N | R1180W | rs566752: | NA | DELETERI | NONSYNC | 0.011 | No | 0.0012 | NA |
| 3 | chr11 | 1651393 | CCTGTGG | C | ENST0000 | ENSG000C | KRTAP5-5 | keratin as | NA | NA | NA | NA | NONFRAN | NA | No | NA | NA |
| 4 | chr19 | 5E+07 | TGGCC | T | ENST0000 | ENSG000C | DLL3 | delta-like | NA | NA | NA | NA | FRAMESH | NA | No | NA | NA |
| 5 | chr19 | 2.4E+07 | G | A | ENST0000 | ENSG000C | ZNF726 | zinc finger | G354R | rs751357C | NA | DELETERI | NONSYNC | 0.019 | No | NA | NA |
| 6 | chr19 | 4.5E+07 | GAGC | G | ENST0000 | ENSG000C | BCL3 | B-cell CLL, | NA | rs752464C | NA | NA | NONFRAN | NA | No | NA | NA |
| 7 | chr2 | 1.5E+08 | A | AT | ENST0000 | ENSG000C | RBM43 | RNA bindi | NA | rs142933E | NA | NA | FRAMESH | NA | No | NA | NA |
| 8 | chr20 | 3.2E+07 | G | A | ENST0000 | ENSG000C | E2F1 | E2F transc | S37F | NA | NA | DELETERI | NONSYNC | 0.014 | No | NA | NA |
| 9 | chr5 | 1.5E+08 | T | G | ENST0000 | ENSG000C | FAXDC2 | NA | Q38P | rs7719051 | NA | NA | NONSYNC | NA | No | NA | NA |
| 10 | chr9 | 4.6E+07 | GAA | G | ENST0000 | ENSG000C | FAM27D1 | family wit | NA | rs782203C | NA | NA | FRAMESH | NA | No | NA | NA |
| 11 | chr9 | 4.6E+07 | GACACAC | G | ENST0000 | ENSG000C | FAM27D1 | family wit | NA | rs782132E | NA | NA | FRAMESH | NA | No | NA | NA |

## Skeletal Dysplasia

ORIGINALITY REPORT

| 19% | 13% | 13% | % |
|---|---|---|---|
| SIMILARITY INDEX | INTERNET SOURCES | PUBLICATIONS | STUDENT PAPERS |

PRIMARY SOURCES

| | | |
|---|---|---|
| 1 | prr.hec.gov.pk<br>Internet Source | 4% |
| 2 | www.ncbi.nlm.nih.gov<br>Internet Source | 1% |
| 3 | www.researchgate.net<br>Internet Source | 1% |
| 4 | authors.library.caltech.edu<br>Internet Source | 1% |
| 5 | www.nature.com<br>Internet Source | <1% |
| 6 | Harold Chen. "Atlas of Genetic Diagnosis and Counseling", Springer Science and Business Media LLC, 2017<br>Publication | <1% |
| 7 | www.karger.com<br>Internet Source | <1% |
| 8 | Samina Yasin, Outi Makitie, Sadaf Naz. "Spondylocarpotarsal synostosis syndrome due to a novel loss of function FLNB variant: a | <1% |